

**Four-Wave Mixing and Phase Conjugation  
in Photorefractive Crystals**

Thesis by  
Jeffrey Owen White

In Partial Fulfillment of the Requirements  
for the Degree of  
Doctor of Philosophy

California Institute of Technology  
Pasadena, California

1984

(Submitted May 11, 1984)

## ACKNOWLEDGEMENTS

First and foremost it is a pleasure to acknowledge the guidance, and supervision of my advisor, Prof. Amnon Yariv. What a privilege it has been to work in the dynamic environment fostered in his group. My colleagues and I thank him for originating the work in this area, suggesting problems to work on, and especially for providing a laboratory where we had the freedom to explore.

Thanks are also due to my colleagues Dr. Mark Cronin-Golomb and Prof. Baruch Fischer who provided the enthusiasm, criticism, encouragement, and intuition which are essential ingredients in graduate work. I am looking forward to the day when we can collaborate on the next project.

With the hope of reciprocating some day, I acknowledge helpful conversations with such people as Profs. William Bridges, Lambertus Hesselink, Dmetri Psaltis, Thomas Caughy, Bengt Fornberg, Bill Kath, and Thad Vreeland.

Desmond Armstrong, Larry Begay, Edith Huang, and Albert Chang have won my eternal respect and gratitude for their willingness to make other people's problems their problems. The technical assistance of Desmond Armstrong and Larry Begay with experimental apparatus was invaluable. Edith Huang and Albert Chang are computer programming consultants extraordinaire.

Constant encourage and perspective have come from my family in New Jersey and friends in California.

## ABSTRACT

This thesis is an experimental and theoretical investigation of nonlinear optics in photorefractive crystals, and applications thereof. Coherent light is used to induce nonlinear, optical frequency polarizations proportional to the cube of the total optical field within these materials. Equivalently, dynamic holography is performed wherein the incident light simultaneously writes, reads and erases index of refraction gratings.

The first part of this thesis is a description of the physics of the photorefractive effect in such crystals as  $\text{Bi}_{12}\text{SiO}_{20}$ ,  $\text{LiNbO}_3$ ,  $\text{KTaO}_3$ , and  $\text{BaTiO}_3$ . Previous microscopic rate equation models are extended to include the dynamics of a second photorefractive center with the aim of explaining several discrepancies with experimental data.

The second part reviews the coupled wave theory of fixed gratings and dynamic gratings formed in photorefractive media. Coupled nonlinear ordinary differential equations describe the interaction between two optical waves; which is caused by the grating that they create. The analysis is extended to the reflection geometry and the ring resonator geometry. The coupling constant is measured in the reflection geometry. Holographic gain is combined with mirror feedback to demonstrate a unidirectional ring oscillator, wherein a optically pumped photorefractive crystal functions as a directional gain element.

The third part extends the analysis to the holographic formulation of four-wave mixing, wherein four waves and up to four gratings exist in the crystal. The equations are solved in the single grating approximation. The object of much of the analysis is to calculate the reflectivity of a four-wave mixing photorefractive phase conjugate mirror. The invention of a passive self-pumped phase conjugate mirror is described.

The last part describes three applications of four-wave mixing. We demonstrate the compensation of intracavity laser distortions by replacing an ordinary mirror in a laser with a passive phase conjugate mirror. We propose and demonstrate a phase conjugate window for one-way transmission of an information bearing optical field through a thin phase distortion. Finally, the multiplicative properties of four-wave mixing are combined with the transforming properties of lenses to construct a coherent optical processor capable of convolving and correlating three input fields containing arbitrary spatial phase and amplitude information.

CONTENTS

1. INTRODUCTION.....	1
1.1 Phase conjugate waves and mirrors .....	1
1.2 Phase conjugate mirrors via linear optics.....	2
1.3 Phase conjugate mirrors via nonlinear optics .....	4
1.4 Outline of thesis .....	6
References for Chapter 1 .....	7
2. THE PHOTOREFRACTIVE EFFECT .....	10
2.1 Introduction .....	10
2.2 Basic mechanism.....	11
2.3 Photorefractive materials .....	13
2.4 Survey of experimental work.....	14
2.5 Microscopic rate equation model of the photorefractive effect .....	19
2.6 Statistical mechanics model of the photorefractive effect.....	31
References for Chapter 2.....	34

CONTENTS

3. TWO-WAVE MIXING.....	38
3.1 Introduction.....	38
3.2 Coupled wave theory of fixed, thick hologram gratings.....	40
3.3 Coupled wave theory of dynamic gratings.....	42
3.4 Oscillation in two-wave mixing.....	45
3.5 Reflection gratings.....	49
3.6 Coupling between waves inside a ring resonator.....	56
References for Chapter 3.....	58
4. FOUR-WAVE MIXING.....	60
4.1 Introduction.....	60
4.2 Holographic formulation of four-wave mixing.....	60
4.3 Single grating, undepleted pumps approximation.....	63
4.4 Pump depletion in the single grating approximation.....	71
4.5 Oscillation in four-wave mixing.....	78
4.6 Self-pumped phase conjugate mirror.....	81
References for Chapter 4.....	82

CONTENTS

5. APPLICATIONS.....	85
5.1 Introduction.....	85
5.2 Laser with dynamic holographic intracavity distortion correc- tion.....	85
5.3 One-way image transmission through inhomogeneous media.....	89
5.4 Spatial convolution and correlation via four-wave mixing.....	98
References for Chapter 5.....	108

## 1. INTRODUCTION

### 1.1 Phase conjugate waves and mirrors

The phase conjugate replica of a monochromatic electromagnetic field is a field, with the same frequency, whose wavefronts, *i.e.*, surfaces of constant phase, take the same shape throughout space, but propagate in the opposite direction at every point. A wave travelling essentially in the positive  $z$  direction is denoted by

$$E_1(\mathbf{r}, t) = A_1(\mathbf{r})e^{i(\omega t - kz)} + A_1^*(\mathbf{r})e^{-i(\omega t - kz)} \quad (1)$$

where the complex amplitude  $A_1(\mathbf{r})$  can describe any spatial amplitude or phase information impressed upon  $E_1$ . Mathematically, its phase conjugate is obtained by complex conjugating the spatial part

$$E_{PC}(\mathbf{r}, t) = A_1^*(\mathbf{r})e^{i(\omega t + kz)} + A_1(\mathbf{r})e^{-i(\omega t + kz)} \quad (2)$$

or changing  $t \rightarrow -t$ , hence the identification of phase conjugation with "time reversal".

That such a phase conjugate wave can exist is proved by showing that it satisfies the same wave equation that the original wave satisfies. The scalar wave equation obeyed by (1) is

$$\nabla^2 A_1 + [\omega^2 \mu \varepsilon(\mathbf{r}) - k^2]A_1 - i2k \frac{\partial A_1}{\partial z} = 0 \quad (3)$$

where  $\mu$  is the uniform magnetic permeability and  $\varepsilon$  is the dielectric constant. The validity of the corresponding equation for (2)

$$\nabla^2 A_1^* + [\omega^2 \mu \varepsilon(\mathbf{r}) - k^2]A_1^* + i2k \frac{\partial A_1^*}{\partial z} = 0$$

follows directly by taking the complex conjugate of (3), provided that  $\varepsilon(\mathbf{r})$  has no imaginary part representing loss or gain.\*

\* In the event that  $\varepsilon(\mathbf{r})$  has an imaginary part that is uniform in space, the proof follows directly from factoring out a uniform attenuation from  $A_1$ .



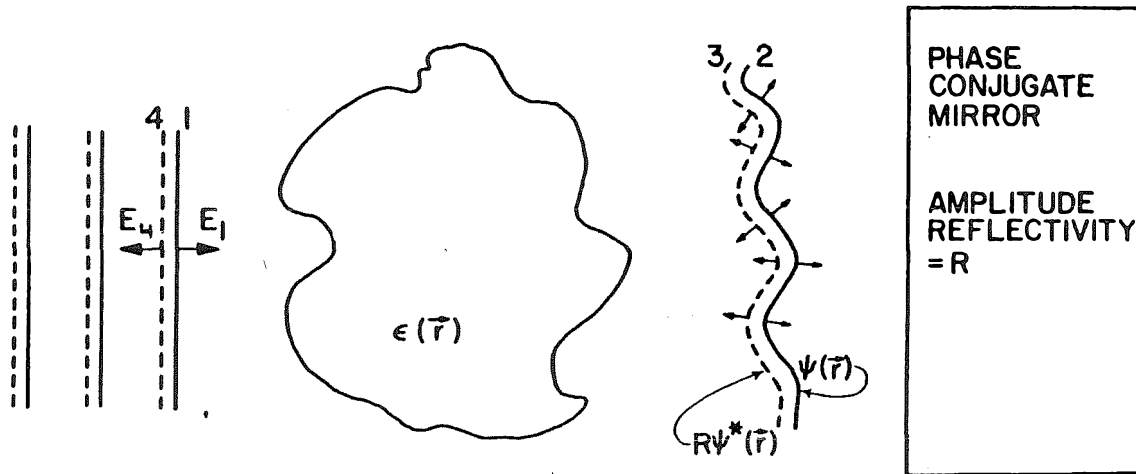
A phase conjugate mirror (PCM) is a device which generates the phase conjugate of an incident wavefront. If we assume that a PCM is located at the plane  $z=z_0$ , then the above arguments hold for all  $z < z_0$ . In a stable two mirror laser cavity, the counterpropagating fields are phase conjugates of each other, so both mirrors are acting as phase conjugate mirrors. However, a true PCM will generate the phase conjugate replica of an incident wavefront possessing arbitrary spatial variation of amplitude, phase, and polarization.

Much of the interest in phase conjugate waves is due to their distortion correcting capability. Figure 1 illustrates the canonical correction scenario where an undistorted wave passes through a region of nonuniform index of refraction, the distorted wave is incident upon a PCM, and the phase conjugate wave returns through the distortion and emerges unscathed. The distortion in the figure could represent modal dispersion in a fiber, atmospheric turbulence, thermal blooming, imperfect optics, etc.

## **1.2 Phase conjugate mirrors via linear optics**

The first implementations of PCM's were arrays of corner cube reflectors. They are technically only pseudo-conjugators because of their effect on the polarization properties of the incident wave and because of the piecewise nature of the reflection. The fidelity of the reflected wave is limited by the size of the individual corner cubes and the flipping of each picture element upon reflection from a corner cube. Technological advancements in micromachining and replicating optics have made available square foot sized arrays with 47,000 corner cubes per square inch [1].

The next realizations were via Coherent Optical Adaptive Techniques. These systems have achieved compensation for aberrated wavefronts with the use of electro-optic devices, acoustic devices, or deformable "rubber" mirrors. The latter are thin metallic reflectors supported by arrays of piezoelectric actuators.



**Figure 1.1.** Typical geometry depicting the ability of phase conjugation to correct for a general spatially dependent phase aberration. A plane wave (1) incident from the left encounters a region of nonuniform dielectric constant. The distorted wavefront (2) is incident upon a PCM, giving rise to (3), which re-traverses the same region. The wave (4) which emerges has the initial planar wavefronts.

The actuators are driven by wavefront error sensors. Such devices are currently in use in lasers, to correct for intracavity distortions, in communications and in astronomy, to image through the atmosphere [2].

Kogelnik pointed out that conventional holographic techniques could be used for imaging through stationary distortions. One need only 1) create a hologram of the distorted object wave and 2) illuminate it with a reconstructing wave counterpropagating to the reference wave. This generates a phase conjugate wave which will retrace the path of the object wave through the distortion and converge to a real image [3].

### 1.3 Phase conjugate mirrors via nonlinear optics

The development of real-time holography, in which holograms are written by interfering two beams in nonlinear media instead of on photographic film, eliminated the time consuming stage of developing the film. The writing and reading (with a third beam) of the transient holograms were considered to be simultaneous but physically distinct, *i.e.*, noninteracting [4-8].

A concurrent development was the discovery that stimulated backscattering (Brillouin, Raman, or Rayleigh) could produce phase conjugate waves. In stimulated Brillouin scattering, an optical wave incident upon a material medium stimulates a forward going acoustical phonon wave whose wavefronts match the optical wavefront. The pressure wave perturbs the index of refraction, retroreflecting up to 80% of the optical wave. In stimulated Raman scattering, a forward going optical phonon wave is generated, and in stimulated Rayleigh scattering, a forward going roton is generated [9-11].

One feature of these stimulated scattering processes is that the frequency of the phase conjugate wave is lower than that of the incident wave by an amount equal to the phonon frequency. Another feature is the existence of intensity thresholds below which there is no gain for the stimulated wave, hence no reflectivity.

The study of all-optical parametric processes in nonlinear media led directly to the current activity in the field. An essential ingredient has been the application of the concepts and techniques of nonlinear optics, including coupled wave theory and Feynman diagrams [12]. One scheme, called three wave mixing (3WM), involves a second order nonlinearity and three optical fields. In this process, difference frequency generation takes place, wherein the incident, signal wave at frequency  $\omega$  and a pump wave at  $2\omega$  induce a nonlinear polarization in the medium which radiates a phase conjugate wave at  $\omega$  [13,14]. The angular

bandwidth of the incident wave is restricted due to phase matching constraints, and the nonlinear medium must lack inversion symmetry in order to possess the second order optical susceptibility, but amplified reflection is possible and there exists no intensity threshold. Another scheme involves a third order susceptibility and four optical fields. The incident wave at  $\omega$  and two counterpropagating waves at  $\omega$  induce a third order nonlinear polarization in the medium [15]. The polarization radiates a fourth, phase conjugate wave at  $\omega$ , hence the name degenerate four-wave mixing (D4WM).

Nonlinear optical implementations of PCM's have several advantages:

- i. The response time is limited only by the nonlinear medium itself. The processing of different parts of the incident wave takes place in parallel.
- ii. The resolution in the near field is limited by the density of the atomic or molecular species participating in the interaction, or the wavelength of the incident light.
- iii. The possibility of gain exists as part of the phase conjugation process itself.
- iv. Wavefront error sensors are not necessary.

and several disadvantages:

- i. Many types of nonlinear media are not available in large sizes of good optical quality. The size of a PCM will limit its resolution in the far field of a distortion.
- ii. In 3WM and 4WM, the pump beams have to be coherent with respect to the signal wave, to a degree determined by the response time of the medium.

Four-wave mixing has become the most important nonlinear optical technique for generating phase conjugate waves because the interaction is automatically phase matched for components of the incident wave at any angle, a third order susceptibility is not forbidden in any material on symmetry grounds, and an

amplified reflection is possible [15-19]. Apart from phase conjugation, 4WM has become a tool for spectroscopy [20, Chap. 8], narrow bandpass filtering [21], converting incoherent to coherent images [22], and image processing [23]. It has been proposed for use in laser fusion [24], generating two photon coherent states [25], temporal signal processing [26], and optical computing [20, Chap. 14].

Many types of nonlinear media have been used as the mixing medium including two-level systems, dyes, semiconductors, radiatively cooled vapors, plasmas, liquid crystals, photorefractive crystals, and aerosols. The photorefractive media are particularly suitable for use with low power continuous wave lasers because of their extraordinary sensitivity, and also because they respond to light continuously throughout the visible spectrum. This is why they were used exclusively in the work described in this thesis.

Several review articles have discussed both theoretical and experimental aspects of phase conjugation, its applications, and the nonlinear media used to date [20,27-29].

#### **1.4 Outline of thesis**

Chapter 2 familiarizes the reader with the photorefractive effect and presents a generalization of existing models designed to address two discrepancies between experimental data and some existing models.

Chapter 3 briefly reviews the coupled wave theory of fixed, thick holograms, and the coupled wave theory of two wave mixing (2WM) in nonlocal, nonlinear media. Two new geometries are examined: energy coupling in the reflection geometry, and a unidirectional ring resonator. Experimental results are presented.

Chapter 4 presents the holographic formulation of four-wave mixing as an

extension of the two-wave mixing formulation in the previous chapter. In this formulation, four plane waves interfere within the medium to write four different gratings. The differences between this formulation and previous formulations of 4WM are emphasized. The resulting coupled wave equations are solved in several approximations including undepleted pump waves, and negligible absorption. The analysis is restricted to cases where only one grating (out of a possible four gratings) is present in the medium. Experimental data supporting the analysis are presented. Oscillation in a new four-wave mixing geometry is considered, which leads to the invention of the self-pumped phase conjugate mirror.

Chapter 5 describes three applications of phase conjugation and four-wave mixing to aberration compensation and image processing. The first application is to correcting intracavity distortions in lasers. This is demonstrated by replacing the end mirror of a commercial argon ion laser with a self-pumped phase conjugate mirror. The second application is to one-way field transmission through inhomogeneous media. We demonstrate the operation of a phase conjugate window which permits the transmission of amplitude and phase information through a thin phase distortion. The third application is a real-time optical processor which performs spatial convolution and correlation of three input object fields.

#### **References for Chapter 1**

1. Reflexite Corp., 199 Whiting St., New Britain Conn. 06051
2. D.L. Fried, guest ed., Special issue on Adaptive Optics, J. Opt. Soc. of Am. **67**, (1977).
3. H. Kogelnik, Bell Syst. Tech. J. **44**, 2451 (1965).
4. H. Boersch, H. Eichler, Z. Angew. Phys. **22**, 378 (1967).
5. H.J. Gerritsen, Appl. Phys. Lett. **10**, 239 (1967).

6. F.S. Chen, J.T. LaMacchia, D.B. Fraser, Appl. Phys. Lett. **13**, 223 (1968).
7. B.I. Stepanov, E.V. Ivakin & A.S. Rubanov, Sov. Phys.-Dokl. **16**, 46 (1971).
8. J.P. Woerdman, Opt. Comm. **2**, 212 (1970).
9. B.Y. Zeldovich, V.I. Popovichev, V.V. Ragul'skii & F.S. Faisulov, Sov. Phys. JETP **15**, 109 (1972).
10. V. Wang and C.R. Giuliano, Opt. Lett. **2**, 4 (1978).
11. B.Ya. Zel'dovich, N.F. Pilipelskii, V.V. Ragul'skii & V.V. Shkunov, Sov. J. Quant. Elect. **8**, 1021 (1978).
12. A. Yariv, IEEE J. Quant. Elect. **13**, 943 (1977).
13. A. Yariv, Appl. Phys. Lett. **28**, 88 (1976).
14. P.V. Avizonis, F.A. Hopf, W.D. Bamberger, S.F. Jacobs, A. Tomita & K.H. Womack, Appl. Phys. Lett. **31**, 435 (1977).
15. A. Yariv and D.M. Pepper, Opt. Lett. **1**, 16 (1977).
16. D.M. Bloom and G.C. Bjorklund, Appl. Phys. Lett. **31**, 592 (1977).
17. S.M. Jensen and R.W. Hellwarth, Appl. Phys. Lett. **32**, 166 (1978).
18. D.M. Pepper, D. Fekete & A. Yariv, Appl. Phys. Lett. **33**, 41 (1978).
19. D.M. Bloom, P.F. Liao & N.P. Economu, Opt. Lett. **2**, 58 (1978).
20. *Optical Phase Conjugation*, (Ed. R.A. Fischer, New York, Academic Press, 1983).
21. J. Nilsen, N.S. Gluck & A. Yariv, Opt. Lett. **6**, 380 (1981).
22. Y. Shi, D. Psaltis, A. Marrakchi & A.R. Tanguay, Jr., Appl. Opt. **22**, 3665 (1983).
23. J. Feinberg, Opt. Lett. **5**, 330 (1980).
24. Y.I. Kruzhilin, Sov. J. Quant. Elect. **8**, 359 (1978).

25. H.P. Yuen & J.H. Shapiro, *Opt. Lett.* **4**, 334 (1979).
26. T.R. O'Meara & A. Yariv, *Opt. Engin.* **21**, 237 (1982).
27. A. Yariv, *IEEE J. Quant. Elect.* **14**, 650 (1978).
28. Special issue on optical phase conjugation, *Opt. Engin.* **21**, no. 2 (1982).
29. C.R. Giuliano, *Phys. Today* **34**, 27 (1981).



## 2. THE PHOTOREFRACTIVE EFFECT

### 2.1 Introduction

Study of the photorefractive effect began with the discovery of optical damage in  $\text{LiNbO}_3$  and  $\text{LiTaO}_3$  [1]. Ashkin *et. al.* noticed that the index of refraction of their crystals was changed by exposure to light, both coherent and incoherent. Visible and ultraviolet wavelengths produced the effect, but not infrared. If the illumination was nonuniform, the optical homogeneity suffered and it was feared that such sensitivity would make  $\text{LiNbO}_3$  less useful as a nonlinear medium. The damage remained when the light was removed, yet the effect was reversible, in contrast to the catastrophic damage that occurs at much higher intensities.

Chen, LaMacchia and Fraser soon realized the opportunities that were there and demonstrated that holograms could be written, stored and erased in  $\text{LiNbO}_3$  [2,3]. In *conventional* holography the interference pattern between an object beam and a reference beam falls on photographic film, recording the amplitude and phase of the object beam. The spatial variation of intensity is mapped into a spatial variation of silver concentration ( or absorption constant ) when the film is developed. In *real-time* holography, the interference pattern fills the crystal, and changes its index as the exposure takes place.

The utility of  $\text{LiNbO}_3$  for frequency doubling was threatened, but the formal equivalence between holography and four wave mixing [4] indicated that a new type of medium was available for nonlinear optics of a different kind. Large nonlinearities became obtainable not only at low powers, but over the entire visible spectrum as well. A speed-sensitivity tradeoff is observed, however, because the degree of response depends on the energy deposited in the crystal, rather than the intensity, as is the case for most nonlinear materials. Charge carriers must migrate from regions of high intensity to low intensity, so the response can never be as fast as that arising from the disturbance of atomic orbitals, or rotation of molecules, etc. Response times in the nanoseconds require  $\text{MW/cm}^2$  intensities

[5].

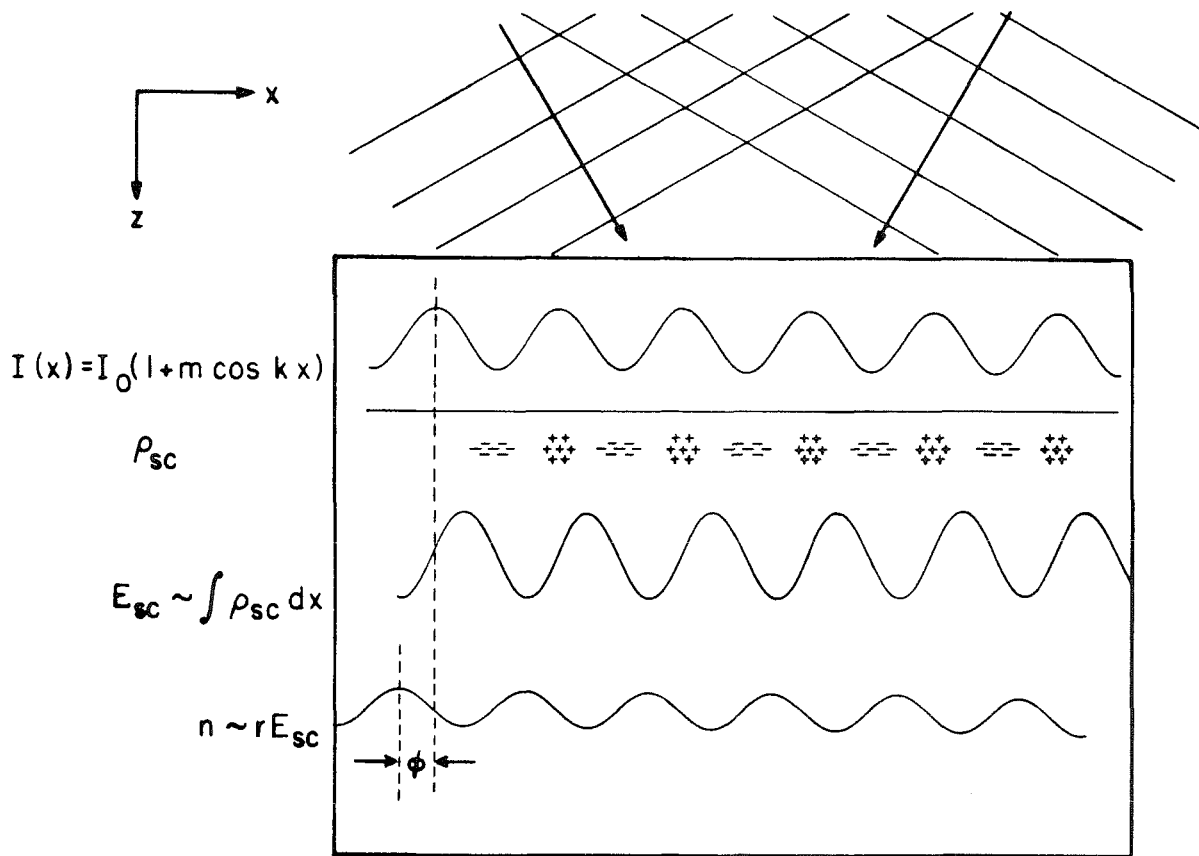
In addition to becoming a new medium for performing nonlinear optics, the photorefractive effect has also become a diagnostic tool. For example, the electron and hole contributions to the photoconductivity in  $\text{LiNbO}_3$  has been determined holographically [6]. Phase and amplitude gratings, created by means other than the photorefractive effect, have been used to measure spatial diffusion rates of electronic excitation in impurity doped solids [7,8], exciton diffusion lengths [9], and energy transport in molecular crystals [10].

The long dark storage times were promising for optical memories except that erasure occurs during readout. A method was discovered whereby the holograms could be fixed if they were recorded at about  $200^\circ\text{C}$  and then cooled to room temperature [11]. Using this technique, 500 holograms were stored in a 1 cm thick crystal of  $\text{LiNbO}_3:\text{Fe}$ . The diffraction efficiency of each hologram was  $\approx 2.5\%$ , and the estimated lifetime of  $10^5$  years is suitable for archival storage.

## 2.2 Basic mechanism

The first explanation of this effect was due to Chen and Amodei [12,13]. Their hypothesis was that charges within the crystal migrated under the influence of the light, creating a space charge field and hence an index change via the electro-optic effect. The charges were thought to occupy states within the energy gap, *i.e.* they were localized or trapped there until excited into the conduction band. They envisioned electrons migrating from intensity maxima to minima, via the conduction band, leaving behind positively ionized donors, *i.e.* trapped holes. The charge separation would produce a space charge field having the same spatial dependence as the pattern of light intensity exposing the crystal (see Fig. 2.1).

The use of photorefractive crystals as holographic storage media depends on the ability to hold a space charge long after exposure. Because the crystal is an insulator in the dark, when the light is turned off, all the electrons must leave the conduction band. The space charge is lost if they all return to ionized sites of the



**Figure 2.1.** The photorefractive mechanism. Two laser beams intersect, forming an interference pattern. Charges are optically excited from traps within the energy gap to the conduction band. Charges return to the traps via collisional recombination. The excitation is preferential in the regions of high intensity, and the trapping is random so there is a net migration of charge from the intensity maxima to the minima. The electric field associated with the space charge density creates a periodic index variation via the electrooptic effect.

original type, *i.e.* if all the electrons recombine with trapped holes. Space charge storage is only possible if a population of holes in the donor sites exists in the dark: nocturnal holes. This requires the presence of alternative sites for the electrons to reside. One cannot simply add more of the positively charged empty donor sites and preserve crystal neutrality, so the additional ingredient is a second type of trap which is neutral when unoccupied.

### 2.3 Photorefractive materials

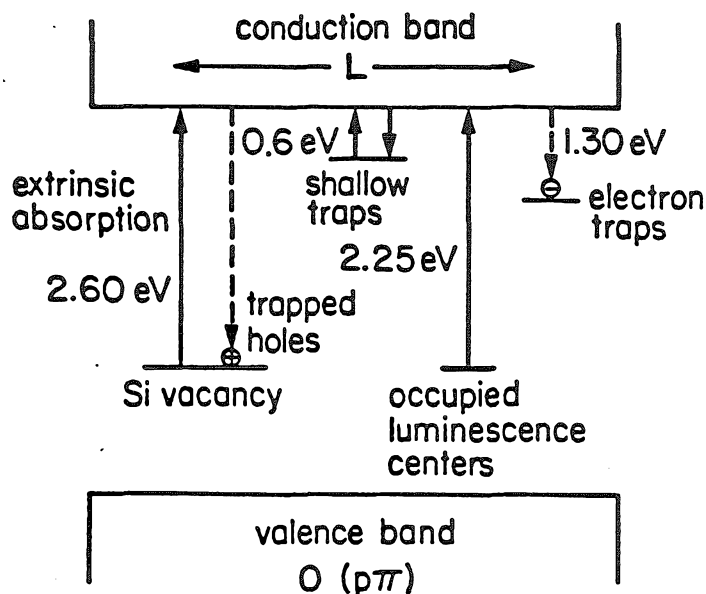
In the broadest sense, photorefractive materials could include any material in which light could produce an index change. Index gratings in ruby have been produced by using an optical interference pattern to generate a spatially varying excitation of the  $\text{Cr}^{3+}$  ion [16]. Gratings have been written in semiconductors by exciting a spatially varying population of electrons in the conduction band [17]. Absorption gratings have been produced by bleaching dyes [18]. In  $\text{CS}_2$  and liquid crystals, polarized light causes the molecules to line up, thus changing the index from ordinary to extraordinary or vice versa [19,20].

The term photorefractive effect is used most commonly today with reference to the combination of a photoinduced space charge field and the electro-optic effect. Only in photoconducting, non-centrosymmetric, crystalline, electrical insulators has this been observed to date, and amongst them only in ferroelectrics and the paraelectric sillenites, bismuth silicon oxide ( $\text{Bi}_{12}\text{SiO}_{20}$ , BSO) and bismuth germanium oxide ( $\text{Bi}_{12}\text{GeO}_{20}$ , BGO).

The energy band diagram of BSO is shown in Fig 2.2. The main source of extrinsic absorption is attributed to Si vacancies, each in a unit cell which is neutral when the vacancy is occupied by an electron. The other operative state in the energy gap is known only to be a source of photoluminescence in a unit cell which is neutral when the center is unoccupied [14].

$\text{BaTiO}_3$ ,  $\text{KNbO}_3$ ,  $\text{LiNbO}_3$ ,  $\text{LiTaO}_3$ ,  $\text{Sr}_{1-x}\text{Ba}_x\text{Nb}_2\text{O}_6$ , and  $\text{Ba}_2\text{NaNb}_5\text{O}_{15}$  are the oxygen octahedra ferroelectrics in which the photorefractive effect has been observed. Since the electro-optic coefficients are linearly related to the spontaneous polarization [21-23], proximity to the phase transition can enhance the electro-optic effect. As an alternative to heating or cooling  $\text{KNbO}_3$ , the transition temperature can be lowered by combining it with  $\text{KTaO}_3$ . The nonlinearities of  $\text{Sr}_{1-x}\text{Ba}_x\text{Nb}_2\text{O}_6$  and  $\text{Ba}_2\text{NaNb}_5\text{O}_{15}$  can be composition controlled as well [27].

Multiple valence transition metals are commonly added because they can

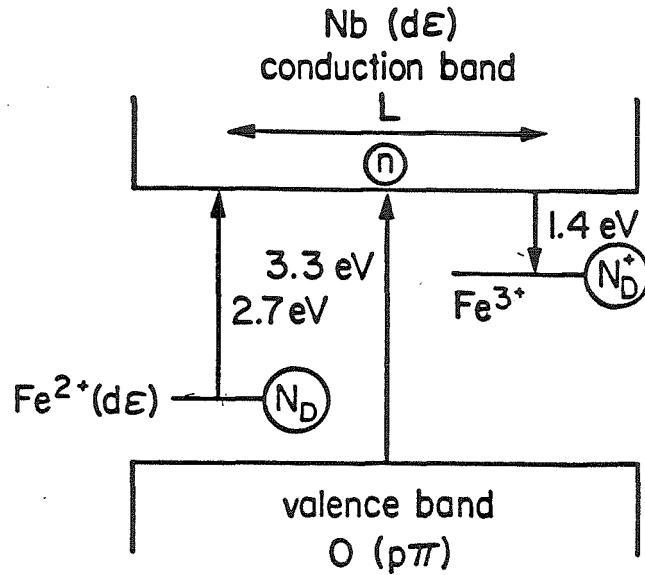


**Figure 2.2.** Energy band diagram of bismuth silicon oxide (after Ref. 14,59).

activate the photorefractive effect by serving as donors and acceptors of electrons. Fe is the most common dopant. The mismatch between the host and a dopant of lower valence can be compensated by oxygen vacancies. Likewise, the valence of the dopant can be changed. The photorefractive sensitivity is correlated with the  $\text{Fe}^{2+}/\text{Fe}^{3+}$  ratio, which can be controlled by oxidation and reduction. For example, removing one O atom frees two electrons which then convert two  $\text{Fe}^{3+}$  ions to  $\text{Fe}^{2+}$  ions. The energy level diagram for  $\text{KNbO}_3$  is shown in Fig. 2.3.

#### 2.4 Survey of experimental work

The photorefractive effect has been explored in many ways. One method is to write a grating with two beams, and monitor its diffraction efficiency with a third, probe beam. If the energy of the probe beam photons is insufficient to excite free electrons, then it will perform a nondestructive readout. The diffracted intensity can be related to the index change (see §3.2), which is the product of the electro-optic coefficient and the electric field. If the probe beam has the same wavelength, and is counterpropagating to one of the writing beams, then the



**Figure 2.3.** Oxygen  $p\pi$  valence band, niobium  $d\varepsilon$  conduction band and  $\text{Fe}^{2+}$  donor and  $\text{Fe}^{3+}$  acceptor levels of  $\text{KNbO}_3$  after Ref. 61.

diffracted beam is the phase conjugate of the other writing beam. The phase conjugate reflectivity is then a measure of the space charge field.

The writing beams themselves can be used to monitor the grating amplitude. During writing, the diffracted component of each writing beam is hard to measure because it is coincident with the undiffracted component of the other beam. If one beam is turned off at any instant, then the diffracted component of the other can be measured as the grating decays. The coupling between the two writing beams is a measure of the grating amplitude and phase, and is manifested as a transfer of power and/or phase between them.

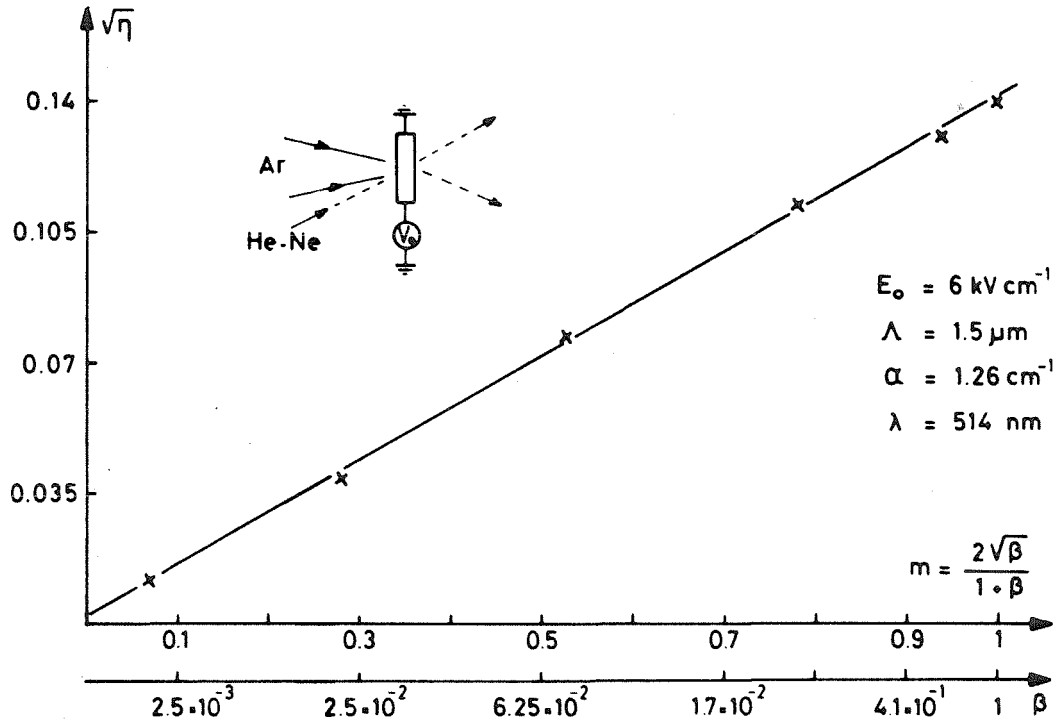
Table 1 summarizes much of the experimental work done to date. The quantities measured are the diffraction efficiency,  $\eta$ , the phase conjugate reflectivity,  $R$ , the two beam coupling constant,  $\Gamma$ , (as defined in §3.3), the index change,  $\delta n$ , and the response time,  $\tau$ . The variables under experimental control are the external, applied field,  $E_0$ , the wavelength,  $\lambda$ , of the writing beam, and the incident intensity

**TABLE 1.** Experimental Studies of the Photorefractive Effect

Crystal	$\lambda$ nm	$\Lambda$ $\mu\text{m}$	$I_0$ $W/\text{cm}^2$	$m=I_1/I_0$	$E_0$ kV/cm	Qty meas'd	Ref.
BGO	604	4.4	>33	0.41,0.14	5-19	$0 < R < 1.5\%$	29
	514.5	.3-.67	?	0.94	0	$.002 < R < .01\%$	30
BSO	514.5	1.05-3	50 $\mu$ -2m	$\sim 1$	0-6	$.01 < \eta < 6.25\%$	31
	"	1.5	5m	0.1-1.0	6	$.01 < \eta < 2\%$	31
	"	"	"	0.14,1.0	"	$0 < R < 0.2\%$	32
	"	0.5-9	10m	?	0-6	$0 < R < 0.2\%$	33
	632.8	3	1-20m	0.18	11.3	$\tau$	34
BaTiO <sub>3</sub>	488.0	?	.002-12	?	0	$\eta$	34
	"	"	0.1-16	?	0	$\tau$	34
	"	0.5-10	?	?	0	$\eta$	34
	514.5	0.4-4.2	.01-.17	?	0	$\tau$	35
	"	2.61	?	?	0-4	$\eta$	35
KNbO <sub>3</sub>	488.0	1.5-10	1	$\sim 1$	0-7	$3 < \eta < 10\%$	36
	"	"	"	"	"	$.2 < \Gamma < 2\text{cm}^{-1}$	36
	"	2	"	0.01-100	?	$.025 < \eta < .6\%$	36
	"	"	"	"	"	$.75 < \Gamma < 2\text{cm}^{-1}$	36
	"	1.6	.001-1	1	0	$10^{-4} < \eta < 10^{-2}$	36
	"	"	"	"	"	$.3 < \Gamma < 1\text{cm}^{-1}$	36
	"	2.2	.01-300	$\sim 1$	0	$.004 < \tau < 4\text{sec}$	37
	592	2.6	>0.1	0.16,0.47	2-13	$0 < R < 10\%$	28
LiNbO <sub>3</sub>	350.7	2.5	?	0.46	-15-15	$0 < \delta n < 10^{-4}$	38
	"	"	"	"	"	$10^{-4} < \delta n < 10^{-3}$	38
	441.6	.35-6.5	10m	?	0	$.06 < \eta < 30\%$	39
	"	"	.1-20m	"	"	$8 < \eta < 12\%$	39
	"	"	?	0.03-0.75	0	$0 < \eta < 30\%$	39
	"	.6	.1-20	0.31	0	$6 < \Gamma < 8\text{cm}^{-1}$	40
	"	"	?	0.02-0.58	0	$4 < \Gamma < 10\text{cm}^{-1}$	40
	"	.35-7	?	0.31	?	$1 < \Gamma < 12\text{cm}^{-1}$	32
SBN	514.5	1.9	100m	0.94	0	$3 < \Gamma < 11\text{cm}^{-1}$	62

variation,  $I = I_0 + I_1 \cos(2\pi x / \Lambda)$ . The fringe spacing is denoted by  $\Lambda$ , and the modulation index of the intensity variation is  $m \equiv I_1 / I_0$ .

The major observation has been that the amplitude of the space charge field,  $E_1$ , is proportional to the modulation index of the intensity variation which creates it [31], hence the diffraction efficiency exhibits a quadratic dependence on  $m$  (Fig. 2.4).

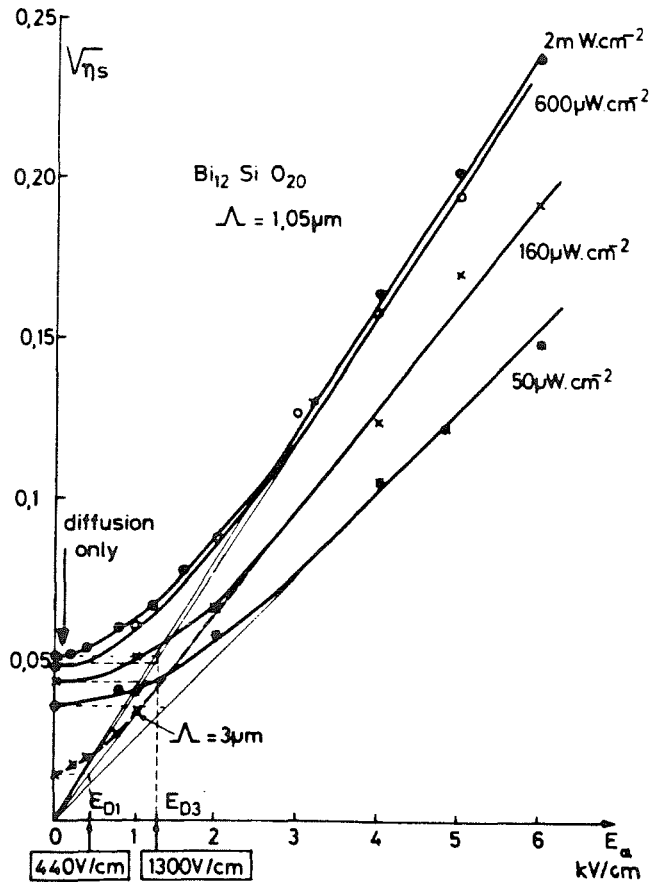


**Figure 2.4.** Square root of diffraction efficiency  $\eta$  versus fringe modulation  $m$ . Incident power  $5 \text{ mW/cm}^2$ . Readout with a HeNe probe beam. From Ref. 31.

The absolute intensity dependence of  $E_1$  has been measured over a wide range of intensities [30,33-40]. The grating amplitude has been found to increase with writing intensity until a gradual saturation. The saturation occurs at  $600 \mu\text{W/cm}^2$  in BSO (Fig. 2.5), and over  $100 \text{ W/cm}^2$  in heavily doped  $\text{KNbO}_3$  (Fig. 2.6).

$E_1$  has a linear dependence on external, applied field,  $E_0$ , in several materials over a range of several  $\text{kV/cm}$ . [28,30,32,35,36,38]. The reflectivity of a phase



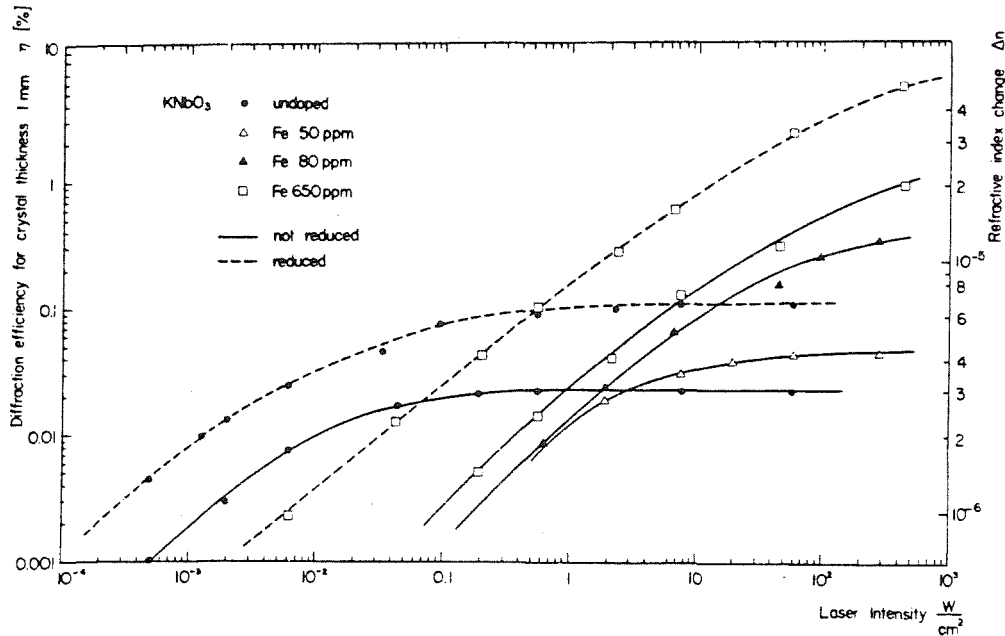


**Figure 2.5.** Square root of steady state diffraction efficiency in BSO crystals vs. applied field for different light intensities; full lines, fringe spacing  $\Lambda = 1\mu\text{m}$ ; dashed line,  $\Lambda = 3\mu\text{m}$ . From Ref. 30.

conjugate mirror was seen to have a quadratic dependence on  $E_0$ , for fringe spacings greater than  $3\mu\text{m}$  [32].

The dependence of  $E_1$  upon fringe spacing,  $\Lambda$ , has also been measured over a range from  $0.5$  to  $10\mu\text{m}$ . It is best studied with zero applied field. In that case, the grating magnitude is proportional to  $1/\Lambda$ . In BSO, an  $E_0 = 2\text{kV/cm}$  was found to yield a phase conjugate reflectivity independent of  $\Lambda$ , *i.e.* a flat modulation transfer function (MTF) for  $1 < \Lambda < 10\mu\text{m}$  [32].

The time dependence of grating formation has been studied less thoroughly. Most data have been interpreted in terms of a single time constant, although recent work has shown more than one time constant in BSO [52-54]. An inverse



**Figure 2.6.** Steady state diffraction efficiency and refractive index modulation vs. laser intensity in  $\text{KNbO}_3:\text{Fe}$  at 488.0 nm. From Ref. 37.

relationship between intensity and response time has been observed over wide ranges in BSO,  $\text{BaTiO}_3$ , and  $\text{KNbO}_3:\text{Fe}$ . At low light levels, the departure from reciprocity appears to be due to the dark conductivity dominating the photoconductivity [37]. Oscillatory writing and erase behavior has been seen in  $\text{LiNbO}_3$  and BSO [31,33].

### 2.5 Microscopic rate equation model of the photorefractive effect

The discussion in this section is intended to provide a theoretical basis for the mathematical form, used throughout this thesis, to represent the index change of photorefractive crystals in response to light. The model of the photorefractive effect presented here is a generalization of previous rate equation models, designed to address two discrepancies with experimental data. A model with a

statistical mechanics approach is discussed in the next section.

Much theoretical effort has been devoted to understanding the data presented in §2.4 [43-51]. The Kukhtarev model [39] agrees well with some measurements made on BSO in steady state, above the saturation intensity [32]. There are two regimes in which discrepancies are present:

- i. Transient measurements disclose the existence of multiple time constants [52-54], while the Kukhtarev model predicts only one.
- ii. Steady state measurements of the space charge field disclose a dependence on absolute intensity below  $600\mu\text{W}/\text{cm}^2$  (Fig. 2.5), which is also not expected from the Kukhtarev model. The particular value of  $600\mu\text{W}/\text{cm}^2$  is an anomaly because the relation between conductivity and intensity, in BSO, is linear except below  $20\text{nW}/\text{cm}^2$  (where the thermal excitation into the conduction band becomes comparable to the optical excitation) and above  $1\text{kW}/\text{cm}^2$  (where the population of the conduction band becomes comparable to the concentration of absorption centers and saturation occurs.)

The intensity saturation at  $600\mu\text{W}/\text{cm}^2$  has been attributed to a complete filling of the less numerous of the two types of traps in BSO, the luminescent centers [30]. According to this explanation, below  $I_{\text{sat}}$  the space charge has contributions from both types of sites, and above  $I_{\text{sat}}$  there is a contribution only from the partially full site. All models of the photorefractive effect to date, in BSO as well as other materials, have considered just one photoactive species (see Ref. 55). The second site is taken to be completely occupied and therefore not participating. The generalization to two photoactive species followed from the hypothesis that i) the second time constant and ii) the intensity saturation could be due to the presence of a second site with different dynamics.

In BSO, the silicon vacancy sites are called donors and the luminescent centers are called acceptors.\* The concentration  $N_D$  includes all sites within the donor

---

\* This terminology can be confusing, especially because the (unoccupied) acceptor states are located closer to the conduction band than the valence band, and the donor states are closer to the valence

band, and we assume that a single absorption cross-section adequately describes the distribution of slightly different sites. We separate  $N_D$  into those sites that are occupied by an electron,  $N_D^\beta(\mathbf{r},t)$  and those that are ionized  $N_D^\dagger(\mathbf{r},t)$ , such that  $N_D = N_D^\beta + N_D^\dagger$ . We separate the acceptor concentration  $N_A$  into those sites that are occupied by an electron,  $N_A^-(\mathbf{r},t)$  and those that are not  $N_A^0(\mathbf{r},t)$ , such that  $N_A = N_A^- + N_A^0$  (Fig. 2.7). The ionization and deionization of the donors is governed by the rate equation

$$\frac{\partial N_D^\dagger}{\partial t} = \alpha_D I (N_D - N_D^\dagger) - \gamma_D n N_D^\dagger \quad (1)$$

where  $\alpha_D$  is the absorption cross-section divided by the photon energy. The recombination coefficient,  $\gamma_D$ , is the cross-section for collisional recombination times the rms thermal velocity of the conduction band electrons.\*\* We assume that the absorption is not limited by availability of states in the conduction band, so that the transition rate is proportional only to the donor concentration. We also limit our consideration to linear recombination.†

The ionization and deionization of the acceptors is governed by the rate equa-

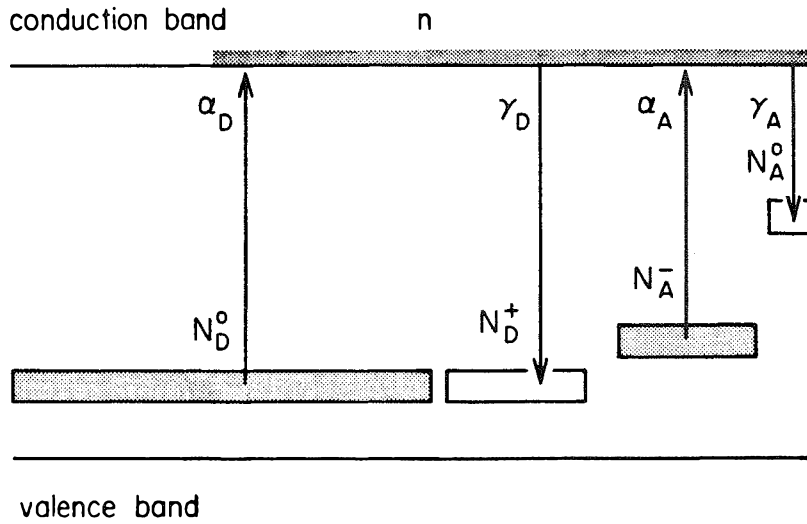
band, in contrast to the situation in doped semiconductors. The terminology for photorefractive crystals arises from a scenario in which every lattice site is neutral initially. Studies of the structure of the defects in BSO indicate that, in this configuration, the Si vacancies are occupied by an electron and the luminescent centers are empty. If charge exchange is to take place, the transfer must be from Si vacancies to luminescent centers, hence the donor/acceptor terminology. However, it is not known whether photorefractive crystals ever assume a form in which every unit cell is neutral. One could just as well ask, "If the crystal is illuminated, allowing the electrons to redistribute, where is an electron most likely to reside?" Based solely on the overwhelming numbers of Si vacancies, one might expect the average electron to reside there, so perhaps in this situation it would be appropriate to call them the acceptors. This suggests a third test on which to base the terminology: if there were an equal number of Si vacancies and luminescent centers in an illuminated crystal, in which trap would the average electron spend the most time? The answer to this question is also not known, but if it were we would be justified in calling that trap the acceptor. We prefer to say that that trap is *more electronegative*, to borrow a term from chemistry. One must remember that trap occupancy is probabilistic and the equilibrium is dynamic with both types of traps accepting and donating electrons to and from the conduction band, through photoexcitation and recombination.

\*\* If we wanted to extend the model to light levels below 20nW/cm<sup>2</sup>, we could add a term to include thermal ionization. The presence of a spatially uniform thermal excitation appears as an effective decrease in the spatial variation of light [56]. The presence of a spatially varying thermal excitation could conceivably contribute to the photorefractive effect, if the thermal conductivity of the crystal were such that localized heating could be maintained.

† If the conductivity were due to holes, we would consider transitions from the valence band to the empty donors. The equations would take an identical form,

$$\frac{\partial N_D^\beta}{\partial t} = \alpha_D' I (N_D - N_D^\beta) - \gamma_D' h N_D^\beta \quad ,$$

where now  $\alpha_D'$  and  $\gamma_D'$  refer to transitions between the donors and the valence band, and  $h$  is the concentration of holes in the valence band.



**Figure 2.7.** Electron trap concentrations and migration paths in BSO. All the symbols are defined in the text. The horizontal widths of the bands are proportional to the log of the concentrations in the special case  $\frac{\alpha_A}{\gamma_A} = \frac{\alpha_D}{\gamma_D}$ .

tion

$$\frac{\partial N_A^0}{\partial t} = \alpha_A I (N_A - N_A^0) - \gamma_A n N_A^0 \quad (2)$$

The current in the conduction band consists of a drift component due to an electric field, and a diffusion component:

$$\mathbf{J} = \mu e n \mathbf{E} + k_B T \mu \nabla n \quad (3)$$

where  $\mu$  is the electron mobility,  $e$  is the electronic charge,  $k_B$  is Boltzman's constant, and  $T$  is the temperature.† The charge and current are related by the continuity equation

† The pyroelectric effect and the bulk photovoltaic effect can contribute to the current in some ferroelectrics. The latter has given rise to an open circuit saturation field of  $10^5 \text{V/cm}$  in Fe doped  $\text{LiNbO}_3$  [57], but none has been observed in BSO.

$$\nabla \cdot \mathbf{J} = -\frac{\partial \rho}{\partial t} = -e \frac{\partial}{\partial t} (N_D^+ - N_A^- - n) \quad (4)$$

Since the crystal as a whole is neutral, we require that the spatial average of the charge density be 0, *i.e.*,

$$\langle \rho \rangle = \langle N_D^+ - N_A^- - n \rangle = 0$$

The charge and the quasi-static electric field are related by Poisson's equation

$$\nabla \cdot \mathbf{E} = \frac{\rho}{\epsilon} = \frac{e(N_D^+ - N_A^- - n)}{\epsilon} \quad (5)$$

where  $\epsilon$  is the dc dielectric constant.

The experimental geometry is shown in Fig. 2.1. The z direction is normal to the crystal face and the x direction is parallel to the face and perpendicular to the fringes. The simplest hologram is a grating formed by the interference of two plane waves

$$I(x) = I_0 + I_1 e^{ikx} + I_1^* e^{-ikx} \quad (6)$$

We are interested in volume holograms but first we consider a slab  $dz$  of photorefractive crystal thin enough so that the intensity throughout is equal to that at the entrance face, *i.e.* known throughout. Later, in Chapters 3 and 4, we will consider the effect of the crystal on the light. We are able to separate the problem in this manner when the variations of the unknown quantities ( $I$ ,  $N_D^+$ ,  $N_A^-$ ,  $n$ ,  $E$ ) are sufficiently different in the directions along and across the fringes.

Since our main interest is volume holograms, in which scattering is confined to Bragg angles, we only consider the fundamental spatial Fourier component in the unknowns  $N_A^-$ ,  $N_D^+$ ,  $n$ , and  $E$ .<sup>\*</sup> Therefore, we take

---

<sup>\*</sup> In actuality, the crystal response includes spatial harmonic generation. However, the two writing (and reading) beams are at Bragg incidence only for a grating with wavevector  $\pm \mathbf{k} = \mathbf{k}_1 - \mathbf{k}_2$ . Our result for the fundamental component differs by little from the result obtained after solving for all the components [39]. Higher components are easily observed in our laboratory by adjusting the angle of incidence of the reading beam. They have been put to good use in image processing as well [58]. Their presence doesn't seem to affect the fundamental grating, for low modulation index  $m = |I_1|/I_0$ , even though the space charge to write higher harmonics must be drawn from the same pool.

$$N_A^0(x,t) = A_0(t) + A_1(t)e^{ikx} + A_1^*(t)e^{-ikx} \quad (7a)$$

$$N_D^{\pm}(x,t) = D_0(t) + D_1(t)e^{ikx} + D_1^*(t)e^{-ikx} \quad (7b)$$

$$n(x,t) = n_0(t) + n_1(t)e^{ikx} + n_1^*(t)e^{-ikx} \quad (7c)$$

$$E(x,t) = E_0(t) + E_1(t)e^{ikx} + E_1^*(t)e^{-ikx} \quad (7d)$$

where the direct (as opposed to alternating) components are spatial averages, *i.e.*,  $A_0(t) = \langle N_A^0(x,t) \rangle$ , *etc.* We have implicitly assumed here that the density of holes ( $A_0$  and  $D_0$ ) is sufficient to resolve the intensity fringes. The only quantity that is known *a priori* is the direct part of the static electric field,  $E_0$ , which can be supplied externally.

*2.5.1 Steady state behavior.* Substituting (6) and (7) into Eqns. 1-5, we obtain, in steady state, seven algebraic equations in seven unknowns. In the small signal approximation, we assume a low modulation index on  $I$ ,  $N_A^0$ ,  $N_D^{\pm}$ , and  $n$ , so that

$$I_1 A_1^* \ll I_0 A_0, \quad n_1 A_1^* \ll n_0 A_0, \quad \text{etc.}$$

In this limit, the direct quantities are related by

$$\frac{\alpha_A \langle N_A^- \rangle}{\gamma_A \langle N_A^0 \rangle} = \frac{\alpha_D \langle N_D^0 \rangle}{\gamma_D \langle N_D^+ \rangle} = \frac{n_0}{I_0} \quad (9)$$

Thus,  $\gamma/\alpha$  can be viewed as a measure of the *electronegativity* of a trap. For a fixed ratio  $n_0/I_0$ , as  $\gamma_A/\alpha_A$  increases,  $\langle N_A^- \rangle/\langle N_A^0 \rangle$  must increase. That is, as the electronegativity of acceptors increases, the probability of acceptor states being occupied increases.

In terms of the intensity and material parameters only, the steady state value of  $D_0$  is given by the cubic equation

$$0 = D_0 - N_A + \frac{\gamma_D D_0 \alpha_A N_A}{\gamma_A \alpha_D (N_D - D_0) + \gamma_D \alpha_A D_0} - \frac{\alpha_D I_0 (N_D - D_0)}{\gamma_D D_0} \quad (10)$$

This equation, and the equation for  $A_0$ , determine the participation of the two sites. The steady state electric field containing the contributions of the charge densities  $A_1$ ,  $D_1$ , and  $n_1$ , is given by

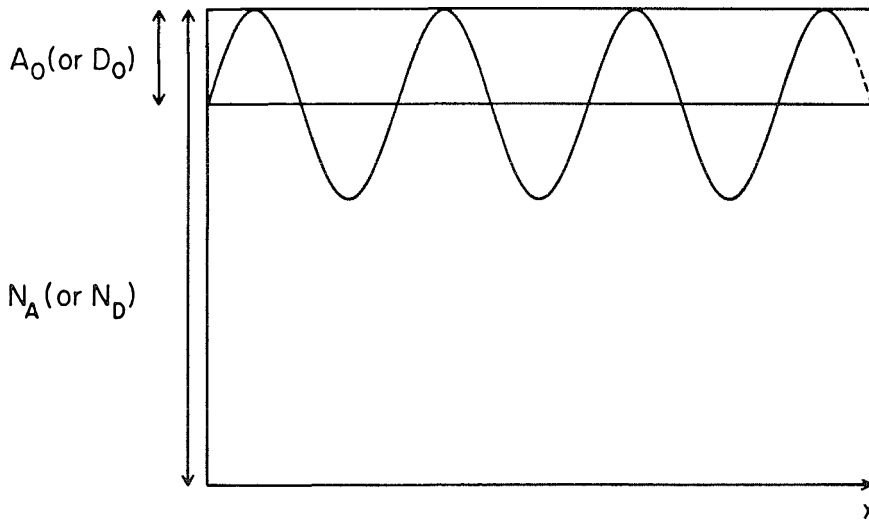
$$E_1 = -i \frac{I_1}{I_0} \frac{E_N(E_0 + iE_f)}{E_0 + i(E_f + E_n + E_N)} \quad (11)$$

This is the field which modulates the index of refraction through the electrooptic effect. The form of (11) motivates the expression for the index of refraction which is used in the remaining chapters (see §3.3). The characteristic fields are defined as follows:

$$E_N \equiv E_D \frac{N_D - D_0}{N_D} + E_A \frac{N_A - A_0}{N_A} \quad E_A \equiv \frac{eA_0}{\epsilon k} \quad E_D \equiv \frac{eD_0}{\epsilon k}$$

$$E_f \equiv \frac{k_B T k}{e} \quad E_n \equiv \frac{e n_0}{\epsilon k}$$

$E_A$ , for example, is the maximum space charge field that could be created with the acceptor sites (Fig. 2.8). Aside from a factor of  $2\pi$ , it corresponds to the field created by a complete charge separation, to a distance equal to one fringe spacing.



**Figure 2.8.** The occupation of the acceptors (and donors) varies periodically, creating a space charge grating.

$E_f$  is the diffusion field, in the sense that diffusion alone will create a space charge



field equal in magnitude (not phase) to that created by an external field  $E_r$ , in the absence of diffusion.

There is implicit intensity dependence in  $n_0$ ,  $A_0$ , and  $D_0$ , hence also in  $E_n$ ,  $E_A$ , and  $E_D$ , so the intensity dependence of the entire expression (11) appears to be quite complicated.\* The intensity dependence is typically less complicated, as shown in §2.5.3.

In view of the way the donors and acceptors contribute to the field in a like fashion, the more general model cannot be excluded on the basis of the data [32] which supports the Kukhtarev model [39].

*2.5.2 Transient behavior.* The first step in the temporal development of holographic recording is for the incident light to excite a population of electrons from both types of traps into the conduction band. We can expect a sudden change in the direct and alternating components of the concentrations of all three species. The electrons in the conduction band ferry charge to and from the acceptor and donor sites, gradually shifting charge from the regions of high intensity to the regions of low intensity, perhaps over many cycles of excitation and recombination. So, we also expect comparatively slow time dependence in  $A_1$  and  $D_1$ . It is these charges, not  $n_1$  that constitute the major part of the space charge density in steady state. As the electrons in the conduction band begin to see the field due to the trapped charge, we expect to see more slow changes in  $n_1$  as well.\*\*

We will consider a step function illumination, with turn-on at  $t=0$ . The time dependent solution requires a second approximation in addition to the small signal approximation. In many situations, the photocurrent has a risetime much shorter than the hologram writing time. The large difference in the time scales allows us to simplify the problem by taking  $n_0$  to be its steady state value for the entire duration of space charge buildup. This is done at the cost of accurate

- 
- \* If  $E_0$  were supplied by a current source, as opposed to a voltage source, an even more complicated intensity dependence could be easily obtained through the photoconductivity.
  - \*\* This feedback is considered to be important in the latter stages of hologram formation [41,46], but can be neglected in the initial stages [47,59]. Mathematically, this would mean the space charge contribution to the electric field in Eqn. 3 could be dropped.

knowledge about the field during times comparable to the risetime of  $n_0$ . No time dependence on this time scale may be extracted from the equations that follow from this approximation.

The steady state value of  $n_0$  depends on  $A_0$  and  $D_0$  which are also taken to have their steady state values, but for a different reason. They are assumed to have reached their equilibrium ratio as a result of prior illumination, either coherent or incoherent. Indeed, a special procedure would be required to bring the ratio of  $A_0$  to  $D_0$  out of equilibrium. Equation (9) is exact for  $I_1 = 0$ , so the relative values of  $A_0$  and  $D_0$  are independent of  $I_0$ . Their absolute values have only a very small intensity dependence through Eqn. 10.

The rate equations for the three populations become three simultaneous linear ordinary differential equations.

$$\dot{A}_1 = \alpha_A [I_1 (N_A - A_0) - I_0 A_1] - \gamma_A [n_1 A_0 + n_0 A_1] \quad (12)$$

$$\dot{D}_1 = \alpha_D [I_1 (N_D - D_0) - I_0 D_1] - \gamma_D [n_1 D_0 + n_0 D_1]$$

$$\dot{A}_1 + \dot{D}_1 - \dot{n}_1 = -\mu e \left[ \frac{en_0}{\epsilon} (D_1 + A_1 - n_1) + ik n_1 E_0 \right] + k_B T \mu k^2 n_1$$

which may be solved by the Laplace transform technique. At this point we can identify some characteristic rates.‡

$$\nu_A \equiv \alpha_A I_0 + \gamma_A n_0 = \frac{\alpha_A I_0 N_A}{A_0} \quad \nu_a \equiv \gamma_A A_0 \quad \frac{\Lambda}{(N_A - A_0)} \equiv \alpha_A I_1$$

$$\nu_D \equiv \alpha_D I_0 + \gamma_D n_0 = \frac{\alpha_D I_0 N_D}{D_0} \quad \nu_d \equiv \gamma_D D_0 \quad \frac{\Lambda}{(N_D - D_0)} \equiv \alpha_D I_1$$

‡ The characteristic rates and fields are related, for example, by

$$E_A \frac{N_A - A_0}{N_A} = \frac{e}{\epsilon k} \frac{I_0}{I_1} \frac{\Lambda}{\nu_A} = \frac{1}{\mu k} \frac{\nu_a \nu_n}{\nu_A}$$

$$\nu_n \equiv \frac{\mu n_0 e}{\epsilon} = \mu k E_n \quad \nu_f \equiv \frac{k_B T \mu k^2}{e} = \mu k E_f \quad \nu_E \equiv \mu k E_0$$

$\nu_n$  is the ratio of the photogenerated conductivity to the dielectric constant which constitutes the inverse of the RC time constant for the material at the given level of illumination. In terms of these rates, the transform of the electric field is given by

$$\left[ s^3 + \nu_2 s^2 + \nu_1^2 s + \nu_0^3 \right] ik \frac{\epsilon}{e} E_1(s) = (A_1(0) + \frac{\Lambda}{s}) \nu_G(s + \nu_D) + (D_1(0) + \frac{\Delta}{s}) \nu_G(s + \nu_A) \quad (13)$$

$$+ ik \frac{\epsilon}{e} E_1(0) \left[ s^2 + s(\nu_A + \nu_a + \nu_D + \nu_d) + \nu_A \nu_D + \nu_a \nu_D + \nu_A \nu_d \right]$$

where  $\nu_2 \equiv \nu_A + \nu_a + \nu_D + \nu_d + \nu_n + \nu_f - i\nu_E$

$$\nu_1^2 \equiv (\nu_f - i\nu_E)(\nu_A + \nu_D) + \nu_A \nu_D + \nu_a \nu_D + \nu_A \nu_d + \nu_n(\nu_A + \nu_a + \nu_D + \nu_d)$$

$$\nu_0^3 \equiv \nu_n(\nu_A \nu_D + \nu_a \nu_D + \nu_A \nu_d) + \nu_A \nu_D (\nu_f - i\nu_E)$$

$\nu_f$  and  $\nu_E$  always appear in the combination  $\nu_f - i\nu_E \equiv \nu_G$ . It is clear from the left side of (13) that consideration of a second photoactive species has generalized the transient behavior to that of multiple time constants.

*2.5.3 Application to bismuth silicon oxide.* Eqn. 9 is relevant to hypothesis (ii). Since  $n_0/I_0$  is independent of  $I_0$  from  $20\text{nW/cm}^2$  to  $1\text{kW/cm}^2$ , the ratio  $\langle N_A^- \rangle / \langle N_A^0 \rangle$  must be constant. Before even computing the values of  $N_A^0$  or  $N_A^-$ , we can conclude that they are independent of  $I_0$ , within this region, because their sum is fixed (see text preceding Eqn. 1). Thus, no change in the occupancy of the acceptors is indicated at  $600\mu\text{W/cm}^2$ , according to this model.

Measurements that have been made on BSO [14] allow one to deduce that

$$N_A = 10^{16} \text{cm}^{-3} \quad N_D = 10^{19} \text{cm}^{-3}$$

$$\alpha_D = \frac{2 \times 10^{-19} \text{cm}^2}{h\nu} = 0.5 \frac{\text{cm}^2}{\text{J}} \quad \gamma_D = 2 \times 10^{-11} \frac{\text{cm}^3}{\text{sec}} \quad \gamma_A = 8 \times 10^{-11} \frac{\text{cm}^3}{\text{sec}}$$

Using a hypothetical value of  $\alpha_A = 2 \frac{\text{cm}^2}{\text{J}}$ , which gives equal electronegativities, we obtain trap occupations which are very nearly independent of  $I_0$ :

$$A_0 = 10^{13} \text{cm}^{-3} \quad D_0 = 10^{16} \text{cm}^{-3}$$

Thus 99.9% the acceptors are filled and 99.9% of the donors remain filled with electrons. Choosing a value of  $I_0 = 0.1 \text{W/cm}^2$ , we obtain

$$n_0 = 5 \times 10^{12} \text{cm}^{-3}$$

Given a dielectric constant of  $\epsilon = 56 \epsilon_0$ , and experimental parameters of  $\Lambda = 1 \mu\text{m}$ ,  $T = 300^\circ\text{K}$ , the characteristic fields take on the values:

$$E_N = 5 \frac{\text{kV}}{\text{cm}} \quad E_A = 5 \frac{\text{V}}{\text{cm}} \quad E_D = 5 \frac{\text{kV}}{\text{cm}}$$

$$E_f = 1.6 \frac{\text{kV}}{\text{cm}} \quad E_r = 2.5 \frac{\text{V}}{\text{cm}}$$

It is then apparent that  $E_1$  has a simpler intensity dependence than shown by (11). Since  $D_0 \ll N_D$ ,  $A_0 \ll N_A$ , and also  $n_0 \ll N_A$  for intensities  $\ll 1 \text{kW/cm}^2$ , we have

$$E_N = E_D \frac{N_D - D_0}{N_D} + E_A \frac{N_A - A_0}{N_A} \approx E_D + E_A = \frac{e}{\epsilon k} (D_0 + A_0) = \frac{e}{\epsilon k} (N_A + n_0) \approx \frac{e N_A}{\epsilon k}$$

which is a material constant independent of intensity. So, the major steady state intensity dependence of the space charge field, and hence the index of refraction variation, is seen to be  $E_1 \propto I_1 / I_0$ , in agreement with experimental results [31].

Concerning the assumption that  $n_0$  reaches its steady state value much faster than  $E_1$ , we note that the risetime of the photocurrent in BSO is 0.4 msec [14], and hologram formation at  $0.1 \text{W/cm}^2$  takes approximately 10 msec [33,60] Using the aforementioned experimental and hypothetical parameters, and the additional

information that  $\mu = 0.03 \text{ cm}^2/\text{Vsec}$ , we obtain

$$\begin{array}{lll} \nu_A = 200\text{Hz} & \nu_a = 800\text{Hz} & \nu_n = 4.8\text{kHz} \\ \nu_D = 50\text{Hz} & \nu_d = 0.2\text{MHz} & \nu_f = 3\text{MHz} \\ \nu_2 = 3\text{MHz} & \nu_1 = 40\text{kHz} & \nu_0 = 5\text{kHz} \end{array}$$

The existence of three time constants is evident from (13), but experimentally two dominant time constants have been observed. In view of the large values of  $\nu_d$  and  $\nu_f$ , possibly  $\nu_E$ , and measurements of hologram risetimes on the order of 10 msec [33,60], we expect the cubic term to be much less than the quadratic term [55]. In this case, there will be two dominant time constants, and the solution will be given by

$$ik \frac{\varepsilon}{e} E_1(t) = \frac{\nu_G(\nu_D \Lambda + \nu_A \Delta)}{\nu_0^3} \left( 1 + A_+ e^{-\frac{t}{\tau_+}} + A_- e^{-\frac{t}{\tau_-}} \right) \quad (14)$$

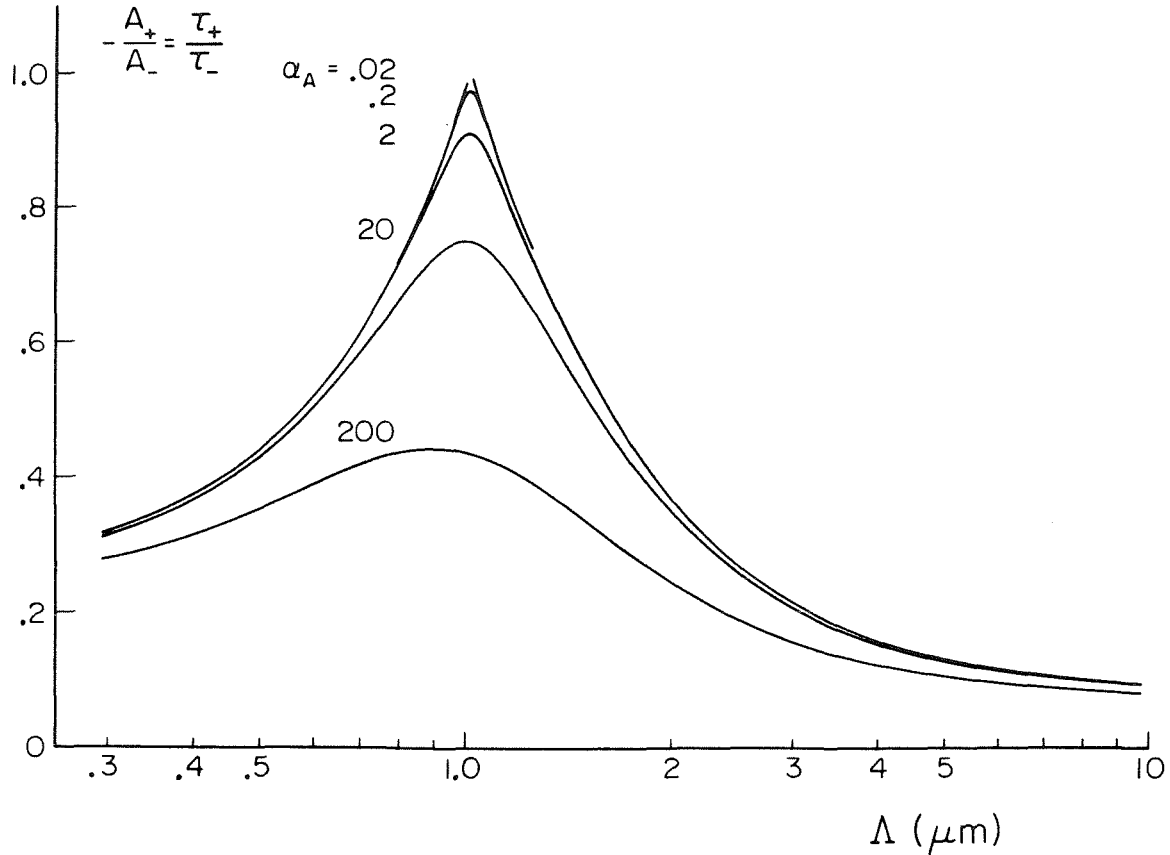
where

$$A_{\pm} \equiv \pm \frac{1}{2} \left( \frac{\nu_1^2}{\sqrt{\nu_1^4 - 4\nu_2\nu_0^3}} \mp 1 \right) \quad \text{and} \quad \frac{1}{\tau_{\pm}} \equiv \frac{\nu_1^2 \pm \sqrt{\nu_1^4 - 4\nu_2\nu_0^3}}{2\nu_2} \quad (15)$$

Using the above parameters, we obtain

$$A_+ = 10 \quad A_- = -11 \quad \tau_+ = 4.8\text{msec} \quad \tau_- = 5.3\text{msec}$$

The ratio  $-A_+/A_- = \tau_+/\tau_-$  is plotted versus fringe spacing for several values of the unknown  $\alpha_A$  in Fig. 2.9. Two time constant behavior should be observed when two conditions are met: 1)  $A_+$  and  $A_-$  are comparable in size, and 2)  $\tau_+$  and  $\tau_-$  are not. The conclusion concerning hypothesis (i) is that the second photoactive species is a possible source of the multiple time constant behavior, for a range of values for  $\alpha_A$  and  $\Lambda$ . At  $\Lambda = 1\mu\text{m}$ , one can see that a) as  $\alpha_A$  decreases (the acceptor states fill with electrons),  $\tau_+$  approaches  $\tau_-$  and the multiple time constant behavior disappears; b) as  $\alpha_A$  increases (the acceptor states become more empty),  $|A_+|$  becomes



**Figure 2.9.** Ratios  $\tau_+/\tau_-$  and  $A_+/A_-$  as a function of the grating period  $\Lambda$ . The parameters used are given in the text. Several hypothetical values of  $\alpha_A$  are used.

much less than  $|A_-|$ , and the multiple time constant behavior disappears again. Experimental work is currently in progress to check the variation of the two time constants with applied field, and grating spacing.

In the event of full traps,  $A_0=0$ ,  $D_0 = N_A+n_0 = N_A$ , and the time dependence simplifies to:

$$\tau = \frac{\nu_D + \nu_d + \nu_n + \nu_f - i\nu_E}{\nu_n\nu_d + \nu_D(\nu_n + \nu_f - i\nu_E)} = \frac{1}{\nu_D} \frac{\frac{\nu_D}{\mu k} + \frac{\nu_d}{\mu k} + E_n + E_f - iE_0}{E_n + E_n + E_f - iE_0} \quad (16)$$

### 2.6 Statistical mechanics model of the photorefractive effect

In the previous section we saw how the rate equation model was stated and how

two approximations were necessary to obtain a solution. An alternative model has been developed by others, which incorporates the same approximations from the beginning, and, not surprisingly, arrives at the same steady state result [35]. The purpose of this section is to introduce the statistical mechanics model, and compare it with the rate equation model.

Recall that

- i. Much of the analysis in the literature treats just one photoactive species.
- ii. Another approximation that is commonly made is to ignore the contribution of the conduction band electrons to the space charge field, *i.e.* ignore their direct contribution but maintain their indirect contribution of allowing a redistribution of trapped charges to take place, in the absence of any tunneling.
- iii. The average concentrations of all species are frequently assumed to reach their steady state values in the early stages of hologram formation.

Accordingly, the hopping model permits a *fixed* concentration of charges,  $N_C$ , to occupy a much larger concentration of identical sites,  $N_S$ , in any of a large number of permutations [35]. Charges reside only in the states within the energy gap, not in the conduction band. In the dark, each charge is immobilized at a site, but when exposed to light it becomes mobile.

Under uniform illumination, the relative probability of two sites  $m$  and  $n$  being occupied is given by statistical mechanics:

$$\frac{W_m}{W_n} = \exp \frac{q(\varphi_n - \varphi_m)}{k_B T}$$

where  $T$  is the lattice temperature, and  $q$  is the charge of the carrier.  $\varphi_n$  is the quasi static potential at site  $n$  due to externally applied fields, to intrinsic chemical potentials *e.g.* the bulk photovoltaic effect, and includes the space charge field itself under conditions of non-uniform illumination. This steady state form is

contrived by choosing the following form for the hopping rate, from site m to n, proportional to

$$\exp \frac{q(\varphi_{nm})}{2k_B T} \quad (17)$$

A spatially varying light intensity causes a rearrangement of this distribution if the tendency to hop from site m is proportional to  $I_m$ . Thus changes in the occupancy of site n depend on the rate of hopping into n from all other sites m and the rate of hopping out of n into any other site:\*

$$\frac{dW_n}{dt} = - \sum_m D_{mn} \left[ W_n I_n \exp \frac{q\varphi_{nm}}{2k_B T} - W_m I_m \exp \frac{q\varphi_{mn}}{2k_B T} \right] \quad (18)$$

As before, variables W and  $\varphi$  are taken to have the form

$$W_n = W_0 + W_1 e^{ikx_n} + W_1^* e^{-ikx_n}$$

$$\varphi_n = \varphi_0 + \varphi_1 e^{ikx_n} + \varphi_1^* e^{-ikx_n}$$

Substituting these expressions into (18), using Poisson's equation, and using the characteristic fields defined in §2.5.1, yields the following:†

$$E_1 = -i D I_0 (k_0 l)^2 \left\{ E_1 \frac{(E_0 - i(E_f + E_N))}{E_N} - i \frac{I_1}{I_0} (E_0 - iE_f) \right\} \quad (19)$$

where D is the adjustable nearest neighbor hopping parameter in the theory. The steady state field amplitude and the time constant are:

$$E_1(\infty) = -i \frac{I_1}{I_0} \frac{E_N (E_0 + iE_f)}{E_0 + i(E_f + E_N)} \quad \tau = \frac{k_B T (N_S)^{2/3}}{D I_0 \varepsilon k (-E_N - E_f + iE_0)} \quad (20)$$

The steady state field agrees well with the rate equation model (11). The equivalent of  $E_n$  does not appear because holes in the valence band are ignored.

\* Factors of 1-W could be added to account for the probability of the final state being unoccupied. The experimental results are actually consistent with leaving out those terms, because the probability is very close to 1. This is equivalent to having  $(N_D - D_0)/N_D = 1$  in §2.5. The experimental results are also consistent with ignoring all hops except between nearest neighbors.

† Now,  $E_f = -\frac{k_B T k}{e}$ , and  $E_N = -\frac{e N_C}{\varepsilon k}$ , because the charge carriers in BaTiO<sub>3</sub> are holes.



The parameter D is unknown, so one cannot compare expression (20) for the time constant with the rate equation result (16) except to say that one could solve for D in terms of the characteristic fields by equating the two results.

### References for Chapter 2

1. A. Ashkin, G.D. Boyd, J.M. Dziedzic, R.G. Smith, A.A. Ballman, J.J. Levinstein & K. Nassau, *Appl. Phys. Lett.* **9**, 72 (1966).
2. F.S. Chen, J.T. LaMacchia & D.B. Fraser, *Appl. Phys. Lett.* **13**, 223 (1968).
3. F.S. Chen, *J. Appl. Phys.* **40**, 3389 (1969).
4. A. Yariv, *Opt. Comm.* **25**, 23 (1978).
5. I.K. Lam, T.Y. Chang, J. Feinberg & R.W. Hellwarth, *Opt. Lett.* **6**, 475 (1981).
6. R. Orlovski and E. Kratzig, *Solid State Comm.* **27**, 1351 (1978).
7. H.J. Eichler, J. Eichler, J. Knof, Ch. Noack, *Phys. Stat. Solidi* **52**, 481 (1979).
8. D.S. Hamilton, D. Heiman, J. Feinberg & R.W. Hellwarth, *Opt. Lett.* **4**, 124 (1979).
9. C.M. Lawson, R.C. Powell, W.K. Zwicker, *Phys. Rev. Lett.* **46**, 1020 (1981).
10. J.R. Salcedo, A.E. Siegman, D.D. Dlott & M.D. Fayer, *Phys. Rev. Lett.* **41**, 131 (1978).
11. D.L. Staebler, W.J. Burke, W. Phillips & J.J. Amodei, *Appl. Phys. Lett.* **26**, 182 (1975).
12. F.S. Chen, *J. Appl. Phys.* **38**, 3418 (1967).
13. J.J. Amodei, *RCA Review* **32**, 185 (1971).
14. S.L. Hou, R.B. Lauer & R.E. Aldrich, *J. Appl. Phys.* **44**, 2652 (1973).
15. G.E. Peterson, A.M. Glass & T.J. Negran, *Appl. Phys. Lett.* **19**, 130 (1971).
16. K.O. Hill, *Appl. Opt.* **10**, 1695 (1971).

17. J.P. Woerdman, *Opt. Comm.* **2**, 212 (1970).
18. E.V. Ivakin, I.P. Petrovich & A.S. Rubanov, *Sov. J. Quant. Elect.* **3**, 52 (1973).
19. S.M. Jensen and R.W. Hellwarth, *Appl. Phys. Lett.* **32**, 166 (1978).
20. I.C. Khoo, *Phys. Rev. A* **23**, 2077 (1981).
21. M.E. Lines and A.M. Glass, *Principles and Applications of Ferroelectrics and Related Materials*, (Clarendon Press, Oxford, 1977).
22. M.D. Domenico, Jr. and S.H. Wemple, *J. Appl. Phys.* **40**, 720 (1969). and p. 735.
23. A.J. Fox, *J. Appl. Phys.* **44**, 254 (1973).
24. W.B. Yelon, W. Cochran, G. Shirane & A. Linz, *Ferroelectrics* **2**, 261 (1971).
25. Landolt-Bornstein, *Numerical Data and Functional Relationships in Science and Technology*, New Series, ed. by K.H. Hellwege (Springer-Verlag, Berlin, 1979) Vol. 11.
26. K. Megumi, H. Kozuka, M. Kobayashi & Y. Furuhata, *Appl. Phys. Lett.* **30**, 631 (1977).
27. B. Fischer, M. Cronin-Golomb, J.O. White, A. Yariv & R. Neurgaonkar, *Appl. Phys. Lett.* **40**, 863 (1982).
28. P.N. Gunter, *Opt. Lett.* **7**, 10 (1982).
29. Y.H. Ja, *Opt. Quant. Elect.* **14**, 363 (1982).
30. J.P. Huignard and F. Micheron, *Appl. Phys. Lett.* **29**, 591 (1976).
31. J.P. Huignard, J.P. Herriau, P. Auborg, & E. Spitz, *Opt. Lett.* **4**, 21 (1979).
32. J.P. Huignard, J.P. Herriau, G. Rivet & P. Gunter, *Opt. Lett.* **5**, 102 (1980).
33. A. Marrakchi, J.P. Huignard & P. Gunter, *Appl. Phys.* **24**, 131 (1981).
34. R.L. Townsend and J.T. LaMacchia, *J. Appl. Phys.* **41**, 5188 (1970).
35. J. Feinberg, D. Heiman, A.R. Tanguay, Jr., & R.W. Hellwarth, *J. Appl. Phys.* **51**, 1297 (1980).

36. A. Krumins and P. Gunter, *Appl. Phys.* **19**, 153 (1979).
37. P. Gunter and F. Micheron, *Ferroelectrics* **18**, 27 (1978).
38. R. Orlowski, E. Kratzig & H. Kurz, *Opt. Comm.* **20**, 171 (1977).
39. N.V. Kukhtarev, V.B. Markov, S.G. Odulov, M.S. Soskin & V.L. Vinetskii, *Ferroelectrics* **22**, 949 (1979).
40. N.V. Kukhtarev, V.B. Markov, S.G. Odulov, M.S. Soskin & V.L. Vinetskii, *Ferroelectrics* **22**, 961 (1979).
41. G.A. Alphonse, R.C. Alig, D.L. Staebler & W. Phillips, *RCA Review* **36**, 213 (1975).
42. Y.H. Ja, *Opt. Comm.* **41**, 159 (1982).
43. Y. Ninomiya, *J. Opt. Soc. of Am.* **63**, 1124 (1973).
44. L. Young, W.K.Y. Wong, M.L.W. Thewalt & W.D. Cornish, *Appl. Phys. Lett.* **24**, 264 (1974).
45. D.M. Kim, R.R. Shah, T.A. Rabson & F.K. Tittel, *Appl. Phys. Lett.* **28**, 338 (1975).
46. S.F. Su and T.K. Gaylord, *J. Appl. Phys.* **46**, 5208 (1975).
47. R. Magnusson and T.K. Gaylord, *J. Appl. Phys.* **47**, 190 (1976).
48. M.G. Moharam and L. Young, *J. Appl. Phys.* **48**, 3230 (1977).
49. B.I. Sturman, *Sov. Phys. Tech. Phys.* **23**, 589 (1978).
50. M.G. Moharam, T.K. Gaylord, R. Magnusson & L. Young, *J. Appl. Phys.* **50**, 5642 (1979).
51. V.L. Vinetskii and N.V. Kukhtarev, *Sov. Phys. Solid State* **16**, 2414 (1975).
52. R.A. Mullen and R.W. Hellwarth, *CLEO '83 Technical Digest*, p. 174 (1983).
53. M.B. Klein, unpublished results.
54. M. Cronin-Golomb & J.O. White, unpublished results.
55. Most of §2.5.2 and part of §2.5.3 were completed when a very similar treatment was published elsewhere. G.C. Valley, *Appl. Opt.* **22**, 3161 (1983). The

differences are that, in Valley's treatment, grating erasure was considered instead of writing, so the steady state field was not analyzed, and the effect of an applied field was not considered. Acknowledgement is also gratefully made for subsequent discussions with G. Valley.

56. M.G. Moharam and L. Young, J. Appl. Phys. **47**, 4048 (1976).
57. A.M. Glass, D. von der Linde & T.J. Negran, Appl. Phys. Lett. **25**, 233 (1974).
58. M.P. Petrov, S.V. Miridinov, S.I. Stepanov & V.V. Kulikov, Opt. Comm. **31**, 301 (1979).
59. M. Peltier and F. Micheron, J. Appl. Phys. **48**, 3683 (1977).
60. J.P. Huignard and J.P. Herriau, Appl. Opt. **16**, 1807 (1977).
61. P. Gunter, Phys. Rep. **93**, 199 (1982).
62. G. Rakuljic, private communication, 1984.

### 3. TWO-WAVE MIXING

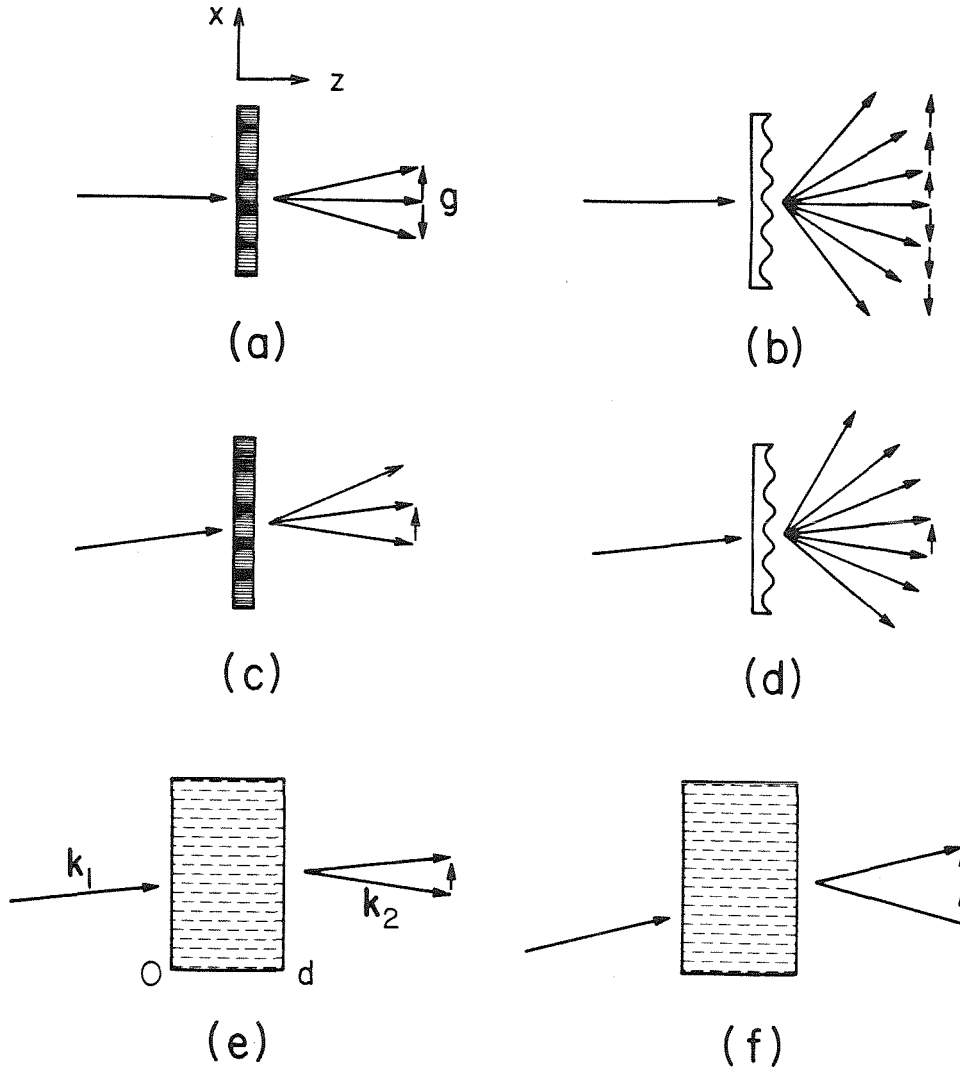
#### 3.1 Introduction

In the previous chapter, the grating formation in photorefractive crystals was explained in terms of nonlinear ordinary differential equations which describe the coupling between the light and the mobile charges within the crystal. A spatially varying intensity was found to cause a redistribution of charge which modulates the index of refraction through the electro-optic effect. The various plane wave components of the incident light are subsequently coupled by the self-induced diffraction. In this chapter, the propagation of light within these crystals is determined by a set of nonlinear ordinary differential equations which describe this coupling.

In the analysis of the previous chapter, the intensity was assumed to be known, *i.e.* equal to the incident intensity, within the thin slice of material that was considered. When the grating thickness is comparable to a fringe spacing, the transmitted field is given simply by the incident field times a multiplicative amplitude to be transmitted,  $t$ , (Fig. 3.1a). The diffracting waves are solutions of the wave equation in a region of simple, *uniform*, index.

If, within the grating, either the exponential absorption constant or the index of refraction is given a sinusoidal modulation, then many diffracted orders appear in accordance with the many Fourier components (Fig. 3.1b). The  $z$  components of the wavevectors need not obey a sum rule, although they may, given the proper angle of incidence (Fig. 3.1c,d). The lack of phase matching in the  $z$  direction isn't important because the medium is infinitesimally thin in the  $z$  direction. The angle of the incident beam is equally unimportant; within the paraxial approximation,  $t$  is independent of the incident angle.

When the wave interaction and diffraction are thus confined to different regions in space, the analysis is quite simple. The diffraction efficiency of thin



**Figure 3.1.** Diffraction from thin and thick gratings.  
a) Thin amplitude grating.  
b) Thin phase or absorption grating.  
c) Phase matching for a thin amplitude grating.  
d) Phase matching for a thin phase or absorption grating.  
e) Zero and first order Bragg diffraction within a thick grating.  
f) Second order Bragg diffraction.

gratings is limited, however, hence the interest in thick gratings.

In a sample of finite (as opposed to infinitesimal) thickness, the nonlinear

interaction and the diffraction occur simultaneously, within the same volume. The wave equation must be solved in a region of *periodic* index variation. The analysis in this chapter is restricted to plane waves in steady state. It is an extension of the coupled wave analysis of thick, fixed hologram gratings, which will be briefly described first.

### 3.2 Coupled wave theory of fixed, thick hologram gratings

In this section, the diffraction of plane waves by thick, fixed, *i.e.* non-erasable gratings is described [1]. Such gratings can be produced in photographic emulsions, dichromated gelatin [2], photopolymer materials [3], and photorefractive crystals that have been fixed after recording [4]. In contrast to thin gratings, for diffraction to occur, the incident beam must be close to Bragg incidence, and only one diffracted beam is radiated (Fig. 3.1e). The transfer of energy into a diffracted component is cumulative in  $z$  only if the diffracted wavevector equals the incident plus the grating vector. Another way of looking at this is that multiple reflections only interfere constructively in certain directions. One can observe higher order reflections, but each order requires illumination at a different angle (Fig. 3.1f).

Propagation inside volume gratings is well described by coupled wave equations derived from the scalar wave equation. As in Chapter two, a grating with only one sinusoidal component is considered. The surfaces of constant index are planes, perhaps tilted with respect to the crystal surface.

$$n = n_0 + \frac{n_1}{2} e^{-i(\mathbf{g}\mathbf{r} + \varphi)} + \frac{n_1}{2} e^{i(\mathbf{g}\mathbf{r} + \varphi)}$$

The optical electric field consists of two fields incident at the Bragg angle whose wavevectors are given by  $\mathbf{k}_1 - \mathbf{k}_2 = \mathbf{g}$ .

$$E(\mathbf{r}) = A_1(z)e^{-i\mathbf{k}_1 \cdot \mathbf{r}} + A_2(z)e^{-i\mathbf{k}_2 \cdot \mathbf{r}}$$

The  $A_i$  are the complex amplitudes representing the envelope of the optical field. The  $z$  dependence of the amplitudes is due to the linear absorption and the coupling caused by the grating. The above expressions are inserted into the scalar wave equation and the terms with equal exponentials are collected in separate equations. The amplitudes are assumed to obey the slowly varying envelope approximation, *i.e.* their second order spatial derivative is neglected in comparison to the optical wavevector times the first derivative. Then, the second order differential equation reduces to the two first order equations:

$$\cos\theta_1 \frac{dA_1}{dz} = -\frac{\alpha}{2} A_1 - i \frac{\pi n_1}{\lambda} e^{-i\varphi} A_2$$

$$\cos\theta_2 \frac{dA_2}{dz} = -\frac{\alpha}{2} A_2 - i \frac{\pi n_1}{\lambda} e^{i\varphi} A_1$$

where  $\theta_i$  is the angle between the  $z$  axis and  $\mathbf{k}_i$ . Separating the amplitudes into a magnitude and phase with the definition  $A_i \equiv \sqrt{I_i} e^{-i\varphi_i}$ , the equations for the intensities can be found.

$$\cos\theta_1 \frac{dI_1}{dz} = -\alpha I_1 + \frac{2\pi n_1}{\lambda} \sqrt{I_1 I_2} \sin(\varphi_1 - \varphi_2 - \varphi) \quad (1a)$$

$$\cos\theta_2 \frac{dI_2}{dz} = -\alpha I_2 - \frac{2\pi n_1}{\lambda} \sqrt{I_1 I_2} \sin(\varphi_1 - \varphi_2 - \varphi) \quad (1b)$$

Note that the phases of  $A_1$  and  $A_2$  appear in the equations, so that at any point in space, if the interference pattern and the grating are out of phase so that  $\varphi_1 - \varphi_2 - \varphi \neq 0$ , the intensities are coupled. This is similar to the case of an electromagnetic field and an oscillating dipole moment, where a temporal phase shift between the two accompanies energy exchange. When the grating is illuminated by a single beam, a complete transfer of energy to the other beam is considered a diffraction efficiency of one. In general the diffraction efficiency is defined to



be:

$$\eta \equiv \left| \frac{\cos\theta_2}{\cos\theta_1} \right| \frac{I_2(l)}{I_1(0)}$$

Notice that if  $|\cos\theta_2| < |\cos\theta_1|$ , then  $I_2(l)$  can be greater than  $I_1(0)$ , where  $I_i = |A_i|^2$  is proportional to the power per unit area perpendicular to  $\mathbf{k}_i$ . Of course for a lossless, passive grating, the flux in the  $z$  direction must be conserved (see (4)). To calculate the diffraction efficiency of a transmission grating, the boundary conditions are  $I_1(0)$  specified, and  $I_2(0)=0$ .

$$\eta = e^{-\alpha d \left( \frac{1}{\cos\theta_1} + \frac{1}{\cos\theta_2} \right)} \sin^2 \frac{\pi n_1 d}{\lambda \sqrt{\cos\theta_1 \cos\theta_2}}$$

This formula is commonly used to interpret the experimental data described in §2.4.

### 3.3 Coupled wave theory of dynamic gratings

To extend the analysis to the *dynamic* case where the grating is written by the very waves that are coupled by it [5], we will derive equations coupling the complex amplitudes of two linearly polarized plane waves

$$\mathbf{E} = \hat{\mathbf{e}}_1 A_1(z) e^{-i\mathbf{k}_1 \cdot \mathbf{r}} + \hat{\mathbf{e}}_2 A_2(z) e^{-i\mathbf{k}_2 \cdot \mathbf{r}}$$

which interfere inside the medium to produce an intensity distribution

$$\begin{aligned} I_1 \equiv \mathbf{E} \cdot \mathbf{E} &= |A_1|^2 + |A_2|^2 + \hat{\mathbf{e}}_1 \cdot \hat{\mathbf{e}}_2 A_1 A_2^* e^{-i(\mathbf{k}_1 - \mathbf{k}_2) \cdot \mathbf{r}} + \hat{\mathbf{e}}_1 \cdot \hat{\mathbf{e}}_2 A_1^* A_2 e^{i(\mathbf{k}_1 - \mathbf{k}_2) \cdot \mathbf{r}} \\ &= I_+ \left[ 1 + \hat{\mathbf{e}}_1 \cdot \hat{\mathbf{e}}_2 \frac{A_1 A_2^*}{I_+} e^{-i(\mathbf{k}_1 - \mathbf{k}_2) \cdot \mathbf{r}} + \hat{\mathbf{e}}_1 \cdot \hat{\mathbf{e}}_2 \frac{A_1^* A_2}{I_+} e^{i(\mathbf{k}_1 - \mathbf{k}_2) \cdot \mathbf{r}} \right] \end{aligned}$$

where  $I_+ \equiv I_1 + I_2$ . We restrict the discussion to waves whose polarization vectors do not change in space, *i.e.*, they are individually eigenpolarizations of the medium, and they are either perpendicular or parallel to the grating planes so

that the coupling does not alter the polarization of either wave. The form for the index is inspired by the expression for the time averaged intensity.

$$n = n_0 + n_1 e^{-i\varphi} \frac{A_1 A_2^*}{I_+} e^{-i(\mathbf{k}_1 - \mathbf{k}_2) \cdot \mathbf{r}} + n_1 e^{i\varphi} \frac{A_1^* A_2}{I_+} e^{i(\mathbf{k}_1 - \mathbf{k}_2) \cdot \mathbf{r}}$$

$n_0$  is the index of the material accompanied by any uniform electro-optic effect. The amplitude of the grating is proportional to the fringe visibility, or modulation index of the intensity distribution,  $2A_1 A_2^* / I_+$ .  $n_1$  is the material response to a unity modulation index, and is given by the amplitude of the space charge field and an effective electro-optic coefficient. For example,

$$n_1 e^{-i\varphi} = -i r_{\text{eff}} \frac{E_N (E_0 + i E_f)}{E_0 + i (E_f + E_n + E_N)} \hat{\mathbf{e}}_1 \cdot \hat{\mathbf{e}}_2 \quad (2)$$

$\varphi$  represents an intrinsic spatial phase shift between the grating and the interference pattern. Substituting these expressions into the scalar wave equation and using the slowly varying envelope approximation yields the following equations:

$$\cos\theta_1 \frac{dA_1}{dz} = -\frac{\alpha}{2} A_1 - i \frac{\pi n_1}{\lambda} e^{-i\varphi} \frac{A_1 A_2^* A_2}{I_+}$$

$$\cos\theta_2 \frac{dA_2}{dz} = -\frac{\alpha}{2} A_2 - i \frac{\pi n_1}{\lambda} e^{i\varphi} \frac{A_1^* A_2 A_1}{I_+}$$

The factor of  $i$  multiplying the coupling term represents a  $90^\circ$  phase shift upon reflection within a medium possessing a periodic index variation. The intensities and phases of the two beams are coupled according to the intrinsic phase of the grating.

$$\cos\theta_1 \frac{dI_1}{dz} = -\alpha I_1 - \frac{2\pi n_1}{\lambda} \sin\varphi \frac{I_1 I_2}{I_+} \quad \cos\theta_1 \frac{d\varphi_1}{dz} = \frac{\pi n_1}{\lambda} \cos\varphi \frac{I_2}{I_+} \quad (3)$$

$$\cos\theta_2 \frac{dI_1}{dz} = -\alpha I_2 + \frac{2\pi n_1}{\lambda} \sin\varphi \frac{I_1 I_2}{I_+} \quad \cos\theta_2 \frac{d\varphi_2}{dz} = \frac{\pi n_1}{\lambda} \cos\varphi \frac{I_1}{I_+}$$

Note that the intensities do not depend on the phase of the optical field, in contrast to Eqns. (1), but depend only on  $\varphi$ , the intrinsic spatial phase shift. The energy balance for the system is the same as that for a fixed grating:

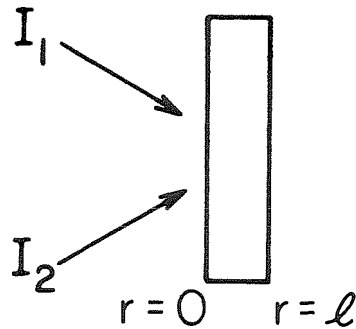
$$\frac{d}{dz} \left[ I_1 \cos\theta_1 + I_2 \cos\theta_2 \right] + \alpha(I_1 + I_2) = 0 \quad (4)$$

which shows that, in the absence of  $\alpha$ , it is the energy flow in the  $z$  direction that is conserved.

The case of a transmission hologram (Fig. 3.2) with symmetric angles of incidence *i.e.*,  $\theta_1 = -\theta_2$ , can be solved by the change of variables

$$J_1 = I_1 e^{\alpha r} \quad J_2 = I_2 e^{\alpha r} \quad J_+ \equiv J_1 + J_2$$

where the path length is denoted by  $r = z / \cos\theta_1$ .



**Figure 3.2.** Two-wave mixing in the transmission geometry.

Noting that  $J_+$  is now constant with respect to  $r$ , the two equations for  $J_1$  and  $J_2$

may be decoupled.

$$\frac{dJ_1}{dr} = -2\Gamma \frac{J_1 J_2}{J_+} = -2\Gamma \frac{J_1(J_+ - J_1)}{J_+}$$

$$\frac{dJ_2}{dr} = 2\Gamma \frac{J_1 J_2}{J_+} = 2\Gamma \frac{(J_+ - J_2)J_2}{J_+}$$

where  $\Gamma = \frac{\pi n_1}{\lambda} \sin\varphi$ . These equations can now be integrated directly and the result expressed in terms of the original variables

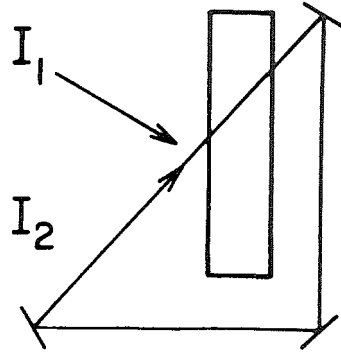
$$I_1 = I_1(0) e^{-ar} \frac{I_1(0) + I_2(0)}{I_1(0) + I_2(0) e^{2\Gamma r}} \quad (5a)$$

$$I_2 = I_2(0) e^{-ar} \frac{I_1(0) + I_2(0)}{I_1(0) e^{-2\Gamma r} + I_2(0)} \quad (5b)$$

For large, positive (negative)  $\Gamma$ , the sum of the intensities of both beams appears in  $I_2$  ( $I_1$ ), aside from the linear absorption.

### 3.4 Oscillation in two-wave mixing

Gain through two beam coupling in transmission was first observed in 1972 [6]. In our laboratory, it has been combined with feedback to produce oscillation in a unidirectional ring resonator [7]. In the configuration of Fig. 3.3, the pump  $I_1$  is supplied externally, but  $I_2$  is not. Scattered light passing through the crystal in many directions is amplified at the expense of  $I_1$ . Scattered light heading in the proper direction is fed back, by the mirrors, into the crystal to be amplified again. In this way, an infinitesimally weak initial beam can build up to a intensity  $I_2$ , comparable to  $I_1$ . The boundary condition appropriate for a ring resonator is  $I_2(0) = (1 - S)I_2(l)$  where  $S$  is the loss due transmitting mirrors, Fresnel reflections from crystal surfaces, etc. Using (3), one can solve for the ratio of oscillating power to pump power



**Figure 3.3.** Two-wave mixing in the ring resonator geometry.

$$\frac{I_2(0)}{I_1(0)} = \frac{1 - S - e^{(\alpha - 2\Gamma)l}}{e^{\alpha l} - (1 - S)}$$

where  $l = d / \cos\theta_1$ . The oscillation condition is

$$2\Gamma l \geq \alpha l - \log(1 - S)$$

independent of pump power. In support of this conclusion, we checked for a pumping threshold. Oscillation was observed to build up for a pump intensity of  $15\text{mW}/\text{cm}^2$ , setting an upper limit for the threshold. The time to reach steady state was approximately eight minutes. At an input intensity of  $1.5\text{W}/\text{cm}^2$ , the time to reach steady state was 8 sec. The "steady state" was characterized by large fluctuations in intensity which made it impossible to quantitatively confirm that the ratio of oscillation to pump intensity was independent of pump intensity. These fluctuations may be due to a mismatch between the longitudinal and transverse modes of the pump laser cavity and the ring cavity. The spectra from the laser and the ring oscillator both had multiple longitudinal modes.

The oscillation was unidirectional, indicating that the  $\Gamma$  coupling the counter-propagating beam to the pump beam was below threshold. Whether it is possible for two counterpropagating beams to be pumped by the same third beam depends on the relative orientation of the crystal through the electro-optic coefficient. The index change in photorefractive crystals depends on the electro-optic coefficient through (2).

The effective electro-optic coefficient is given by

$$r_{\text{eff}} = \varepsilon_{ij}(r_{ijk}\mathbf{g}_k) \varepsilon_{ij} / (g n_o^3 n_\lambda) \quad (6)$$

where  $\varepsilon_{ij}$  is the dielectric tensor of the material,  $\mathbf{g} = \mathbf{k}_1 - \mathbf{k}_2$  is the grating vector,  $\mathbf{g}_k$  is the component of  $\mathbf{g}$  in the  $k$  direction,  $g = |\mathbf{g}|$ , and  $n_\lambda$  is the index of refraction (either ordinary or extraordinary) appropriate for the polarization of the mixing beams.

For crystals of the point group  $4mm$ , such as SBN and  $\text{BaTiO}_3$ , the nonzero electrooptic coefficients and their conventional contracted notations are  $r_{zzz} \equiv r_{33}$ ,  $r_{xxz} = r_{yyz} \equiv r_{13}$ , and  $r_{yzy} = r_{zxx} \equiv r_{42}$ . Equation (6) reduces to

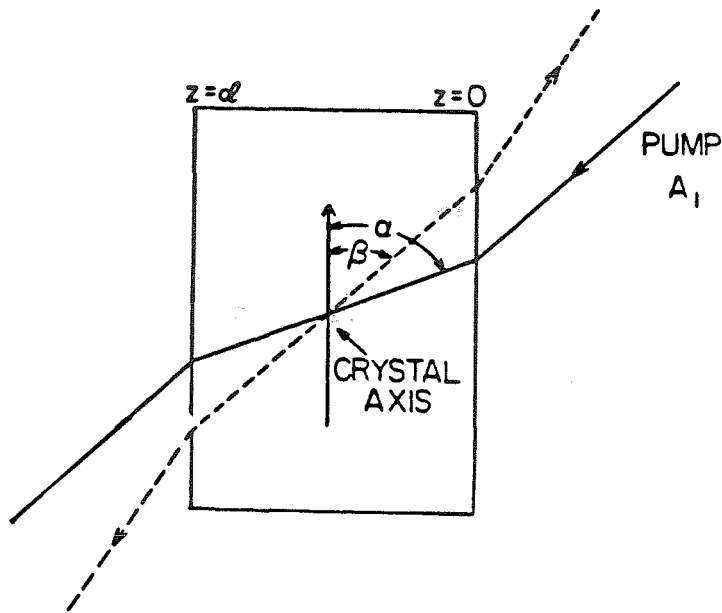
$$r_{\text{eff}} = r_{13} \sin \frac{\alpha + \beta}{2}$$

for mixing beams of ordinary polarization and

$$r_{\text{eff}} = \left( n_e^4 r_{33} \sin\alpha \sin\beta + 2n_e^2 n_o^2 r_{42} \cos^2 \frac{\alpha + \beta}{2} + n_o^4 r_{13} \cos\alpha \cos\beta \right) \frac{1}{n_e n_o^3} \sin \frac{\alpha + \beta}{2}$$

for mixing beams of extraordinary polarization.  $\alpha$  and  $\beta$  are the angles of the pump beams and oscillation beam(s) with respect to the optic axis of the crystal as shown in Fig. 3.4.

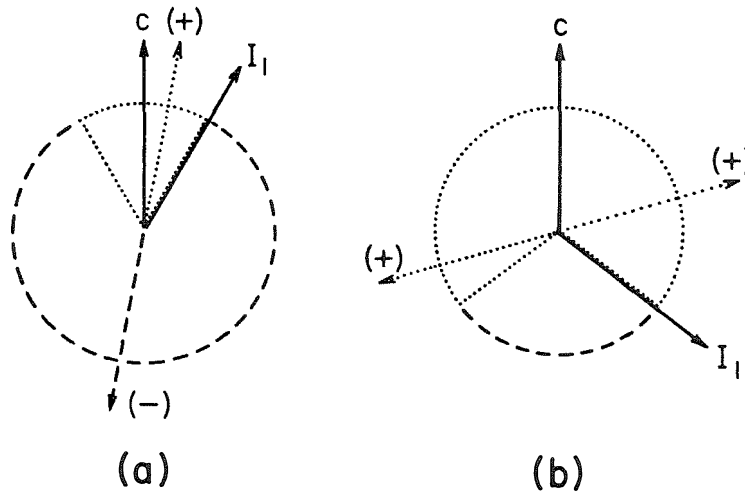
In  $\text{BaTiO}_3$  the large electrooptic coefficient is  $r_{42} = 820\text{pm/V}$  [9]. To observe the largest effects it is necessary to use extraordinary polarization and to orient the crystal so that the grating vector is not parallel to any of the crystal axes.



**Figure 3.4.** Two-wave mixing geometry showing the pump beam (solid), the oscillation beam(s) (dashed), and the c axis of the crystal.

In SBN,  $r_{33}$  is large ( $= 10^{-9}$  m/V) so that extraordinary polarization must be used, although the grating vector can be parallel to the optic axis.

If we only consider the  $r_{42}$  term in BaTiO<sub>3</sub>, when two waves intersect, the one with the  $\mathbf{k}$  closest to the c axis gets amplified at the expense of the other, via the grating formed between them. Given an acute angle between the pump beam and the c axis, the pump will amplify one member of a pair of counterpropagating beams and attenuate the other member (Fig. 3.5a). Given an obtuse angle between the pump beam and the c axis, the pump will amplify each of two counter-propagating beams *individually* (Fig. 3.5b). However, a two-beam coupling analysis cannot predict the gain when all three beams are present because each beam will interact with the superposition of two or three different gratings. We have not been able to observe in our laboratory a bidirectional ring oscillator pumped by a single beam.

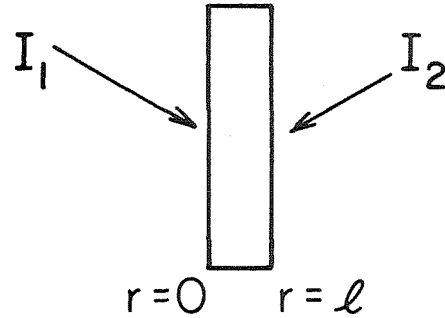


**Figure 3.5.** Diagram showing amplification and attenuation through two beam coupling. The pump wave is  $I_1$  and the optic axis is denoted by  $c$ . Signal waves heading in directions spanned by the dotted region of the circle will be amplified. Signal waves heading in directions spanned by the dashed region of the circle will be attenuated. In (a) and (b), the angle between the pump wave and the  $c$  axis is acute and obtuse, respectively.

### 3.5 Reflection gratings

Up to this point, only transmission gratings have been discussed. Both reflection and transmission gratings are described by the same differential equations (3), but the boundary conditions differ (see Fig. 3.6). In the former case, the two incident waves are specified at the same interface, and both values are sought at the opposite interface, *i.e.* they have the same entrance face and the same exit face. In the latter case, the incident waves are specified at opposite faces. In practice, reflection gratings are written by beams that are more nearly counterpropagating, and transmission gratings are written by beams that are more nearly copropagating. Very short period transmission gratings, and very long period reflection gratings can be written, but as the beams approach grazing incidence, a hologram of finite extent will intercept less and less of the beam.





**Figure 3.6.** Two-wave mixing in the reflection geometry.

A special case of the reflection geometry is where the beams are counterpropagating. It is important to understand the coupling between counterpropagating beams because they are one constituent of the four-wave mixing implementation of phase conjugate mirrors.

The key to solving the two-point boundary value problem can be derived from (3)

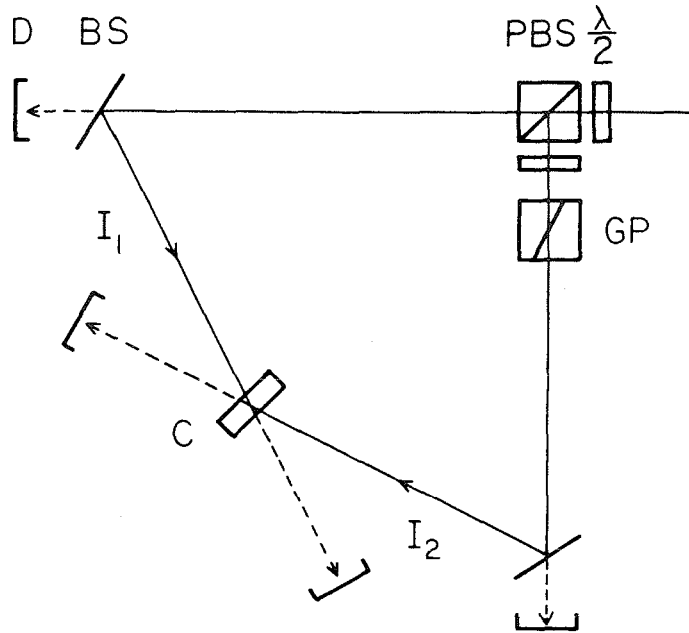
$$\frac{d}{dr}(I_1 I_2) = 2\Gamma I_1 I_2$$

*independent* of the absorption constant,  $\alpha$ . The path length is denoted by  $r = z / \cos\theta_1$ . The intensities at the two faces are therefore related by

$$\frac{I_1(l)I_2(l)}{I_1(0)I_2(0)} = e^{2\Gamma l} \quad (7)$$

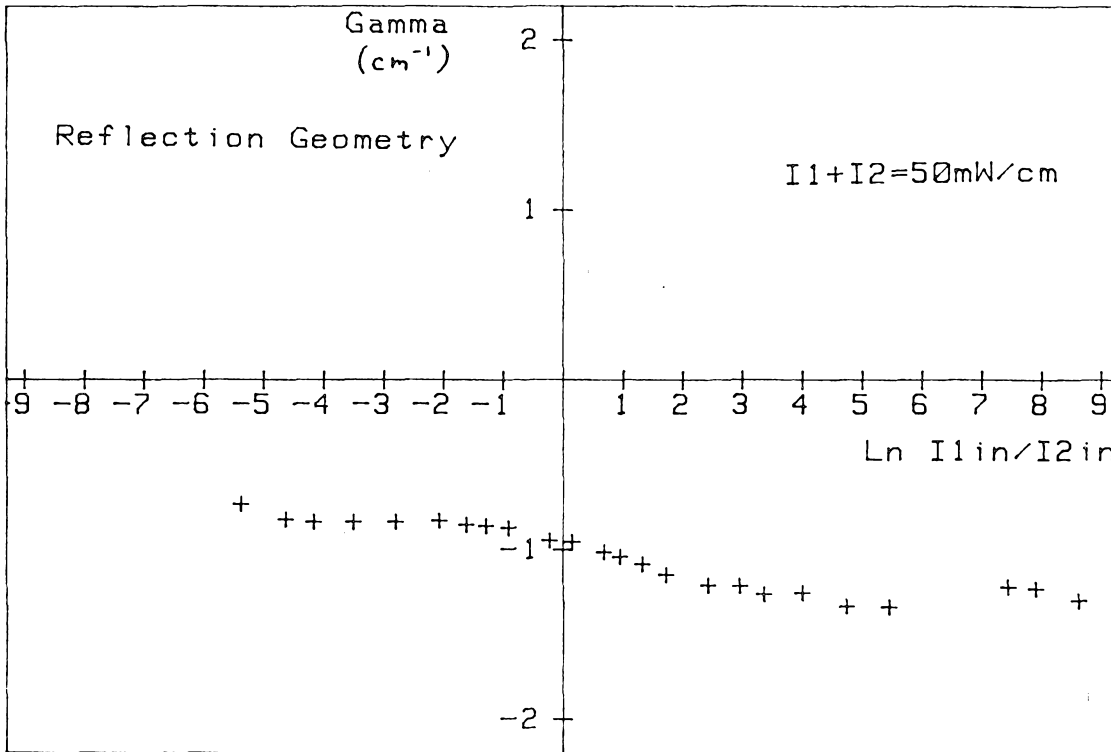
in which all the intensity dependence is explicit.  $\Gamma$  should only depend on the grating vector and the crystal orientation.

Before solving the reflection grating problem, an experimental test of equation (7) will be described. The experimental apparatus is shown in Fig. 3.7.



**Figure 3.7.** Experimental configuration for two-beam coupling in the reflection geometry.  
C: crystal  
D: detector  
GP: glan prism  
BS: beamsplitter  
PBS: polarizing beamsplitter  
 $\lambda/2$ : half-wave plate

The two input and two output intensities are measured by the four detectors, which are monitored by a minicomputer. The half-wave plate - polarizing beam-splitter combination serves as a no loss beamsplitter with a transmission/reflection ratio that can be varied by simply rotating the half-wave plate. The sum of the two input intensities was held constant and the coupling constant  $\Gamma$  was calculated as the ratio was varied. The results are shown in Fig. 3.8, in which  $\Gamma$  changes by only a factor of two while the ratio of the two input intensities changes by six orders of magnitude. Eqn. 7 inspires a change of variables which is helpful in solving for the output intensities in the reflection



**Figure 3.8.** The two-beam coupling constant vs. the ratio of the intensities of the two input beams.

geometry

$$J_1 = I_1 e^{-\Gamma r} \quad J_2 = I_2 e^{-\Gamma r}$$

Now,  $J_1 J_2$  is constant with respect to  $r$ , allowing the equations for  $J_1$ , and  $J_2$  to be decoupled and integrated. Using this change of variables in (3), we obtain

$$\frac{dJ_1}{dr} = (\Gamma - \alpha)J_1 - 2\Gamma \frac{J_1 J_2}{J_1 + J_2} = (\Gamma - \alpha)J_1 - 2\Gamma \frac{J_1(0)J_2(0)}{J_1 + \frac{J_1(0)J_2(0)}{J_1}}$$

$$\frac{dJ_2}{dr} = (\Gamma + \alpha)J_2 - 2\Gamma \frac{J_1 J_2}{J_1 + J_2} = (\Gamma + \alpha)J_2 - 2\Gamma \frac{J_1(0)J_2(0)}{\frac{J_1(0)J_2(0)}{J_2} + J_2}$$

In terms of the original variables, the variation of  $I_1$  and  $I_2$  with  $r$  is given by [10]:

$$e^{-(\Gamma + \alpha)r} = \left[ \frac{(\Gamma - \alpha)I_1^2(0) - (\Gamma + \alpha)I_1(0)I_2(0)}{(\Gamma - \alpha)I_1^2 e^{2\Gamma r} - (\Gamma + \alpha)I_1(0)I_2(0)} \right]^{\frac{\Gamma}{\Gamma - \alpha}} \frac{I_1 e^{\Gamma r}}{I_1(0)} \quad (8a)$$

$$e^{-(\Gamma - \alpha)r} = \left[ \frac{(\Gamma + \alpha)I_2^2(0) - (\Gamma - \alpha)I_1(0)I_2(0)}{(\Gamma + \alpha)I_2^2 e^{2\Gamma r} - (\Gamma - \alpha)I_1(0)I_2(0)} \right]^{\frac{\Gamma}{\Gamma + \alpha}} \frac{I_2 e^{\Gamma r}}{I_2(0)} \quad (8b)$$

$I_2(0)$  is still an unknown which must be solved for by evaluating (8b) at  $r=l$ .

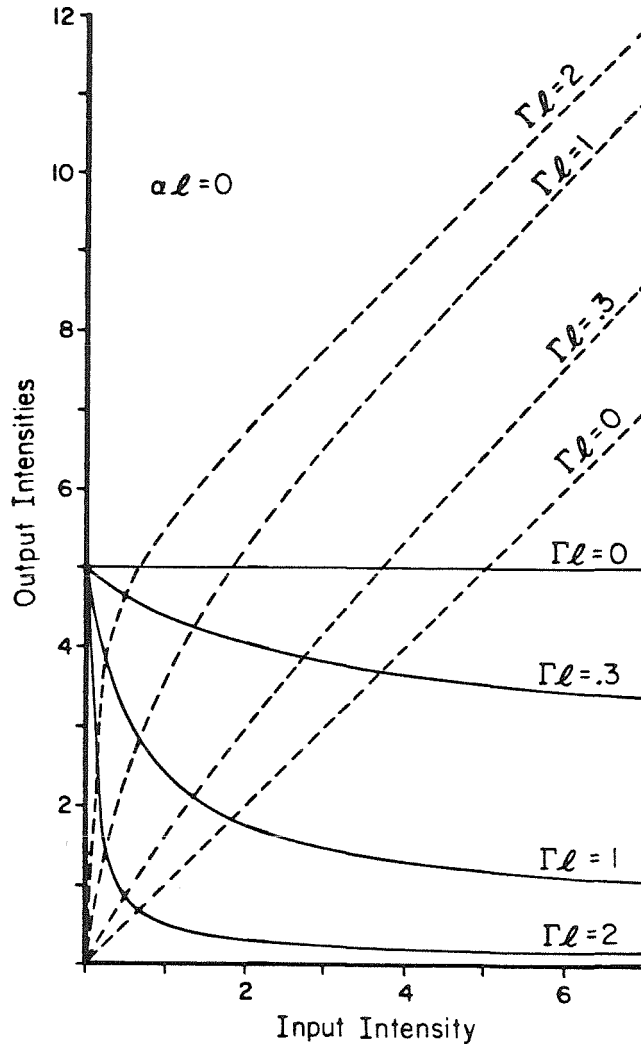
Input/output curves for this amplifier are shown in Fig. 3.9, for the case  $\alpha = 0$ . They are obtained by numerical solutions of (B). The donor, or pump, beam is fixed in intensity and the signal beam is varied from zero to twice the intensity of the donor beam. These curves show the changes in both output intensities as the intensity of the one input is varied.

In the limit  $\alpha \rightarrow 0$ , one can show, from (B), that

$$I_1(l) = I_1(0) \frac{I_1(0) + I_2(l)}{I_1(0) + I_2(l) e^{2\Gamma l}}$$

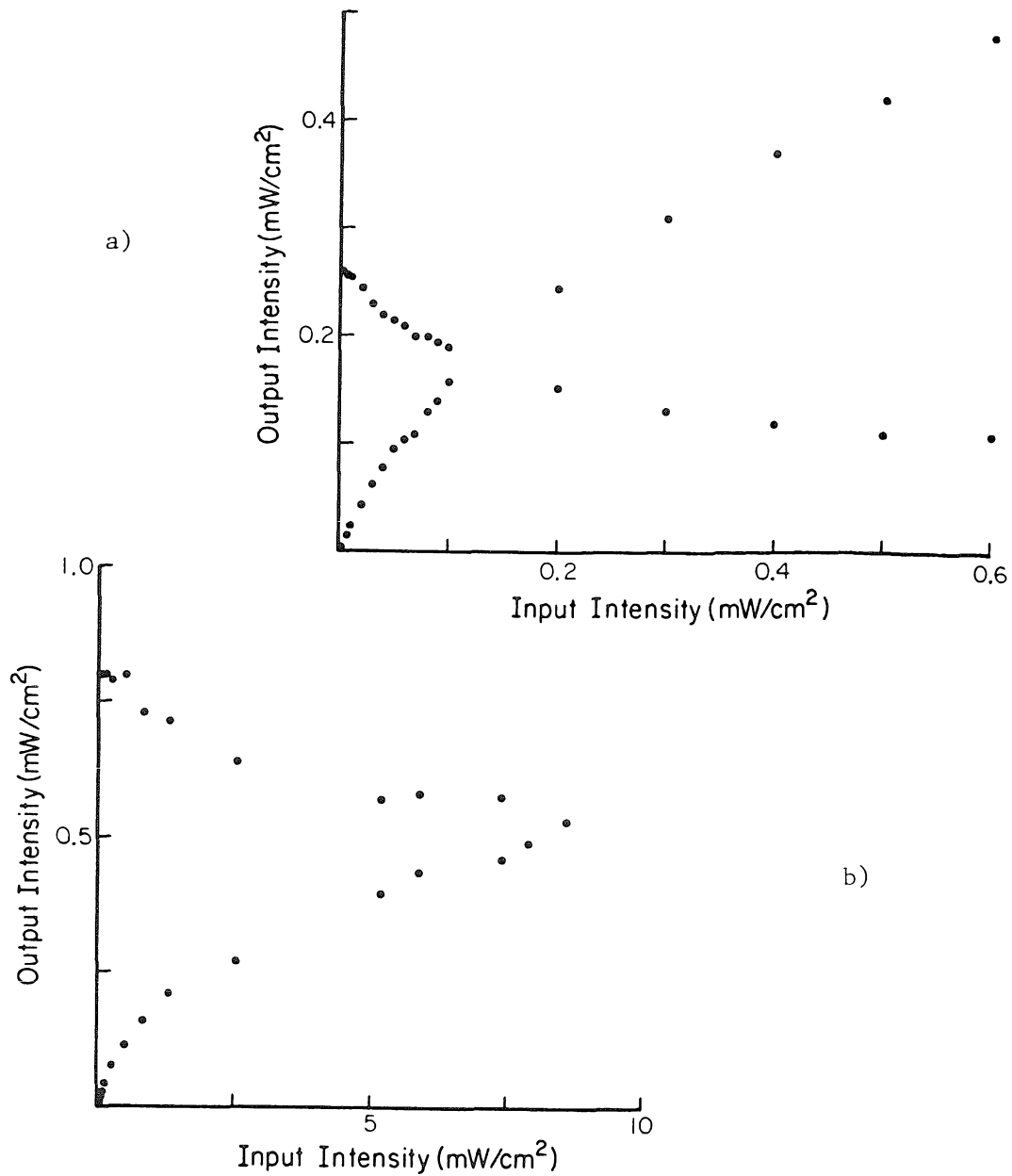
$$I_2(0) = I_2(l) \frac{I_1(0) + I_2(l)}{I_1(0) e^{-2\Gamma l} + I_2(0)}$$

which are identical to (5a) and (5b) under the interchange  $I_2(0) \rightarrow I_2(l)$ . Therefore an amplifier with  $\alpha = 0$  and a transmission geometry will have the same operating curves, and the design of an amplifier should be concerned with maximizing  $\Gamma$  and need not be prejudiced in favor of either geometry.



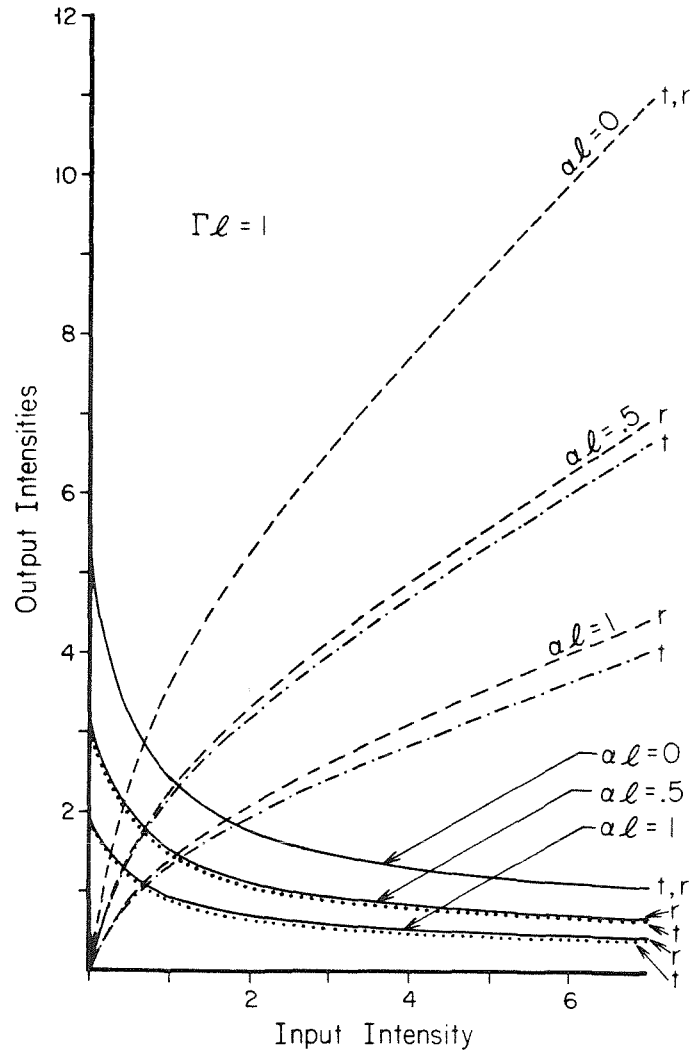
**Figure 3.9.** Diagram showing the operation of a two-beam coupling amplifier. The intensities of the two output beams are plotted vs. the intensity of one of the two input beams. The dashed line is the amplified beam and the solid line is the attenuated beam. The intensity of the second input beam is fixed at 5 (arbitrary units).

Experimental data demonstrating qualitative agreement with this analysis are shown in Fig. 3.10. The data were taken with the apparatus shown in Fig. 3.7. One should not expect Figs. 3.10a and 3.10b to be identical because the coupling constants for the cases are different. A quantitative comparison between Figs. 3.9 and 3.10 has not been attempted because the analysis has neglected Fresnel reflections at the crystal surfaces.



**Figure 3.10.** Experimental values for the output intensities of an amplifier with the (a) transmission geometry (b) reflection geometry.

A difference between the two amplifier geometries appears for a non-zero  $\alpha$ , and this is shown in Fig. 3.11. This figure shows that if two beams are sent through a photorefractive crystal in the reflection geometry, the combined intensity of the two beams which emerge is larger than if the same two beams



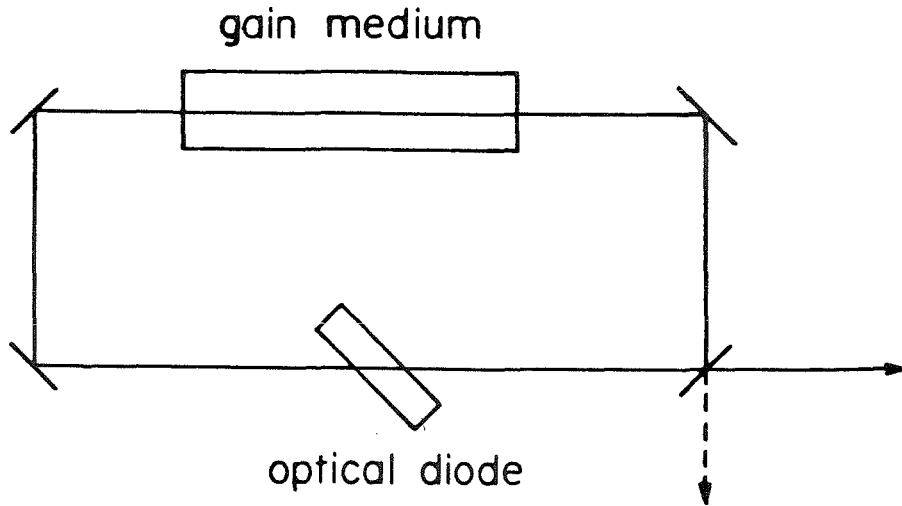
**Figure 3.11.** Diagram showing the operation of two-beam coupling amplifiers, in the transmission and reflection geometries, with absorption present. The value of the donor beams is 5, and  $\Gamma l = 1$ . The output intensities of the acceptor beams are plotted vs. their input intensities.

are sent through in the transmission geometry. (Same coupling strength and absorption constant in both cases.)

### 3.6 Coupling between waves inside a ring resonator

The power flow, from one wave to another, in two-wave mixing suggests the use of an electro-optic crystal as a uni-directional element inside a ring laser cavity (Fig. 3.12). The preferred one-directional power flow could enhance the

clockwise oscillation at the expense of the counter-clockwise oscillation, if the two counter-propagating waves were coupled with a reflection grating.



**Figure 3.12.** A ring laser containing a gain medium and an optical diode, or uni-directional element.

A bi-directional ring laser has standing wave nodes which prevent complete utilization of the inversion inside the gain medium [11,12]. Increased mode stability and a four-fold increase in power output results from eliminating the oscillation in one direction, hence the interest in optical diodes. Currently, Faraday rotators are combined with Brewster windows to provide a 1% difference in round trip loss between the competing directions. This difference in loss combined with the competition for the gain is sufficient to keep the oscillation in one direction below threshold.

The holographic coupling only exists when both beams are present, so the best one could hope for would be a situation where one direction was dominant



and only a small amount of power remained in the other direction to maintain the coupling. Unfortunately, for gain media that do not possess any directionality in their own right, a *steady state* solution does not exist. For example, for gain media characterized by

$$\gamma = \frac{\gamma_0}{1 + \frac{I}{I_{\text{sat}}}}$$

where  $I_{\text{sat}}$  is the saturation intensity, the intensities within the gain medium obey the relation

$$\frac{d}{dz}(I_1 I_2) = 0 \quad \text{or} \quad I_1(0)I_2(0) = I_1(l)I_2(l)$$

which is incompatible with Eqn. 5.

A brief experimental investigation was performed with a ring dye laser and a poled single crystal of SBN. We were unable to get either the clockwise or counter-clockwise waves to go below threshold. The intensities of both beams had periodic fluctuations on a millisecond time scale. This corresponded closely to the response time of the photorefractive effect at the intensity level within the cavity.

### References for Chapter 3

1. H. Kogelnik, Bell Syst. Tech. J. **48**, 2909 (1969).
2. T. Shankoff, Appl. Opt. **7**, 2101 (1968).
3. D.H. Close, A.D. Jacobson, J.D. Margerum, R.G. Brault & F.J. McClung, Appl. Phys. Lett. **14**, 159 (1969).
4. D.L. Staebler, W.J. Burke, W. Phillips & J.J. Amodei, Appl. Phys. Lett. **26**, 182 (1975).
5. D. W Vahey, J. Appl. Phys. **46**, 3510 (1975).

6. D. L. Staebler and J. J. Amodei, J. Appl. Phys. **43**, 1042 (1972).
7. J. O. White, M. Cronin-Golomb, B. Fischer & A. Yariv, Appl. Phys. Lett. **40**, 450 (1982).
8. F. Laeri, T. Tschudi, J. Albers, Opt. Comm. **47**, 387 (1983).
9. A. Yariv, *Quantum Electronics*, (Wiley, New York, 1975).
10. This problem has been subsequently solved by two others. Y.H. Ja, Opt. Quant. Elect. **14**, 547 (1982). P. Yeh, Opt. Comm. **13**, 323 (1983).
11. M. Sargent III, Appl. Phys. **9**, 127 (1976).
12. G. Marowsky and K. Kaufman, IEEE J. Quant. Elect. **12**, 207 (1976).

## 4. FOUR-WAVE MIXING

### 4.1 Introduction

The holographic formulation of four-wave mixing (4WM) is an extension of the two-wave mixing formulation presented in the previous chapter. We continue to consider the same third-order nonlinearity, but now four waves are present in the medium. Four-wave mixing has a commensurate increase in versatility over two-wave mixing, and, in particular, is the most important nonlinear technique for generating phase conjugate wavefronts.

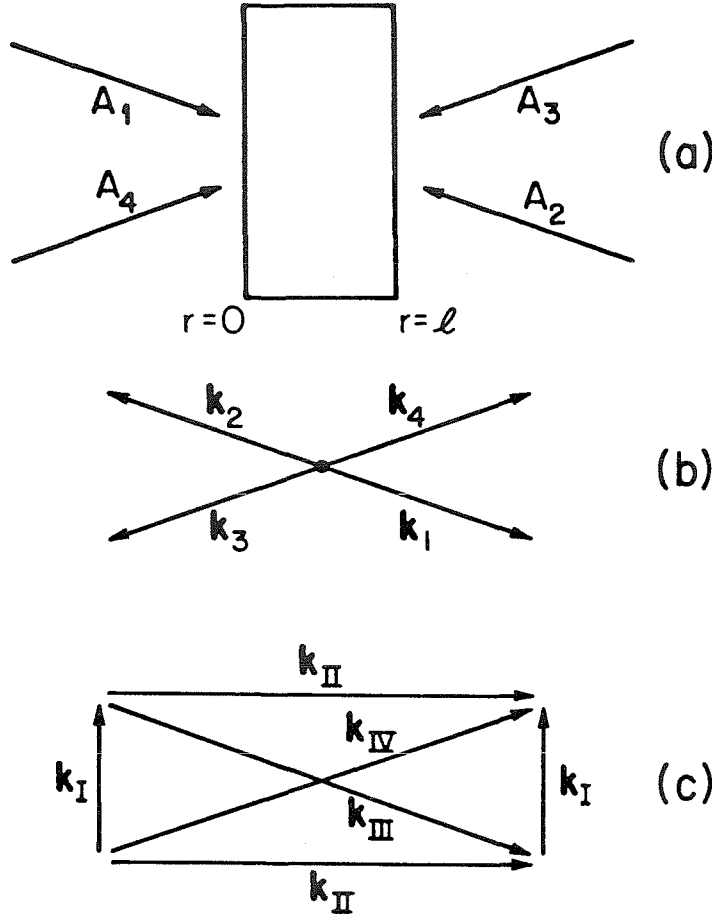
The differences between photorefractive media and other nonlinear media will be further explored in this chapter, especially with regard to their impact on four-wave mixing. Experimental results supporting our analysis will be presented.

### 4.2 Holographic formulation of four-wave mixing

The four-wave mixing implementation of a phase conjugate mirror consists of a medium possessing a third order susceptibility pumped by two counter-propagating beams. By convention,  $A_1$  and  $A_2$  are taken to be the counter-propagating pump beams (Fig. 4.1a).  $A_4$  is the incident signal, object, or probe beam and  $A_3$  is the phase conjugate wave. In the plane wave approximation, we calculate the reflectivity for only one plane wave component of the object beam, *i.e.*, the analysis includes only two pairs of counterpropagating plane waves.  $A_1(0)$ ,  $A_2(l)$ , and  $A_4(0)$  are the known, inputs (Fig. 4.1a).  $A_3$  is not input, *i.e.*,  $A_3(l) = 0$ , but it is generated within the medium. The unknown, outputs are  $A_1(l)$ ,  $A_2(0)$ ,  $A_3(0)$ , and  $A_4(l)$ . Let the electric field amplitude associated with the  $j$ th beam be

$$E_j(\mathbf{r}, t) = A_j(\mathbf{r}) e^{i(\mathbf{k}_j \cdot \mathbf{r} - \omega t)} + \text{c.c.}$$

where c.c. stands for complex conjugate. The four beams write four distinct gratings labelled with Roman numerals I-IV (Fig. 4.1c).



**Figure 4.1.** Geometry of four-wave mixing in a nonlinear or holographic medium.

$A_1$  and  $A_2$  are the counterpropagating pump beams.

$A_4$  and  $A_3$  are the incident and phase conjugate beams, respectively.

$k_1$  through  $k_4$  are the optical wavevectors.

$k_I$  through  $k_{IV}$  are the grating vectors.

$$n = n_0 + \frac{n_I e^{i\varphi_I}}{2} \frac{A_1^* A_4 + A_2 A_3^*}{I_+} e^{i k_I \cdot r} + c.c. + \frac{n_{II} e^{i\varphi_{II}}}{2} \frac{A_1 A_3^* + A_2^* A_4}{I_+} e^{i k_{II} \cdot r} + c.c.$$

$$+ \frac{n_{III} e^{i\varphi_{III}}}{2} \frac{A_1 A_2^*}{I_+} e^{i k_{III} \cdot r} + c.c. + \frac{n_{IV} e^{i\varphi_{IV}}}{2} \frac{A_3^* A_4}{I_+} e^{i k_{IV} \cdot r} + c.c.$$

where  $I_+ = \sum_{j=1}^4 I_j$ . The grating vectors are determined by the wavevectors of the

incident beams.

$$\mathbf{k}_I \equiv \mathbf{k}_4 - \mathbf{k}_1 = \mathbf{k}_2 - \mathbf{k}_3 \quad \mathbf{k}_{II} \equiv \mathbf{k}_1 - \mathbf{k}_3 = \mathbf{k}_4 - \mathbf{k}_2 \quad \mathbf{k}_{III} \equiv \mathbf{k}_1 - \mathbf{k}_2 \quad \mathbf{k}_{IV} \equiv \mathbf{k}_4 - \mathbf{k}_3$$

The complex amplitudes of each of the index gratings are in general different, depending upon the polarization state of the light and the magnitude and direction of the grating vector in conjunction with the properties of the medium ( $r_{\text{eff}}$ ,  $E_N$ ,  $E_f$ ,  $E_n$ , etc.) and applied fields, as outlined in Chapter 2.

Substituting this form for the index into the Helmholtz wave equation,  $(\nabla^2 + \omega^2 \mu \epsilon)E = 0$ , and using the slowly varying envelope approximation (§3.2), we arrive at the following coupled wave equations: [1]

$$\cos\theta \frac{dA_1}{dz} = -i \frac{\pi n_I}{\lambda} e^{-i\varphi_I} \frac{A_1 A_4^* + A_2^* A_3}{I_+} A_4 - i \frac{\pi n_{II}}{\lambda} e^{i\varphi_{II}} \frac{A_1 A_3^* + A_2^* A_4}{I_+} A_3 \quad (1a)$$

$$-i \frac{\pi n_{III}}{\lambda} e^{i\varphi_{III}} \frac{A_1 A_2^*}{I_+} A_2 - \frac{\alpha}{2} A_1$$

$$\cos\theta \frac{dA_2}{dz} = i \frac{\pi n_I}{\lambda} e^{i\varphi_I} \frac{A_1^* A_4 + A_2 A_3^*}{I_+} A_3 + i \frac{\pi n_{II}}{\lambda} e^{-i\varphi_{II}} \frac{A_1^* A_3 + A_2 A_4^*}{I_+} A_4 \quad (1b)$$

$$+ i \frac{\pi n_{III}}{\lambda} e^{-i\varphi_{III}} \frac{A_1^* A_2}{I_+} A_1 + \frac{\alpha}{2} A_2$$

$$\cos\theta \frac{dA_3}{dz} = i \frac{\pi n_I}{\lambda} e^{-i\varphi_I} \frac{A_1 A_4^* + A_2^* A_3}{I_+} A_2 + i \frac{\pi n_{II}}{\lambda} e^{-i\varphi_{II}} \frac{A_1^* A_3 + A_2 A_4^*}{I_+} A_1 \quad (1c)$$

$$+ i \frac{\pi n_{IV}}{\lambda} e^{-i\varphi_{IV}} \frac{A_3 A_4^*}{I_+} A_4 + \frac{\alpha}{2} A_3$$

$$\cos\theta \frac{dA_4}{dz} = -i \frac{\pi n_I}{\lambda} e^{i\varphi_I} \frac{A_1^* A_4 + A_2 A_3^*}{I_+} A_1 - i \frac{\pi n_{II}}{\lambda} e^{i\varphi_{II}} \frac{A_1 A_3^* + A_2^* A_4}{I_+} A_2 \quad (1d)$$

$$-i \frac{\pi n_{IV}}{\lambda} e^{i\varphi_{IV}} \frac{A_3^* A_4}{I_+} A_3 - \frac{\alpha}{2} A_4$$

Here  $\vartheta$  is the angle of incidence of each wave and  $\alpha$  is the the absorption constant. This formulation differs from previous formulations of four-wave mixing [2] in several respects:

- i. The complex part of the coupling coefficients represents a spatial phase shift (between a grating and the interference pattern that generates it), rather than the more common temporal phase shift (between an optical frequency electric field and the response of an atomic dipole moment, for example.) The four beams propagate in different directions in space, but the same direction in time. Accordingly, any temporal phase shift will have the same sign for all beams, while any spatial phase shift will be positive with respect to two beams, and negative with respect the other two.
- ii. The normalizing factor in the denominator ( $I_+$ ) is peculiar to the photorefractive effect. Nonlinearities higher than third order are clearly present in the response of photorefractive media.
- iii. Missing from here are terms, *e.g.*,  $A_1 A_1^* A_1$ , which give rise to self focusing in some media, but are not holographic in origin. For a plane wave  $A_1$ ,  $A_1^* A_1$  is constant in the plane perpendicular to  $\mathbf{k}_1$ , and contains no grating fringes. Also, in some media possessing a true third order susceptibility, waves with perpendicular polarizations can interact, whereas in the holographic formulation, only terms representing waves that interfere are included in the expression for the index.

### 4.3 Single grating, undepleted pumps approximation

Having generated all the terms in Eqns. 1, it was found that only a small number of terms are needed to describe BaTiO<sub>3</sub> in many situations. In the single grating approximation, we assume that, out of a possible four index gratings, only one is present. There are several reasons why the other gratings may be absent.

- i. If beams two and four are incoherent with respect to each other, or have orthogonal polarizations, then the time averaged  $A_2^* A_4$  terms vanish, and do not represent a static interference pattern.
- ii. If two waves do interfere, but the period of the interference pattern is shorter than the mean distance between traps, then it will not produce a space charge field. The spatial frequency response of the medium can thus limit grating formation.
- iii. Even if two waves do produce a space charge field, if the field is in a direction for which the effective electro-optic coefficient vanishes, then it will not produce an index grating.

In the undepleted pumps approximation, we assume that the two pump beams are unaffected by the nonlinear interaction. This is typically true when the pump beams are much more intense than the other beams. This is a safe assumption in media with local response, but in photorefractive media one has to be aware of the possible energy exchange between the pump beams themselves as discussed in §3.5.

*4.3.1 Transmission grating* If the transmission grating is dominant, we have from (1)

$$\frac{dA_1}{dr} = -\frac{\alpha}{2}A_1 \quad (2a)$$

$$\frac{dA_2}{dr} = \frac{\alpha}{2}A_2 \quad (2b)$$

$$\frac{dA_3}{dr} = \frac{\alpha}{2}A_3 + \gamma \frac{A_1 A_4^* + A_2^* A_3}{I_+} A_2 \quad (2c)$$

$$\frac{dA_4^*}{dr} = -\frac{\alpha}{2}A_4^* + \gamma \frac{A_1 A_4^* + A_2^* A_3}{I_+} A_1^* \quad (2d)$$

where  $\gamma \equiv i \frac{\pi n_I}{\lambda} e^{-i\phi_I}$ , and  $r = z / \cos\vartheta$ . The first two equations are immediately

integrable.

$$A_1 = A_1(0) e^{-\frac{\alpha}{2}r} \quad A_2 = A_2(l) e^{\frac{\alpha}{2}(r-l)} \quad I_+(r) = I_1(0) e^{-\alpha r} + I_2(l) e^{\alpha(r-l)}$$

To uncouple the remaining two equations we make use of the relation

$$\frac{d}{dr}(A_1^* A_3 - A_2 A_4^*) = 0 \quad \text{or} \quad A_1^* A_3 - A_2 A_4^* \equiv c \quad (3)$$

The equation for  $A_3$  then can be written

$$\frac{dA_3}{dr} = \left(\gamma + \frac{\alpha}{2}\right)A_3 - \frac{c\gamma A_1}{I_+} \quad \text{or} \quad A_3 = c\gamma A_1(0) \int_r^l \frac{e^{-(\gamma + \alpha)(r-r')} dr'}{I_+(r')}$$

using the boundary condition  $A_3(l) = 0$ . To solve for  $c$ , the expression for  $A_3$  can be inserted into Eqn. 3 and evaluated at  $r = 0$ .

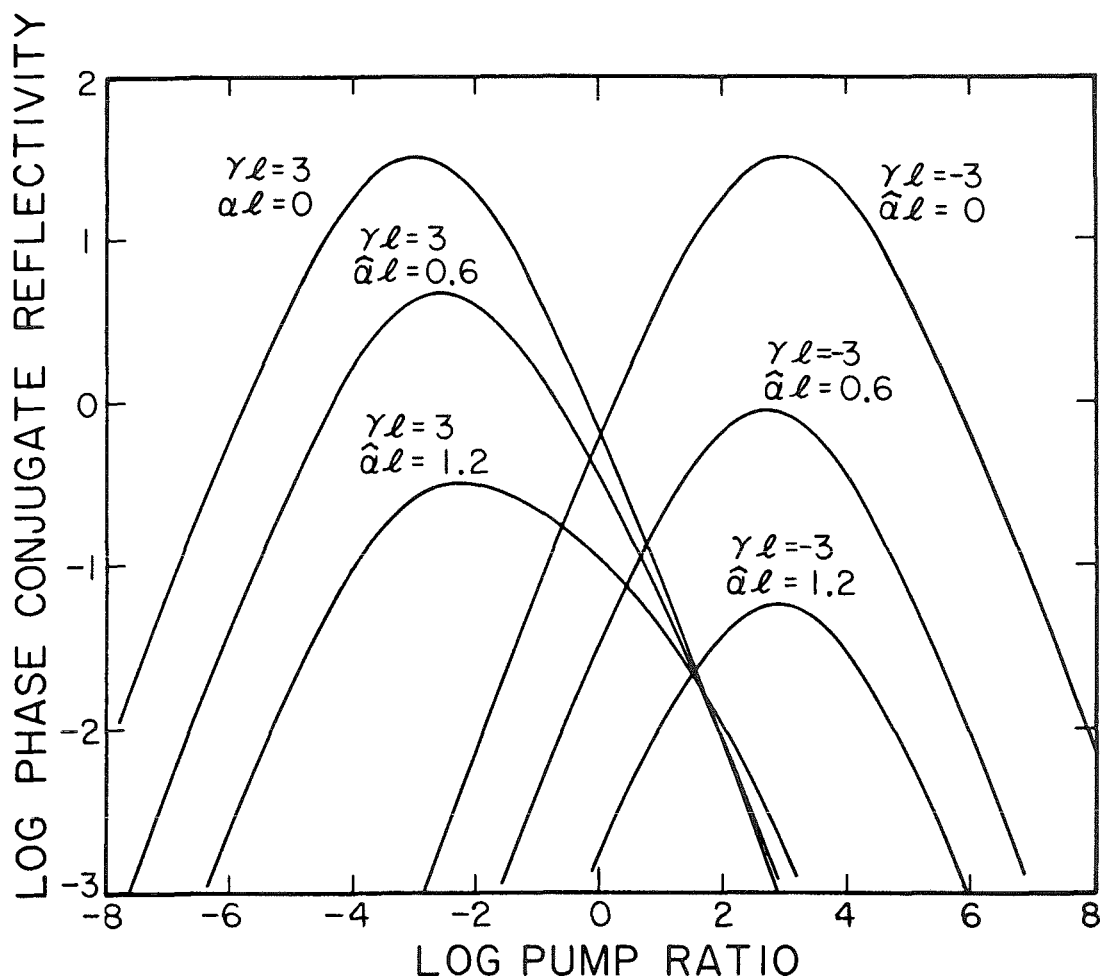
$$c = \frac{A_2(l) A_4^*(0) e^{-\frac{\alpha}{2}l}}{\gamma I_1(0) \int_0^l \frac{e^{(\gamma + \alpha)r'} dr'}{I_+(r')} - 1}$$

The phase conjugate amplitude reflectivity is given by

$$\rho = \frac{A_3(0)}{A_4^*(0)} = \gamma A_1(0) A_2(l) e^{-\frac{\alpha}{2}L} \frac{\int_0^l \frac{e^{-(\gamma + \alpha)(r-r')} dr'}{I_+(r')}}{\gamma I_1(0) \int_0^l \frac{e^{(\gamma + \alpha)r'} dr'}{I_+(r')} - 1}$$

In Fig. 4.2, the phase conjugate intensity reflectivity is plotted versus the pump ratio,  $p$ . The pump ratio is defined according to the *function* of the two pump beams with respect to the probe wave,  $A_4$ , i.e.,  $p$  is the ratio of the intensity of the pump which reads out the grating written by  $A_4$ , to the intensity of the pump which writes the grating with  $A_4$ . From Eqns. 2c & 2d, we can see that pump 1 writes a grating with  $A_4$ , and pump 2 reads out the grating, therefore, for the transmission grating,  $p \equiv I_2(l)/I_1(0)$ . The reflectivity is plotted for  $\gamma l = \pm 3$  and several values of  $\hat{\alpha} = \alpha/\gamma$ . We see that the effect of increasing linear absorption

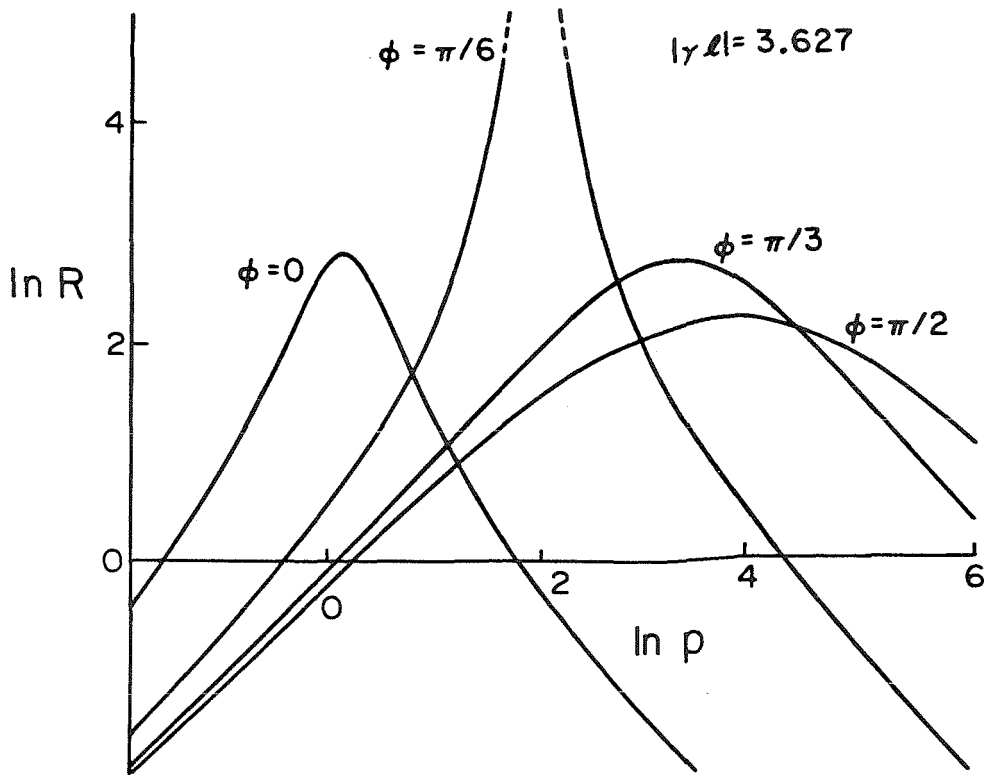




**Figure 4.2.** Phase conjugate intensity reflectivity of the transmission grating in the undepleted pumps approximation vs. the pump ratio  $I_2(l)/I_1(0)$ . The coupling strength is  $\gamma l = \pm 3$  and the reflectivity is shown for various values of the normalized linear absorption  $\hat{\alpha} = \alpha/\gamma$ .

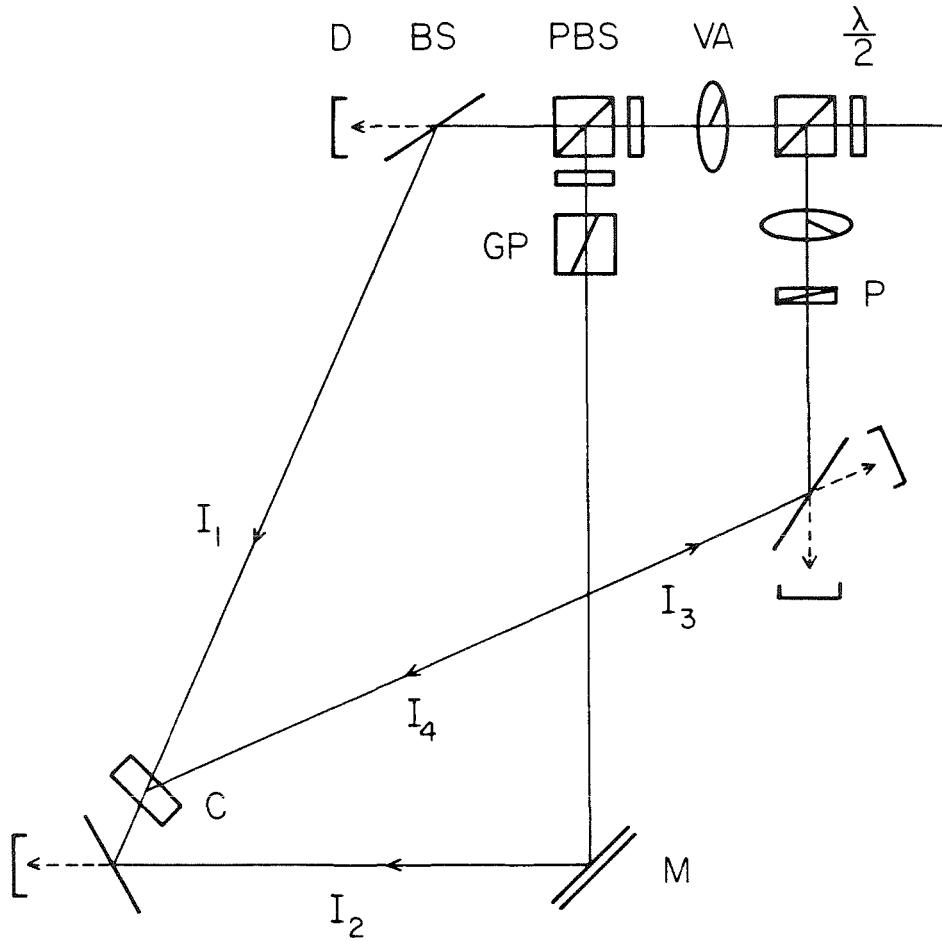
is primarily to decrease the reflectivity, with the greater decrease being for negative  $\gamma l$ .

The dependence of phase conjugate reflectivity on the pump ratio is a manifestation of the same phase shift which produced the directionality in two-wave mixing. Fig. 4.3 shows how the optimum pump ratio varies with  $\varphi_1$ . Media with local response ( $\varphi_1 = 0$ ) display an optimum pump ratio of unity. A measurement



**Figure 4.3.** Phase conjugate reflectivity in the undepleted pumps approximation for coupling strength  $\gamma l = -3.627$  and various phase angles,  $\phi$ . Mirrorless self-oscillation occurs here for  $\phi = \pi/6$  and  $p = 6.13$ .

of phase conjugate reflectivity vs. pump ratio has been made using the experimental apparatus shown in Fig. 4.4. The half-wave plate / polarizing beam-splitter combination forms a lossless beamsplitter with a transmission/reflection ratio that can be varied simply by rotating the half-wave plate. An experimental curve of reflectivity vs. pump ratio is shown in Fig. 4.5. The nonlinear medium is a poled,  $4 \times 4 \times 7 \text{ mm}^3$  single crystal of  $\text{BaTiO}_3$ . All three input beams at 514.5 nm are supplied by the same argon ion laser. Their total intensity is  $27.5 \text{ W/cm}^2$ .



**Figure 4.4.** Experimental configuration for measuring phase conjugate reflectivity as a function of pump ratio.

- |                |                               |
|----------------|-------------------------------|
| C: crystal     | BS: beamsplitter              |
| D: detector    | PBS: polarizing beamsplitter  |
| P: polarizer   | $\lambda/2$ : half-wave plate |
| GP: Glan prism | VA: variable attenuator       |

The fringe spacing is  $1.9\mu\text{m}$ .

The expression for the reflectivity can be simplified when  $\alpha = 0$ .

$$R = p \left| \frac{e^{-\gamma l} - 1}{e^{-\gamma l} + p} \right|^2 \quad (4)$$

R is invariant under the interchange  $p \rightarrow 1/p$  and  $\gamma l \rightarrow -\gamma l$ , meaning that probe beams travelling in opposite directions to each other, incident upon opposite

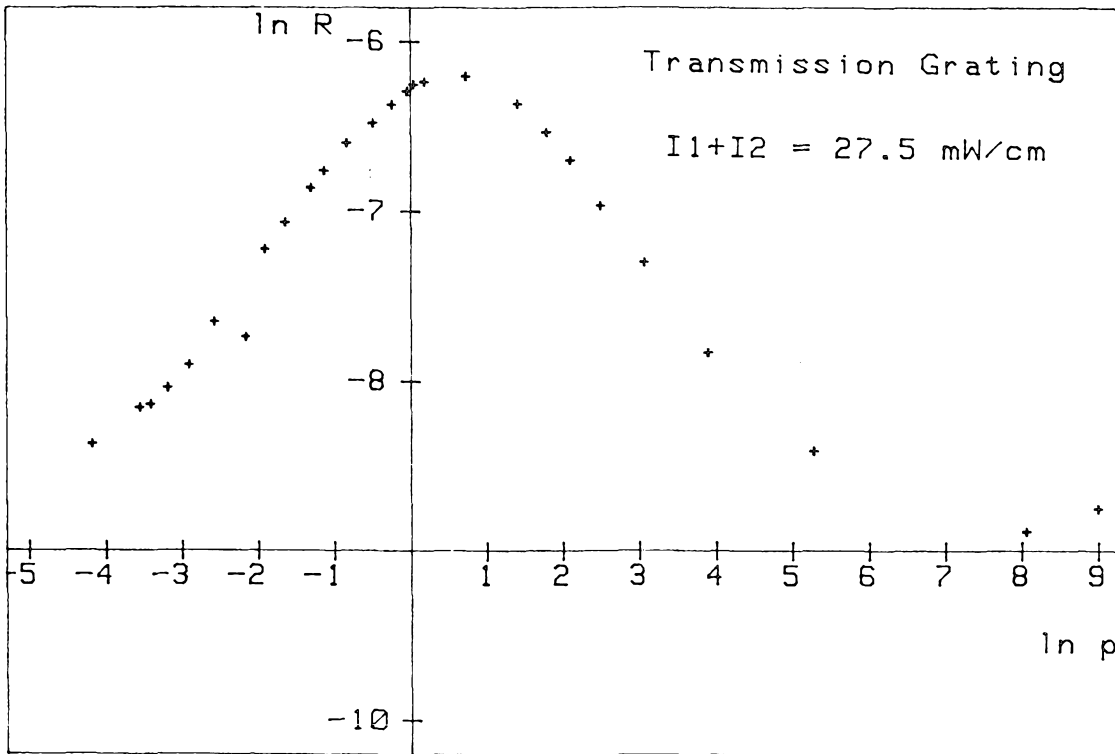


Figure 4.5. Experimental curve of phase conjugate reflectivity vs. pump ratio.

faces of a photorefractive PCM, will experience the same reflectivity.

The condition for an infinite reflectivity is

$$\text{Im}(-\gamma l) = \pm\pi, \pm 3\pi, \dots \quad \text{and} \quad \text{Re}(-\gamma l) = \ln p$$

Of course, pump depletion occurs long before infinite reflectivities. While this condition cannot be satisfied for  $\varphi_1 = \pi/2$ , reflectivities exceeding 100% are within reach of finite coupling strengths at all phase angles. The phase angle can be controlled by applying an electric field to the crystal, and also by detuning

the pump and probe beams. In the latter case the finite response time of the photorefractive effect causes the grating to lag behind the moving fringes. This departure from a ninety degree phase shift can restore the possibility of infinite reflectivity or self oscillation [3].

As the signal intensities approach the intensities of the pumps, we must expect pump depletion. Even if no signal is supplied, a PCM with gain can produce oscillation when provided with positive feedback such as in a mirror resonator. In this case, pump depletion determines the steady state oscillation strength. The theoretical approach to this problem is the subject of §4.4 .

*4.3.2 Reflection grating* If the reflection grating is dominant, we have from (1)

$$\frac{dA_1}{dr} = -\frac{\alpha}{2}A_1$$

$$\frac{dA_2}{dr} = \frac{\alpha}{2}A_2$$

$$\frac{dA_3}{dr} = \frac{\alpha}{2}A_3 + \gamma \frac{A_1^*A_3 + A_2A_4^*}{I_+}A_1$$

$$\frac{dA_4^*}{dr} = -\frac{\alpha}{2}A_4^* + \gamma \frac{A_1^*A_3 + A_2A_4^*}{I_+}A_2^*$$

where the definition of the coupling constant for the reflection grating,

$\gamma = i \frac{\pi \Omega_{\Pi}}{\lambda} e^{-j\varphi_{\Pi}}$ , is analogous to that for the transmission grating. In the absence

of absorption, we see that the equations are the same as (2) under the interchange of  $A_1$  and  $A_2$ . This is in accordance with the exchange of their functions, because now beam 2 writes a grating with the incident beam, and beam 1 reads it out. Thus Eqn. 4 also applies to the reflection grating case, when  $\alpha = 0$ , if  $p$  is changed to  $p = I_1(0)/I_2(l)$  in accordance with its definition in §4.3.1.

#### 4.4 Pump depletion in the single grating approximation

The influence of pump depletion on four-wave mixing has been analyzed previously using a Lagrangian method [4,5,6]. The analysis applied to four *colinear* waves inside a medium with a *local* response. Another method has been used to solve a very general class of nonlinear parametric processes including 4WM [7]. However, it has not been applied to nonlocal nonlinear susceptibilities, such as are present in photorefractive media. The method for treating *nonlocal* media presented in this section is not restricted to a colinear geometry, but is restricted to a symmetrical geometry where all waves have the same angle of incidence [8].

As a starting point, we allow for the  $r$  dependence of beams one and two but do not consider the effect of more than a single grating on the interactions of the four beams, and restrict ourselves to the case where  $\alpha l \ll 1$ . The equations now under examination are intermediate in complexity between Eqns. 1 and Eqns. 2.

*4.4.1 Transmission grating* When only  $n_1$  is present, Eqns. 1 take the form

$$\frac{dA_1}{dr} = -\gamma \frac{A_1 A_4^* + A_2^* A_3}{I_+} A_4$$

$$\frac{dA_2^*}{dr} = -\gamma \frac{A_1 A_4^* + A_2^* A_3}{I_+} A_3^*$$

$$\frac{dA_3}{dr} = \gamma \frac{A_1 A_4^* + A_2^* A_3}{I_+} A_2$$

$$\frac{dA_4^*}{dr} = \gamma \frac{A_1 A_4^* + A_2^* A_3}{I_+} A_1^*$$

We are chiefly interested in calculating phase conjugate reflectivities so it is enough to solve for the ratios  $A_3/A_4^*$  and  $A_1/A_2^*$ . The differential equations for

the ratios can be decoupled with the use of the relations

$$A_1 A_2 + A_3 A_4 \equiv \frac{c}{2} \quad \text{and} \quad A_1 A_3^* - A_2^* A_4 \equiv \frac{d}{2} \quad (5)$$

The flux conservation equations are retained from the two-wave mixing case (3.4).

$$f_+ \equiv I_1 + I_4 \quad f_- \equiv I_2 + I_3 \quad f \equiv f_+ - f_- \quad (6)$$

The fluxes are known, *i.e.*, they are given by the boundary conditions. Substituting the above constants into the differential equations for  $A_{34} \equiv A_3/A_4^*$ , and  $A_{12} \equiv A_1/A_2^*$ , we obtain

$$\frac{dA_{34}}{dr} = \frac{\gamma}{I_+} \left[ \frac{c}{2} - f(A_{34}) - \frac{c^*}{2}(A_{34})^2 \right]$$

$$\frac{dA_{12}}{dr} = -\frac{\gamma}{I_+} \left[ \frac{c}{2} + f(A_{12}) - \frac{c^*}{2}(A_{12})^2 \right]$$

which can be integrated directly, because  $I_+$  is a constant with respect to  $r$ .

$$\frac{-c^* A_{34}|_l - f - \sqrt{f^2 + |c|^2}}{-c^* A_{34}|_l - f + \sqrt{f^2 + |c|^2}} \frac{-c^* A_{34}|_0 - f + \sqrt{f^2 + |c|^2}}{-c^* A_{34}|_0 - f - \sqrt{f^2 + |c|^2}} = e^{\sqrt{f^2 + |c|^2} \frac{\gamma L}{I_+}}$$

and a corresponding equation for  $A_{12}$  obtained by replacing  $f \rightarrow -f$ , and  $\gamma \rightarrow -\gamma$ . We now invoke consistency between the completed integrations and Eqns. (5) which allowed the problem to be separated. Making the substitutions

$$A_{34}|_0 = \rho \quad A_{34}|_l = 0 \quad A_{12}|_0 = \frac{I_1(0)}{\frac{c^*}{2} - \rho^* I_4(0)} \quad A_{12}|_l = \frac{c}{2 I_2(l)}$$

we obtain a pair of transcendental equations which can be solved for  $|c|^2$ , and  $R = |\rho|^2$ . The three input intensities appear only in the two combinations  $p = I_2(l)/I_1(0)$  and  $q = \frac{I_4(0)}{I_1(0) + I_2(l)}$ . As the probe ratio,  $q$ , increases, we

expect to see more pump depletion. A contour plot of  $R$  vs.  $p$  and  $q$ , for  $\gamma l = -3$ , is shown in Fig. 4.6.

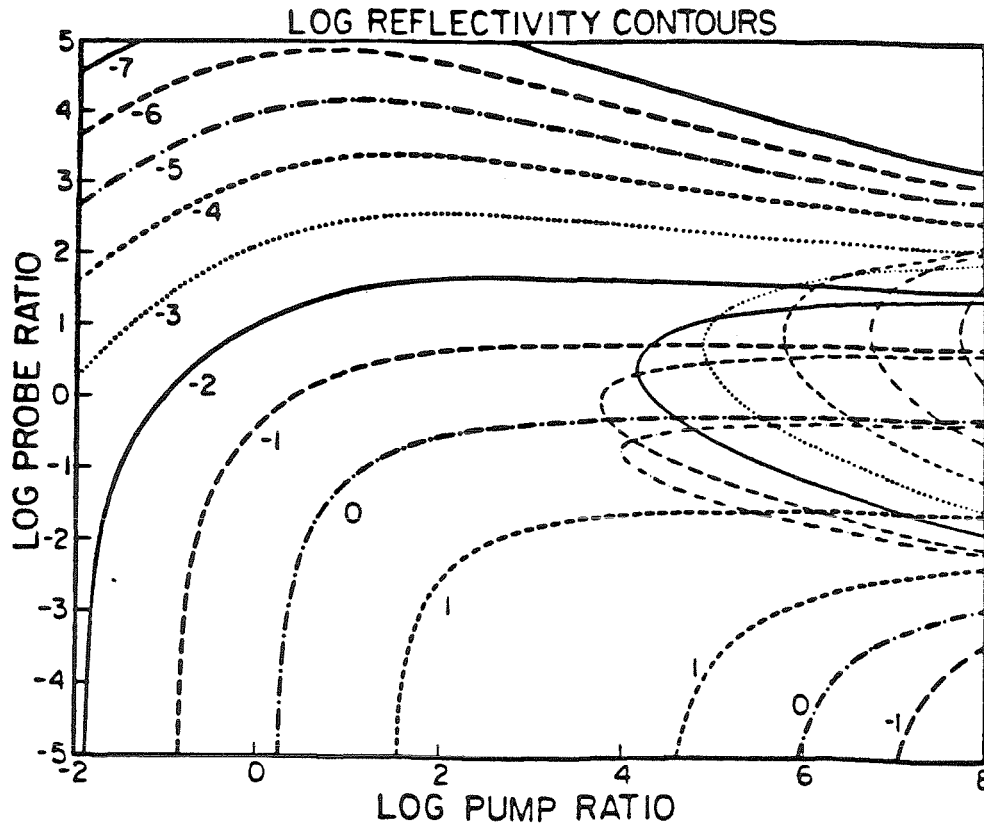
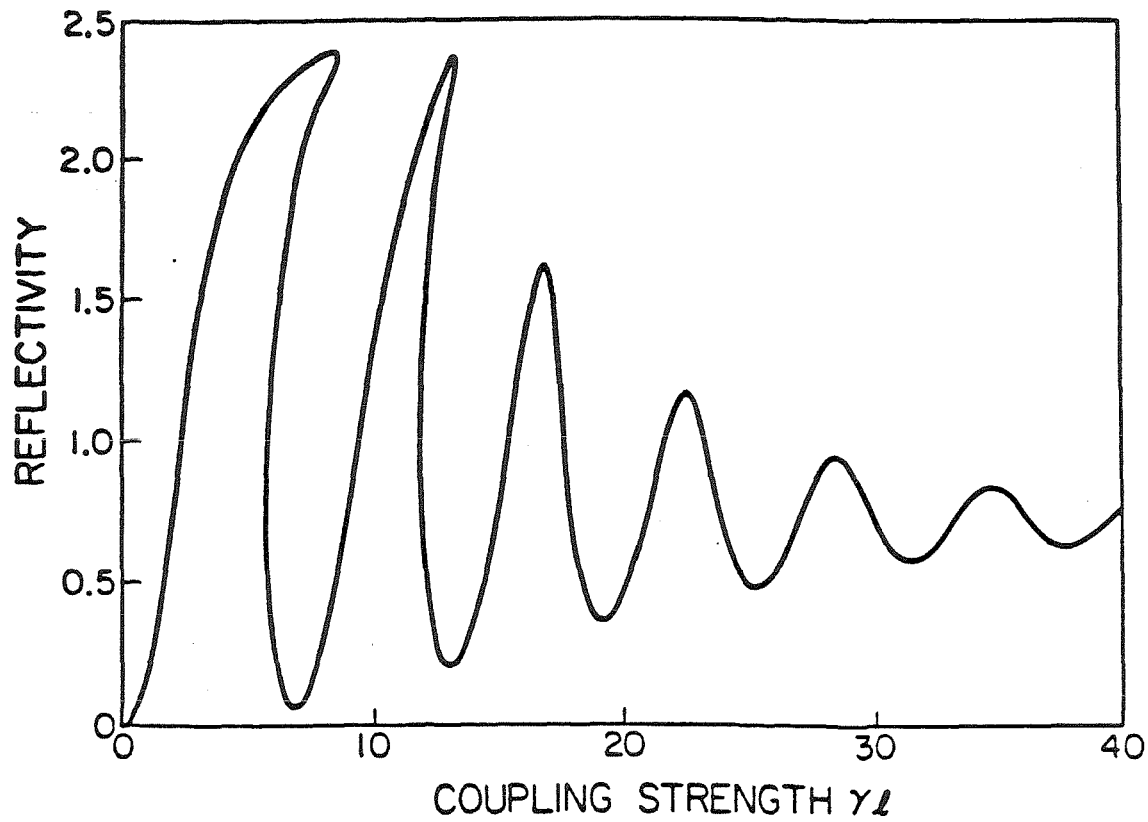


Figure 4.6. Contour plot of phase conjugate reflectivity for  $\gamma l = -3$  as a function of the pump ratio  $I_2(l)/I_1(0)$  and the probe ratio  $I_4(0)/[I_1(0) + I_2(l)]$ . The transmission grating is operative.

The figure suggests that  $R$  remains finite as  $p \rightarrow \infty$ . A plot of  $R$  vs.  $|\gamma l|$  is shown in Fig. 4.7. The phase shift between the grating and the interference fringes is  $5^\circ$ .





**Figure 4.7.** Reflectivity of a photorefractive PCM vs. coupling strength magnitude  $|\gamma l|$ . The transmission grating is operative. The phase shift between the grating and the interference fringes is  $5^\circ$ .

The intensities of the two pumping beams are equal ( $p = 1$ ) and the probe intensity is 20% of the total pumping intensity ( $q = 0.2$ ). The top of the graph corresponds to the reflectivity that would result if all the power of beam 2 were transferred to beam 3. This is the maximum reflectivity consistent with the conservation laws (5). The peaks in the curve correspond to the poles in the

reflectivity of a PCM with no pump depletion and no phase shift between the grating and the interference fringes.

4.4.2 *Reflection grating* When the reflection grating is dominant, Eqns. (1) take the form

$$\frac{dA_1^*}{dr} = \gamma \frac{A_1^* A_3 + A_2 A_4^*}{I_+} A_3^*$$

$$\frac{dA_2}{dr} = \gamma \frac{A_1^* A_3 + A_2 A_4^*}{I_+} A_4$$

$$\frac{dA_3}{dr} = \gamma \frac{A_1^* A_3 + A_2 A_4^*}{I_+} A_1$$

$$\frac{dA_4^*}{dr} = \gamma \frac{A_1^* A_3 + A_2 A_4^*}{I_+} A_2^*$$

where  $\gamma \equiv i \frac{\pi n_{II}}{\lambda} e^{-i\phi_{II}}$ . The reflection grating can be solved in the same manner as the transmission grating by decoupling the differential equations for the beam ratios with relations analogous to Eqns. (5) and (6).

$$A_1 A_4^* - A_2^* A_3 \equiv \frac{c}{2} \quad \text{and} \quad A_1 A_2 - A_3 A_4 \equiv \frac{d}{2}$$

$$f_{13} \equiv I_1 - I_3 \quad f_{42} \equiv I_4 - I_2 \quad f \equiv f_{13} + f_{42}$$

We now have

$$\frac{dA_{34}}{dr} = \frac{\gamma}{I_+} \left[ \frac{d}{2} + f(A_{34}) - \frac{d^*}{2} (A_{34})^2 \right] \quad (7a)$$

$$\frac{dA_{12}}{dr} = -\frac{\gamma^*}{I_+} \left[ \frac{d}{2} + f(A_{12}) - \frac{d^*}{2} (A_{12})^2 \right] \quad (7b)$$

where the flux  $f$  is no longer known.  $I_+$  is no longer a constant with respect to  $r$ , but is coupled to the grating term  $\frac{g}{2} \equiv A_1^* A_3 + A_2 A_4^*$ .

$$\frac{dI_+}{dr} = \frac{|g|^2}{2I_+}(\gamma + \gamma^*) \quad \frac{dg}{dr} = \gamma g$$

This system is easy to solve, since  $g$  is not coupled to  $I_+$ .

$$g(r) = g(0)e^{\gamma r} \quad I_+^2(r) - I_+^2(0) = |g(r)|^2 - |g(0)|^2 \quad (8)$$

where  $g(0)$  is unknown. Eqns. 7 can then be integrated

$$\frac{-d^*A_{34})_l + f - \sqrt{f^2 + |d|^2}}{-d^*A_{34})_l + f + \sqrt{f^2 + |d|^2}} \frac{-d^*A_{34})_0 + f + \sqrt{f^2 + |d|^2}}{-d^*A_{34})_0 + f - \sqrt{f^2 + |d|^2}}$$

$$= \left\{ \frac{I_+(l) - I_+(-\infty)}{I_+(l) + I_+(-\infty)} \frac{I_+(0) + I_+(-\infty)}{I_+(0) - I_+(-\infty)} \right\}^{\frac{\gamma \sqrt{f^2 + |d|^2}}{(\gamma + \gamma^*)I_+(-\infty)}}$$

where  $I_+^2(-\infty)$  is given by Eqn. (8). The equation for  $A_{12}$  is obtained with the substitution  $A_{34} \rightarrow A_{12}$ , and  $\gamma \rightarrow -\gamma^*$ . The unknowns are  $f$ ,  $\rho = A_{34})_0$ ,  $|d|^2$ ,  $I_+(0)$ , and  $I_+(l)$ . With the addition of three more equations, we can solve for  $R = |\rho|^2$ .

$$I_+(0) + f = 2(I_1(0) + I_4(0))$$

$$I_+(l) - f = 2I_2(l)$$

$$\frac{I_+^2(l) - I_+^2(0)}{e^{2\gamma l} - 1} = \frac{I_4(0)}{I_1(0)} \left[ |\rho|^2 (I_1(0) + I_4(0))^2 + \frac{|d|^2}{4} + \frac{\rho d^* + \rho^* d}{2} (I_1(0) + I_4(0)) \right]$$

The third equation is obtained by substituting  $\rho$ ,  $d$ , etc., into expression (8) for  $g$ .

A slightly different method can be used to solve both the transmission grating and the reflection grating. It makes use of the solutions for  $I_+(r)$  and  $g(r)$  obtained above. When  $\gamma \in \mathbb{R}$  we can make use of the change of variables

$$du = \frac{\gamma}{I_+} e^{\gamma r} dr \quad \text{or} \quad e^{|g_0|u(r)} = \frac{|g_0| e^{\gamma r} + \sqrt{|g_0|^2 e^{2\gamma r} + I_+^2(-\infty)}}{|g_0| + \sqrt{|g_0|^2 + I_+^2(-\infty)}}$$

to transform the system of equations (6). Note that  $u$  has the same sign as  $\gamma$ .  $g_0$  is an abbreviation for  $g(0)$ , i.e.,  $g_r \equiv g(r)$ .

$$\frac{d}{dr} \begin{pmatrix} A_1 \\ A_3 \end{pmatrix} = \frac{\gamma}{I_+(r)} \begin{pmatrix} 0 & g^*(r) \\ g(r) & 0 \end{pmatrix} \begin{pmatrix} A_1 \\ A_3 \end{pmatrix} \rightarrow \frac{d}{du} \begin{pmatrix} A_1 \\ A_3 \end{pmatrix} = \begin{pmatrix} 0 & g_0^* \\ g_0 & 0 \end{pmatrix} \begin{pmatrix} A_1 \\ A_3 \end{pmatrix}$$

$$\frac{d}{dr} \begin{pmatrix} A_4 \\ A_2 \end{pmatrix} = \frac{\gamma}{I_+(r)} \begin{pmatrix} 0 & g^*(r) \\ g(r) & 0 \end{pmatrix} \begin{pmatrix} A_4 \\ A_2 \end{pmatrix} \rightarrow \frac{d}{du} \begin{pmatrix} A_4 \\ A_2 \end{pmatrix} = \begin{pmatrix} 0 & g_0^* \\ g_0 & 0 \end{pmatrix} \begin{pmatrix} A_4 \\ A_2 \end{pmatrix}$$

The solutions, in terms of the unknown  $g_0$ , are given by:

$$\begin{pmatrix} A_1 \\ A_3 \end{pmatrix} = \frac{A_1(0)e^{-|g_0|L} + A_3(l) \frac{g_0^*}{|g_0|}}{2 \cosh |g_0|L} e^{|g_0|u} \begin{pmatrix} 1 \\ \frac{g_0}{|g_0|} \end{pmatrix} \quad (9a)$$

$$+ \frac{A_1(0)e^{|g_0|L} - A_3(l) \frac{g_0^*}{|g_0|}}{2 \cosh |g_0|L} e^{-|g_0|u} \begin{pmatrix} 1 \\ -\frac{g_0}{|g_0|} \end{pmatrix}$$

$$\begin{pmatrix} A_4 \\ A_2 \end{pmatrix} = \frac{A_4(0)e^{-|g_0|L} + A_2(l) \frac{g_0^*}{|g_0|}}{2 \cosh |g_0|L} e^{|g_0|u} \begin{pmatrix} 1 \\ \frac{g_0}{|g_0|} \end{pmatrix} \quad (9b)$$

$$+ \frac{A_4(0)e^{|g_0|L} - A_2(l) \frac{g_0^*}{|g_0|}}{2 \cosh |g_0|L} e^{-|g_0|u} \begin{pmatrix} 1 \\ -\frac{g_0}{|g_0|} \end{pmatrix}$$

where  $L \equiv u(l)$ . When  $A_3(l) = 0$ , the phase conjugate reflectivity is given by

$$R = \left| \frac{A_3(0)}{A_4^*(0)} \right|^2 = \frac{I_1(0)}{I_4(0)} \tanh^2 |g_0|L \quad (10)$$

To solve for  $|g_0|L$ , we return to equation (7) for  $g$ , used to separate the problem, and evaluate  $g$  at  $r = 0$  and  $r = l$  using Eqns. (9).

$$\frac{g_0}{2} = -(I_1(0) + I_4(0)) \frac{g_0}{|g_0|} \tanh |g_0|L + \frac{A_2(l)A_4^*(0)}{\cosh |g_0|L}$$

$$\frac{g_0}{2} e^{\gamma l} = I_2(l) \frac{g_0}{|g_0|} \tanh |g_0|L + \frac{A_2(l)A_4^*(0)}{\cosh |g_0|L}$$

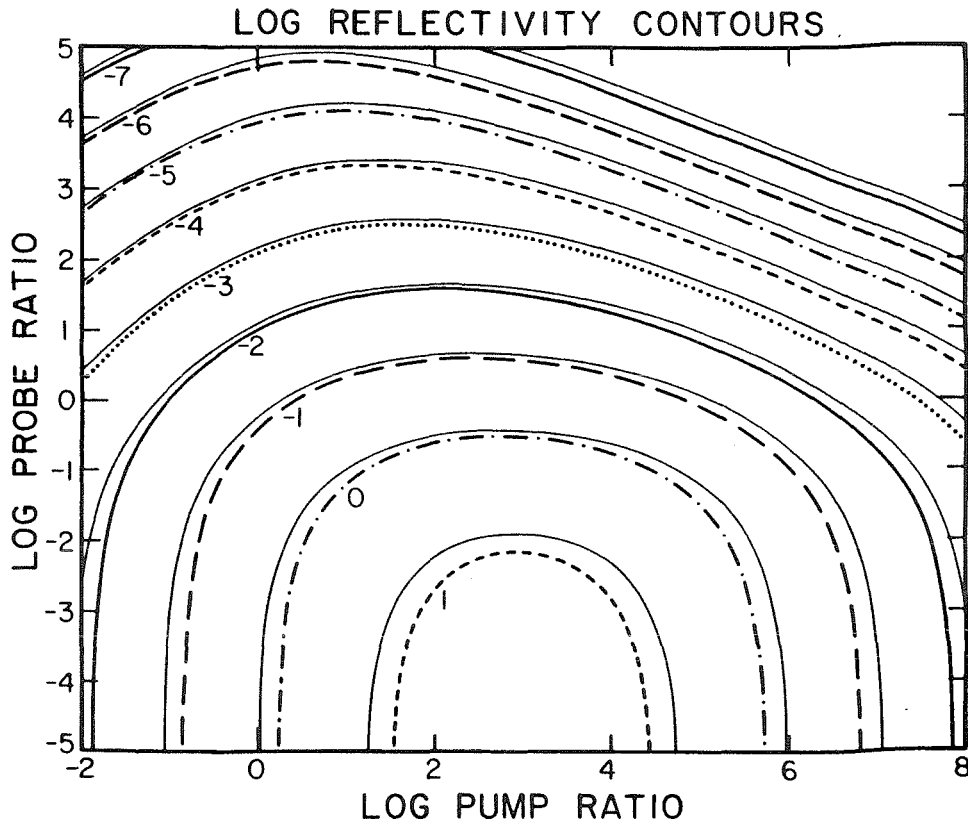
Solving the above equations for  $g_0$  and taking the magnitude yields two equations in  $|g_0|$  and  $|g_0|L$ . Eliminating  $|g_0|$ , we obtain:

$$\sinh |g_0|L = \frac{\sqrt{I_2(l)I_4(0)(1 \pm e^{-\gamma l})}}{I_1(0) + I_2(l)e^{-\gamma l} + I_4(0)} = \frac{\sqrt{(p+1)q(1 \pm e^{-\gamma l})}}{p + e^{-\gamma l} + (p+1)q} \quad (11)$$

Combining (10) and (11), we have an explicit expression for the reflectivity of the reflection grating as a function of the pump and probe ratios. As the probe ratio  $q \rightarrow 0$ , we expect the reflectivity to reduce to the solution obtained, in §4.3, with the undepleted pumps approximation. Of the two solutions above, only the one with the minus sign reduces to the proper answer. A contour plot of this solution, for  $\gamma l = -3$ , is shown in Fig. 4.8. Associated with each proper solution is an improper solution, obtained with the minus sign in (11), and shown by the fine solid lines in Fig. 4.8.

#### 4.5 Oscillation in four-wave mixing

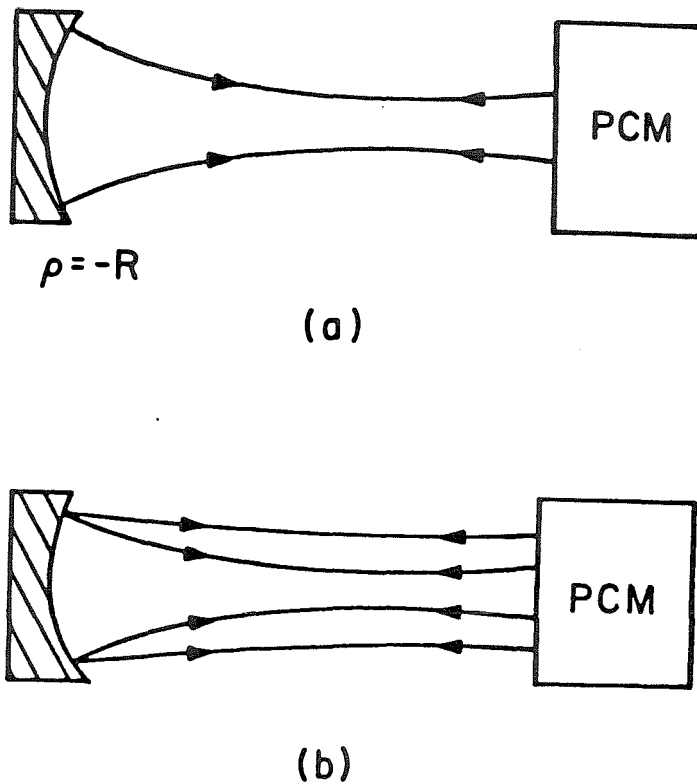
Oscillation in four-wave mixing was predicted in 1977 [2] and first observed in 1979 [9]. A PCM alone can oscillate if the reflectivity,  $R$ , of the mirror is infinite. A phase conjugate resonator (PCR), *i.e.*, a PCM, normal mirror pair, can oscillate if  $R$  is sufficient to overcome the losses (Fig. 4.9a). A loaded PCR, *i.e.*, a PCR containing an auxiliary source of gain, can oscillate if the combined gain is sufficient to overcome the losses. The first observation of oscillation was in the last category. The PCM was a  $\text{CS}_2$  cell pumped by a Q-switched ruby laser. The auxiliary gain was also a flash lamp pumped ruby rod. Subsequently, continuous wave oscillators have been constructed with a single domain crystal of  $\text{BaTiO}_3$  pumped with 514.5 nm light from an argon ion laser [10], strontium barium niobate



**Figure 4.8.** Contour plot of phase conjugate reflectivity for  $\gamma l = -3$  as a function of the pump ratio  $I_1(0)/I_2(l)$  and the probe ratio  $I_4(0)/[I_1(0) + I_2(l)]$ . The reflection grating is operative.

pumped with 488.0 nm light [11], and with a Na vapor cell pumped with a resonant wavelength from a tunable dye laser [12].

Much of the interest in PCR's is due to their unique stability and frequency spectrum. The standard stability analysis uses the ABCD matrix technique to



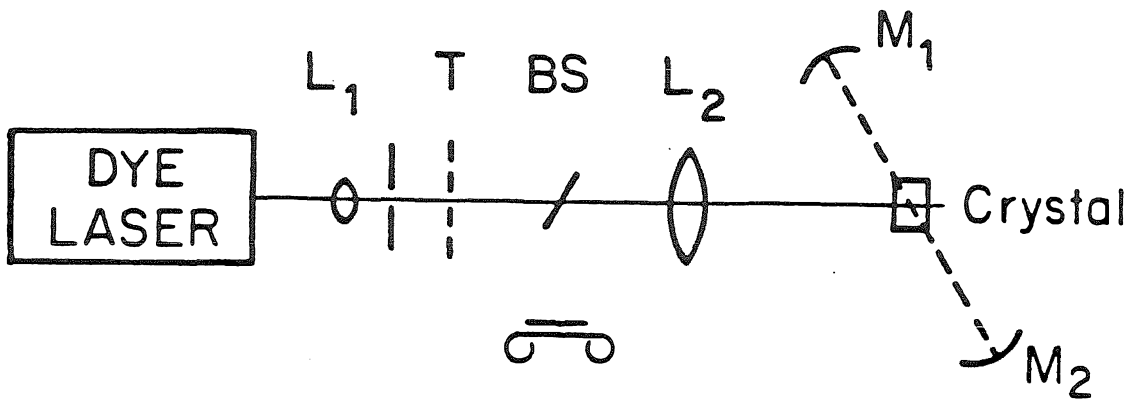
**Figure 4.9.** Sketch of a typical allowed PCR Gaussian mode for the degenerate case and demanding self-consistent field solutions for one (a) and two (b) round trips.

trace the evolution of the characteristics (spot size and wavefront curvature) of a Gaussian beam as it traverses a resonator. If the stability criterion is that the characteristics exactly repeat after one roundtrip, then the matrix analysis indicates that, at the normal mirror, the radii of curvature of the Gaussian beam and the mirror must be equal. Thus, both concave and convex normal mirrors are stable, independent of cavity length (Fig. 4.9a). Another unique feature is the existence of modes that repeat only after two round trips (Fig. 4.9b), for which there are no criteria for stability, *i.e.*, any wavefront will repeat after two

round trips [9].

#### 4.6 Self-pumped phase conjugate mirror

Oscillation has been observed in several configurations other than PCR's [13,15], of which perhaps the most interesting is shown in Fig. 4.10.



**Figure 4.10.** Self-pumped phase conjugate mirror geometry. The incident wave is shown by a solid line and the oscillation beams which it induces are dashed. The oscillation beams then serve as counterpropagating pumps and phase conjugate the incident wave.

The gain is provided by the two-beam coupling discussed in Chapter 3. The pump beam is the single beam incident upon the photorefractive crystal, which is situated within a Fabry-Perot resonator. The oscillation which builds up is shown by the dotted line. To the extent that the oscillating beams are phase conjugates of each other, they will act as the pump waves  $A_1$  and  $A_2$  of Fig. 4.1, and generate the phase conjugate of  $A_4$ . One would not necessarily expect the oscillation beams to be phase conjugates of each other, in view of the



inhomogeneous gain provided by an incident beam with any spatial information. However, a phase conjugate wave has been observed propagating backward relative to  $A_4$ . An imaging experiment has demonstrated the phase conjugation of a field containing pictorial information [14]. This configuration is called a *self-pumped phase conjugate mirror* because the oscillation beams do not have to be supplied externally [13,14]. Reflectivities greater than one are impossible in steady state, but reflectivities approaching one are theoretically possible and 30% has been observed. The alignment of the Fabry-Perot cavity is critical, but the alignment of the cavity relative to the incident wave is not. The acceptance angle has been measured to be  $20^\circ$  on either side of the crystal.

The single grating analysis of §4.4 can be applied to the PPCM [14]. The boundary conditions are no longer  $I_1(0)$  and  $I_2(l)$ , but are the reflectivities of the mirrors,  $M_1$  and  $M_2$ .

$$M_1 = I_{12}(0) \quad M_2 = 1 / I_{12}(l)$$

The cavity is assumed to be in resonance.  $M_1$  and  $M_2$  can be generalized to include other losses, *e.g.*, Fresnel reflections from the crystal surfaces, but not absorption losses within the crystal. A contour plot of  $R$  vs.  $M_1$  and  $M_2$  is shown in Fig. 4.11. It is apparent that  $R$  can be multivalued and is insensitive to  $M_1$  in the region of small  $M_1$  and large  $M_2$ . This corresponds to the region of Fig. 4.6, where  $R$  is insensitive to  $p$ , since as  $M_1 \rightarrow 0$ ,  $p \rightarrow \infty$ . The following section describes an experiment which proves that  $R$  remains finite even when  $M_1 = 0$ .

#### References for Chapter 4

1. B. Fischer, M. Cronin-Golomb, J.O. White & A. Yariv, Opt. Lett. **6**, 519 (1981).
2. A. Yariv and D.M. Pepper, Opt. Lett. **1**, 16 (1977).
3. J.F. Lam, Appl. Phys. Lett. **42**, 155 (1983).

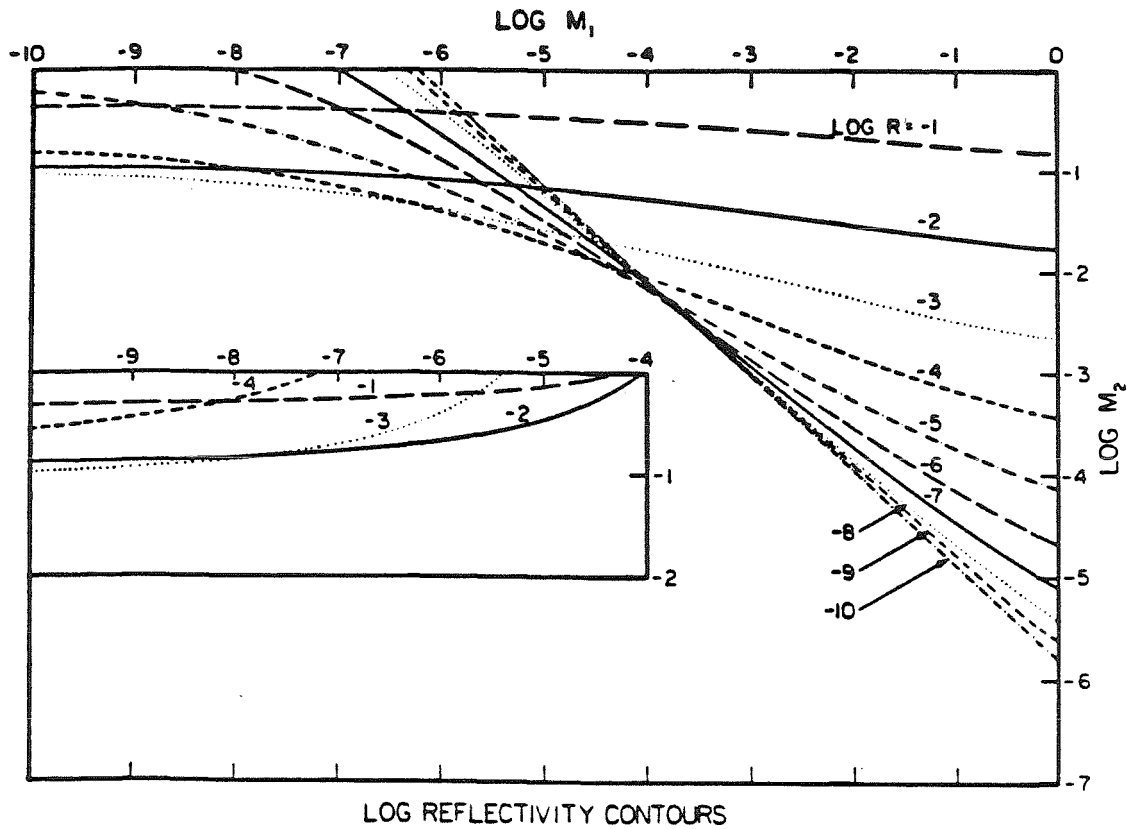


Figure 4.11. Contour plots of the reflectivity of the passive phase conjugate mirror. The coupling strength  $\gamma l = -3$ . Some of the contours at low  $M_1$  and high  $M_2$  have been redrawn as an insert.

4. J.H. Marburger and J.F. Lam, Appl. Phys. Lett. **34**, 389 (1979).
5. J.H. Marburger and J.F. Lam, Appl. Phys. Lett. **35**, 249 (1979).
6. H.G. Winful and J.H. Marburger, Appl. Phys. Lett. **36**, 613 (1980).
7. A.R. Kessel and V.M. Musin, Opt. Comm. **44**, 133 (1982).
8. M. Cronin-Golomb, J.O. White, B. Fischer & A. Yariv, Opt. Lett. **7**, 313 (1982).

9. J. Au Yeung, D. Fekete, D.M. Pepper & A. Yariv, IEEE J. Quant. Elect. **15**, 1180 (1979).
10. J. Feinberg and R.W. Hellwarth, Opt. Lett. **5**, 519 (1980). ; **6**, 257 (1981).
11. B. Fischer, M. Cronin-Golomb, J.O. White, A. Yariv & R. Neurgaonkar, Appl. Phys. Lett. **40**, 863 (1982).
12. R.C. Lind and D.G. Steel, Opt. Lett. **6**, 554 (1981).
13. J.O. White, M. Cronin-Golomb, B. Fischer & A. Yariv, Appl. Phys. Lett. **40**, 450 (1982).
14. M. Cronin-Golomb, B. Fischer, J.O. White & A. Yariv, Appl. Phys. Lett. **41**, 689 (1982).
15. M. Cronin-Golomb, B. Fischer, J.O. White & A. Yariv, Appl. Phys. Lett. **42**, 919 (1983).

## 5. APPLICATIONS

### 5.1 Introduction

The applications that are currently envisioned for four-wave mixing and phase conjugation may be outlined as follows:

- I. Spatial domain applications
  - A. Aberration compensation
  - B. Spatial information processing
  - C. Interferometry
- II. Temporal and frequency domain applications
  - A. Frequency filtering
  - B. Temporal signal processing
- III. Nonlinear spectroscopy

4WM has also been proposed for generating two-photon coherent states, which could be a fourth category.

In this chapter, three applications to aberration compensation and spatial information processing are described.

### 5.2 Laser with dynamic holographic intracavity distortion correction

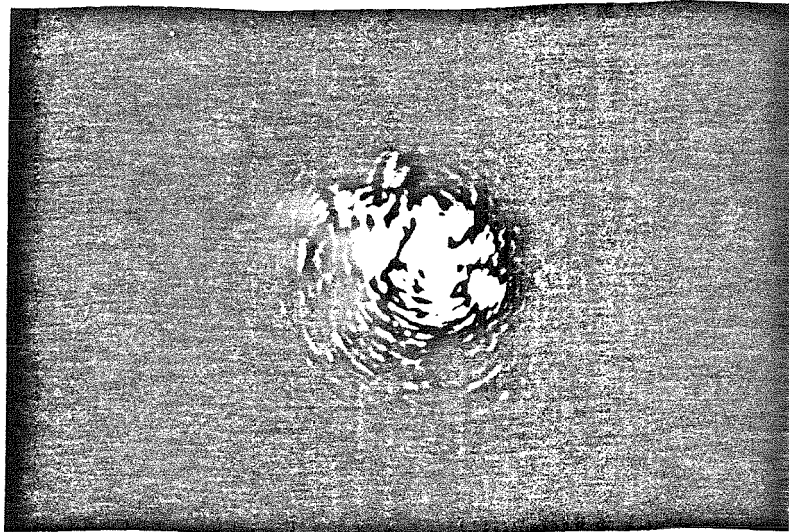
Phase conjugate resonators employing PCM's make use of both the spatial and frequency characteristics of 4WM (see §4.5). Distortions in laser resonators with normal mirrors commonly arise because of defects in laser rods, turbulence in gaseous gain media, imperfect optics, thermal effects, and nonlinear effects. By using the passive (self-pumped) phase conjugate mirror (PPCM) described in §4.6 as one mirror of a laser, we were able to demonstrate its distortion correcting capability [1]. The possibility of using real-time holography to compensate for intracavity distortions had been proposed [2].



Fig. 5.1a shows the starting arrangement. Lasing is initially induced at the high gain line, 488nm, between mirror  $M_1$  and beamsplitter BS. Light transmitted through the beamsplitter pumps the crystal C which is placed in the  $M_3$ - $M_4$  resonator. Gain through two-beam coupling (see Chapter 3) causes an oscillation to build up in the resonator. Reflecting mirror  $M_2$  can be used to assist in the buildup. With oscillation established, the beamsplitter and the retroreflecting mirror  $M_2$  are removed, as in Fig. 5.1b. The starting procedure described above is required since the coherence of the fluorescence is insufficient to allow the formation of the required refractive index grating in the crystal. Once the grating is established, the configuration of Fig. 5.1b corresponds to an equilibrium state, and the grating in the crystal is continuously maintained by the very beams which it couples together.

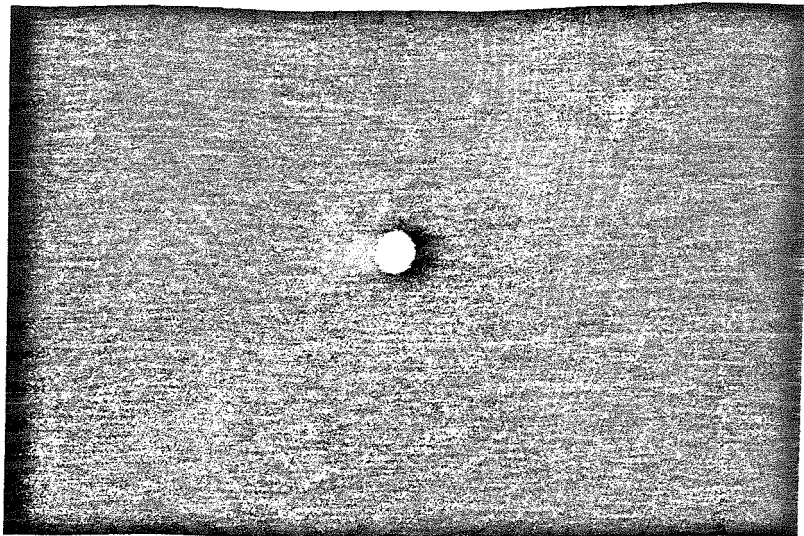
According to the theory of the PPCM, there is a certain two-beam coupling strength, in the crystal, above which it is possible to maintain oscillation between the crystal and  $M_3$  even in the absence of mirror  $M_4$  (see Fig. 4.11). We were able to demonstrate such oscillation in our resonator. Fig. 5.1c depicts the starting arrangement. Once oscillation involving mirror  $M_3$  was established, the beamsplitter and  $M_2$  were removed and the laser continued to oscillate, as in Fig. 5.1d. In this configuration, the crystal looks much like a distortion correction element to be inserted into an existing laser cavity without replacing either mirror.

The distortion correcting capability of the laser is apparent from the pictures of the output shown in Fig. 5.2. The photographs in Fig. 5.2 were taken 1 m from the output mirror  $M_1$ . Inserting the etched glass into the normal laser cavity destroyed the mode and lowered the output power from 2W to 1 mW, at 38A tube current. Replacing the normal mirror with a PPCM restored the mode shape and boosted the power output back to 500mW. The distortion correction indicates that each of the oscillations - one in the  $M_1$ /crystal arm and the other in the



(a)

5mm



(b)

5mm

**Figure 5.2.** Experimental comparison of the mode quality of a laser with and without distortion correction by a PPCM.

- a. Output of normal laser with distortion inside the cavity.
- b. Output with one mirror replaced with PPCM.

$M_3$ /crystal arm - is composed of two oppositely traveling waves which are phase conjugates of each other (Fig. 5.1d). This mode of oscillation may not be the

only allowed stable configuration but in the presence of spatial filters such as the plasma bore tube, it is the minimum diffraction loss configuration and thus the one surviving in a laser oscillator.

The amount of light lost from the PCM is small. At a 24A tube current, the beam extending straight through the crystal from the discharge tube had an intensity of 6mW. The beam extending straight through the crystal from  $M_3$  had an intensity of 16mW. These are to be compared with an intensity of 600mW in the  $M_1$ /crystal cavity.

The pump beams in a PPCM are not independent of each other or of the input beam, in contrast to an ordinary PCM. This loss of independence means that the half-axial,  $c/4L$  longitudinal modes of an ideal PCR are not observed. (L stands for the mirror spacing.) The frequency spectrum of the original laser was multi-mode, with the  $c/2L$  mode spacing of an ordinary resonator.

In other laboratories, several self-pumped mirrors have been developed, subsequent to our work, all of which make use of the photorefractive effect. One version makes use of total internal reflection from crystal faces to replace the external Fabry-Perot cavity [3]. Another version has been used as the end mirror on a Cu vapor laser, wherein the spontaneous emission from the laser is sufficient to initiate operation [4].

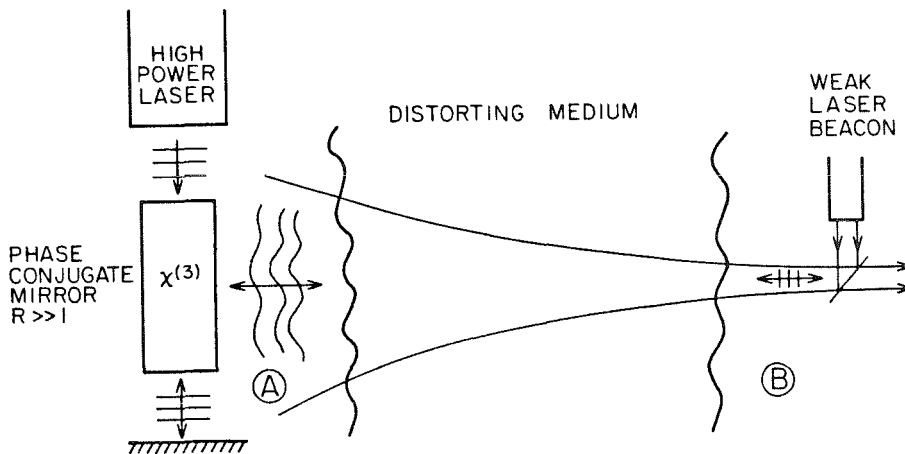
### **5.3 One-way image transmission through inhomogeneous media**

Aberration compensation can be performed before a distorted image is received (predetection) or after (postdetection). In the latter category, iterative techniques have been proposed for restoring linearly degraded images [5], restoring finite energy optical objects from limited spatial and spectral information [6], and optically implementing Gerschberg-type algorithms for reconstructing an object from the modulus of its Fourier transform [7] and image extrapolation [8]. Coherent optical processors for solving the above restoration problems and



processors designed to solve differential and integral equations [9,10] rely on mirrors to send a wavefront on multiple passes through some kind of filter. It has been proposed that PCM's should find use here because of their wavefront reversal properties and because the possibility of reflection with gain should breathe new life into systems which in the past were deemed impractical because of reflection losses [11].

An example in the predetection category is a scheme for transmitting a laser beam from point A to point B through a distorting medium, say the atmosphere [12].



**Figure 5.3.** Scheme for transmitting a laser beam from point A to point B through a distorting medium.

A beam will normally spread due to the finite size of the aperture at A. If diffraction were the only factor present, the size of the beam at B would be diffraction limited, and could be made smaller only through the use of a waveguide. Other factors make the diffraction limit difficult to achieve. The beam can be distorted by atmospheric turbulence, or, if the beam is intense enough, it will also encounter, or create, distortions such as thermal blooming.

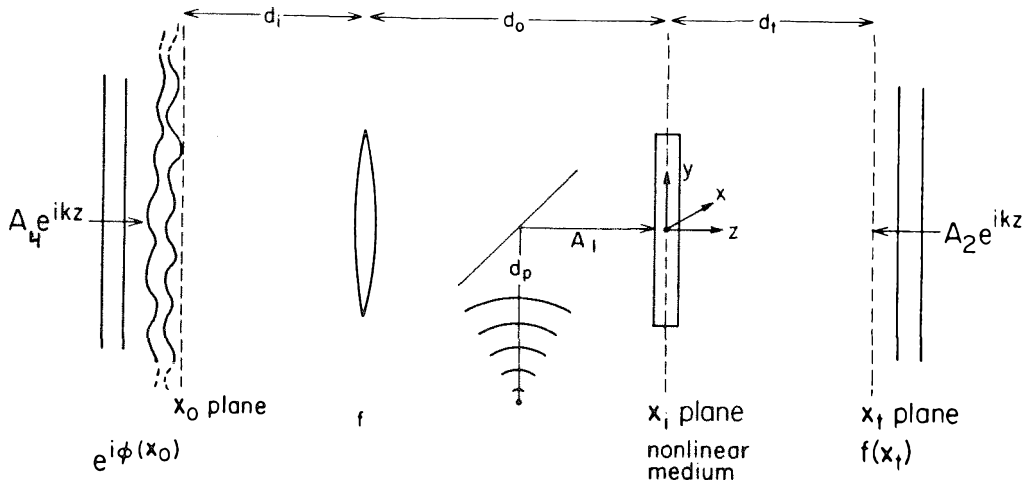
To solve the latter two sources of degradation, we may first transmit a *beacon* or probe beam from B to A, so that it acquires or measures the total distortion in transit (Fig. 5.3). Next the phase conjugate is generated at A. Upon reversing its path, the phase conjugate wave should arrive at B with the same phase and amplitude distribution as the originally transmitted wave. To correct for *non-linear* stationary, lossless distortions, the PCM must have a reflectivity of unity [13].

The finite size (resolution) of the PCM will limit the severity of the distortions in the far field (near field) which can be corrected. Such imaging by phase conjugation requires that the picture field pass twice through the distortion which is a major disadvantage in the large number of practical situations where the pictorial information is to be transmitted in a single direction only.

A holographic scheme for dealing with this situation has been proposed and demonstrated [14]. It requires the presence of a reference wave originating on the same side of the distortion as the object. If both waves propagate through essentially the same path, on the receiving side the distortions can be removed in the recording process by mixing the two distorted waves. Conventional or real-time holography provides such a mixing operation. The reconstruction takes place at the receiving station when the hologram is illuminated with an undistorted reference to obtain an aberration free image.

For situations where the object and reference are located on opposite sides of an aberrating path, a new scheme for one way image transmission has been proposed and demonstrated in our laboratory [15,16]. It does not involve wavefront reversal *per se* but it does utilize 4WM. The technique is limited to purely phase distortions characterized by a multiplicative complex amplitude to be transmitted  $t = e^{i\varphi(x,y)}$ . If the distortion and its conjugate,  $t^* = e^{-i\varphi(x,y)}$ , were in contact, the combination of the two would be homogeneous, *i.e.*  $tt^* = 1$ , independent of  $x$  and  $y$ . Our technique consists of creating the conjugate distortion in real-time

within a nonlinear medium (NLM) and imaging the NLM and the distortion together with a lens (Fig. 5.4).



**Figure 5.4.** Technique for one-way field transmission through a thin phase distortion.

The conjugate distortion is created by nonlinear mixing of a distorted and an undistorted reference wave. The undistorted reference originates on the same side of the distortion as the object. The distorted reference originates on the opposite side of the distortion, and propagates through the distortion and the lens. Both references are incident upon the NLM and a phase hologram is formed which is a conjugate replica of the distortion. The object wave  $E_2$  is then able to pass unaberrated through the hologram-lens-distortion combination.

The technique of one-way image transmission can be understood in more detail by a) propagating each of the three fields from their respective starting planes to the NLM, b) obtaining the third-order nonlinear polarization,  $P_{NL}$ , in the medium, and c) calculating the field, radiated by  $P_{NL}$ , which propagates back through the distortion. The undistorted reference wave  $E_1$  is a spherical wave originating at a point source of amplitude  $A_1$  situated at  $r_p$

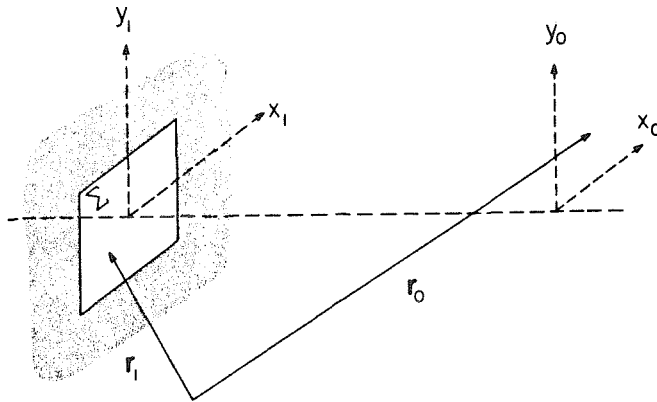
$$E_1(\mathbf{x}_i, z) = A_1 \frac{e^{ik|\mathbf{r}_p - \mathbf{r}_i|}}{i\lambda|\mathbf{r}_p - \mathbf{r}_i|} = A_1 \frac{\exp ik(d_p + z + \frac{|\mathbf{x}_i|^2}{2(d_p + z)})}{i\lambda(d_p + z)} \quad (1)$$

$$\equiv A_1(z) \exp ik(d_p + z + \frac{|\mathbf{x}_i|^2}{2(d_p + z)})$$

Here  $\mathbf{r}_i$  is a vector which spans the NLM,  $\mathbf{x}_i = (x_i, y_i)$  is the transverse part of  $\mathbf{r}_i$ , and  $z$  is the longitudinal part. The above approximation, called the Fresnel approximation, is valid when

$$z^3 \gg \frac{\pi}{4\lambda} |\mathbf{x}_p - \mathbf{x}_i|_{\max}^4$$

The spatial information to be transmitted  $f(\mathbf{x}_i)$  is recorded in a transparency and illuminated by a plane wave  $A_2$ . The field,  $E(\mathbf{r}_0)$ , radiated by an extended source,  $E(\mathbf{r}_1)$ , specified over an aperture  $\Sigma$ , is given by the Rayleigh-Sommerfeld diffraction formula (see Fig. 5.5).



**Figure 5.5.** Diffraction of a plane wave by an aperture  $\Sigma$ . The field at the aperture is treated as an extended source, spanned by  $\mathbf{r}_1$ . The field at  $\mathbf{r}_0$  can be calculated with the Rayleigh-Sommerfeld diffraction formula.

$$E(\mathbf{r}_0) = \int_{\Sigma} E(\mathbf{r}_1) \frac{\exp ik|\mathbf{r}_0 - \mathbf{r}_1|}{i\lambda|\mathbf{r}_0 - \mathbf{r}_1|} d^2\mathbf{r}_1 \quad (2)$$

Applying the Fresnel approximation again we obtain

$$E(\mathbf{r}_0) = \int_{\Sigma} E(\mathbf{r}_1) \frac{\exp ik \left[ z_0 - z_1 + \frac{|\mathbf{x}_0 - \mathbf{x}_1|^2}{2(z_0 - z_1)} \right]}{i\lambda(z_0 - z_1)} \quad (3)$$

Thus, within the NLM, the field  $E_2$  is given by

$$E_2(\mathbf{x}_i, z) = \int A_2 f(\mathbf{x}_t) \frac{\exp ik \left[ d_t - z + \frac{|\mathbf{x}_t - \mathbf{x}_i|^2}{2(d_t - z)} \right]}{i\lambda(d_t - z)} d^2\mathbf{x}_t \quad (4)$$

The  $z$  dependence of the denominator can be dropped, providing the NLM is thin enough such that within it,  $z \ll d_t$ .

The distorted reference wave is obtained by illuminating the distortion with a beacon, plane wave  $A_4$ . If  $d_o$ ,  $d_i$ , and  $f$  satisfy the lens law,  $\frac{1}{d_o} + \frac{1}{d_i} = \frac{1}{f}$ , then the distortion is imaged into the NLM. The imaging properties of lenses can be derived by using Fresnel diffraction to describe the propagation between the object plane and the image plane. Propagation through the lens is described by a multiplicative transmission function

$$t(\mathbf{s}) = \exp ik(n\Delta - |\mathbf{s}|^2 / 2f) \quad (5)$$

where  $n$  is the index of refraction of the lens,  $\Delta$  is the on-axis thickness, and  $\mathbf{s}$  is a vector in the plane of the lens. The field in the neighborhood of the image plane,  $E_i(\mathbf{x}_i, z)$ , is related to the field at the object plane,  $E_o(\mathbf{x}_o)$ , by

$$E_i(\mathbf{x}_i, z) = -\frac{d_o}{d_i} E_o\left(-\mathbf{x}_i \frac{d_o}{d_i}\right) \exp ik \left\{ \xi + \frac{|\mathbf{x}_i|^2}{2d_i} \left(1 + \frac{d_o}{d_i}\right) \right\} \quad (6)$$

where  $\xi = d_o + n\Delta + d_i$ . We have assumed that the lens has infinite transverse extent, *i.e.*, no aperture, and that the  $z$  dimension of the NLM is thin enough so that

$$\exp\left[-\frac{ikz}{2d_i^2}|\mathbf{s}-\mathbf{x}_i|_{\max}^2\right] = 1 \quad (7)$$

If the distortion is characterized by a random phase  $\varphi(\mathbf{x}_o)$ , then, according to (6), the distorted reference will be of the form

$$E_4(\mathbf{x}_i, z) = -\frac{d_o}{d_i}A_4 \exp\left[i\varphi\left(-\mathbf{x}_i \frac{d_o}{d_i}\right)\right] \exp ik\left[\xi + \frac{|\mathbf{x}_i|^2}{2d_i}\left(1 + \frac{d_o}{d_i}\right)\right] \quad (8)$$

Here we have used a Born type approximation, having assumed that the non-linear interaction is weak enough so that the three input fields are unaffected, *i.e.*, known everywhere. In reality, the three input fields are coupled, in the manner described in Chapter 4, to each other and to new waves generated within the NLM.

In NLM possessing a third-order susceptibility,  $\chi^{(3)}$ , a polarization is induced which is proportional to the cube of the total field. The particular term of interest is

$$P_{NL} = \chi^{(3)}E_1E_2E_4^* \quad (9)$$

which radiates a field, propagating backward relative to  $E_4$ , of the same frequency. The field  $E(\mathbf{r}_o)$  radiated by such a polarization is given by a Green's function solution

$$E(\mathbf{r}_o) = \frac{4\pi^2}{\lambda^2} \int P_{NL}(\mathbf{r}_1) \frac{\exp ik|\mathbf{r}_o-\mathbf{r}_1|}{|\mathbf{r}_o-\mathbf{r}_1|} d^3\mathbf{r}_1 \quad (10)$$

The similarity between (2) and (10) indicates that, by applying the Fresnel approximation to (10), we can show that the field radiated by  $P_{NL}$  is also imaged by the lens, in analogy to (6)

$$E_3(\mathbf{x}_o) = -\int_{-i/2}^{i/2} \frac{d_i}{d_o} \frac{4\pi^2}{\lambda} P_{NL}\left(-\mathbf{x}_o \frac{d_i}{d_o}, z\right) \exp ik\left[\xi + z + \frac{|\mathbf{x}_o|^2}{2d_o}\left(1 + \frac{d_i}{d_o}\right)\right] dz \quad (11)$$

$$= 4\pi^2 \chi^{(3)} \frac{A_1 A_2 A_4^*}{i\lambda d_t} \frac{t}{\lambda} \exp i k (d_p + d_t + \frac{|\mathbf{x}_o|^2}{2d_p} \frac{d_i^2}{d_o^2}) e^{-i\varphi(\mathbf{x}_o)} \int f(\mathbf{x}_t) \exp i k \frac{|\mathbf{x}_t + \mathbf{x}_o \frac{d_i}{d_o}|^2}{2d_t} d^2 \mathbf{x}_t$$

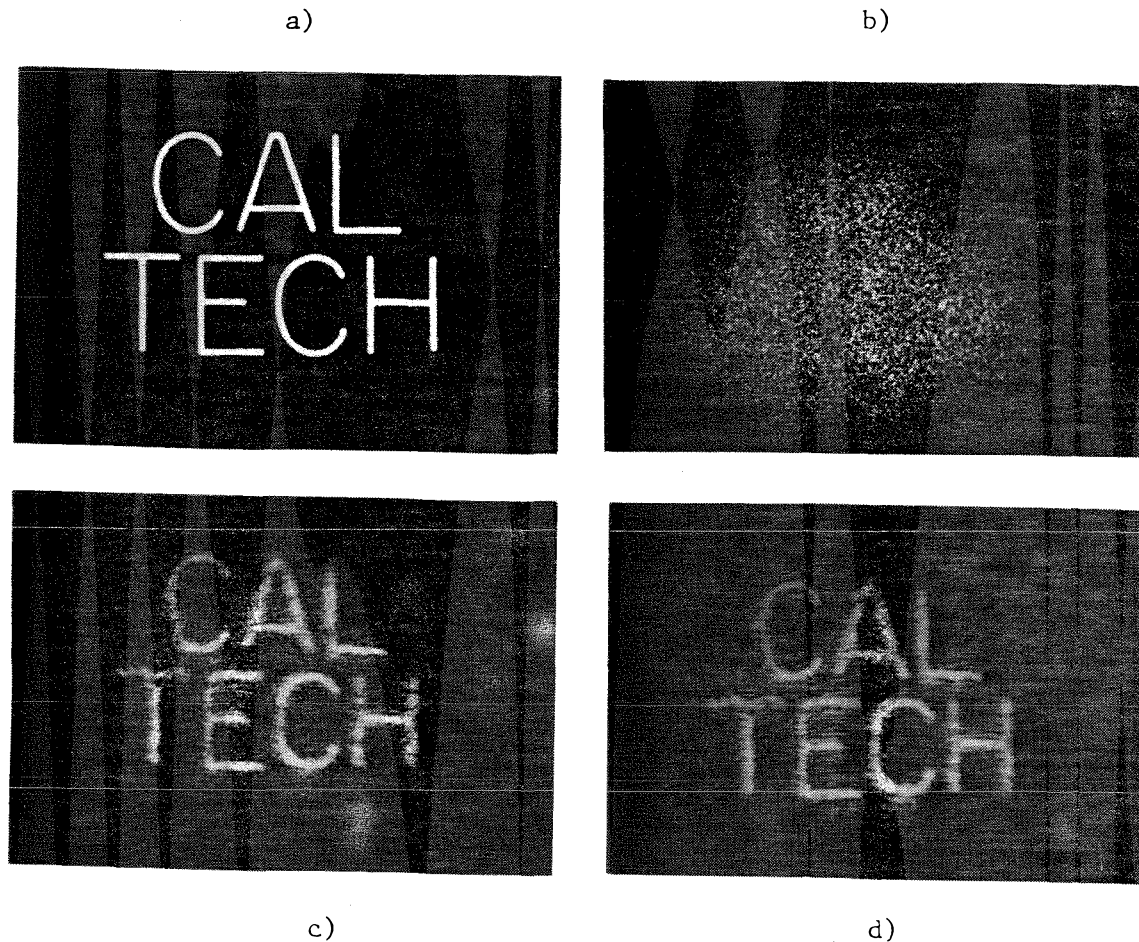
where we have substituted (1), (4), and (8) into (9), and used an approximation similar to (7).

We see that the field incident upon the distortion from the right has been pre-multiplied by the complex conjugate of the distortion transmission function, so that the transmitted field will contain no trace of the distortion. If  $d_p \rightarrow \infty$ , *i.e.*, the undistorted reference is a plane wave, then the field which is transmitted through the distortion will be an inverted version of (4), the original object field,  $E_2$ , as it was incident upon the NLM. The combination of distortion, lens, and NLM thus behaves like a homogeneous medium for fields incident from the right.  $E_2$  may be amplified for sufficiently strong fields  $A_1$ , and  $A_2$ , and may be rescaled by  $d_i/d_o$ .

In practice, the angular separation between the two reference beams forms a carrier spatial frequency, within the hologram, which is then modulated with the information about the distortion.

The object used in the experiment was a transparency containing the letters "CALTECH", shown in Fig. 5.6a. The distortion is a piece of ground glass. The object and distortion are both illuminated in transmission. The nonlinear medium is a poled  $7 \times 4.5 \times 4 \text{ mm}^3$  single crystal of  $\text{BaTiO}_3$ . All three waves incident upon the crystal are provided by the same argon ion laser operating at 514.5 nm.

An attempt to photograph the object through the ground glass is shown in Fig. 5.6b. The wavefront is obliterated by the random phase distortion. Fig. 5.6c is an image of the object field transmitted through the phase conjugate window, showing almost complete reconstruction. Fig. 5.6d is an image of the object field transmitted through the crystal alone, showing that the residual aberrations are



**Figure 5.6.** Experimental results for one-way field transmission obtained with the configuration of Fig. 5.4.

- a. The object to be transmitted.
- b. An attempt to photograph the object through the distortion without any compensation, showing the severity of the distortion.
- c. A photograph of the field transmitted through the phase conjugate window.
- d. A photograph of the field transmitted through the phase conjugate window without the ground glass distortion, *i.e.*, transmitted through the crystal alone.

due to inhomogeneities within the crystal itself.



#### 5.4 Spatial convolution and correlation via four-wave mixing

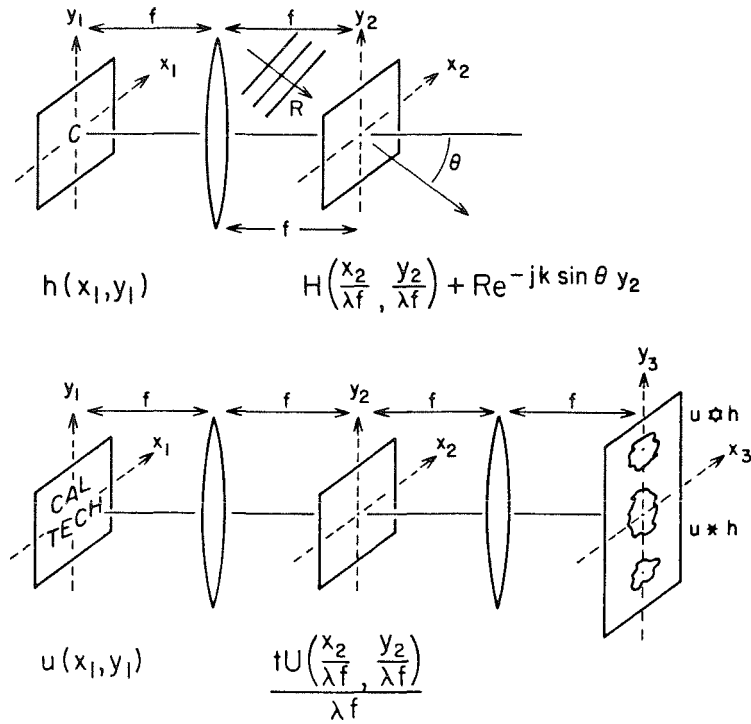
Coherent and incoherent optical processors have been used for pattern recognition, guidance systems, image deblurring, edge enhancement, and synthetic aperturing. The special type of nonlinearity present in the photorefractive effect can be used to advantage in edge enhancement [17,18]. The utility of gratings for optical processing has been demonstrated [19]. For example, a grating placed in the filter plane of a coherent optical processor can translate, add, and subtract input pattern functions. Multiple gratings can also be used to obtain first- or higher-order derivatives of intensity distributions, and restore smeared or multiply exposed images [19].

The concept can be generalized beyond gratings in the filter plane to the production of more complicated Van der Lugt filters [20]. In the Van der Lugt technique, a filter with impulse response  $h(x,y)$  is first synthesized by exposing film to the interference pattern of a plane reference wave,  $R$ , and the Fourier transform,  $H = F\{h\}$  (Fig. 5.7a).  $H$  is obtained in the back focal plane of a lens when  $h$  is in the front focal plane (see (13) below). The film is developed to produce a transparency with an amplitude transmittance proportional to the intensity incident during exposure

$$t(x_2, y_2) \propto I(x_2, y_2) = |R|^2 + \frac{|H|^2}{\lambda^2 f^2} + R^* e^{ik \sin \theta y_2} \frac{H}{\lambda f} + R e^{-ik \sin \theta y_2} \frac{H^*}{\lambda f}$$

The developed film is then reinserted into the filter plane, and the object  $u(x,y)$  to be processed is inserted into the input plane in place of  $h$  (Fig. 5.7b). Now the field  $U$  is incident upon the filter and one component of the field leaving the transform plane is proportional to the product  $HU$ . Propagating through the second lens gives  $h * u$  at the output plane, by the convolution theorem, where  $*$  denotes convolution.

A nonlinear medium can be substituted for the film, allowing for rapid



**Figure 5.7.** The Van der Lugt technique.

- a. Constructing the Van der Lugt or matched filter.
- b. Convolving and correlating an input pattern function with the impulse response of the Van der Lugt filter.

modification of the filter. Some caution must be exercised when making such a substitution. Strictly speaking, for an object in the front focal plane of a lens, the exact Fourier transform only exists at one plane in space, the back focal plane. Depending on the confocal parameter of the system, a good or bad approximation to the transform may exist in some noninfinitesimal region about the focal plane [20]. This puts a limit on the thickness,  $t$ , of both volume filters and film emulsions,

$$t < 2f^2\lambda / r_{\max}^2, \quad (12)$$

where  $r_{\max}$  is the spatial extent of the largest input field, and  $f$  is the focal length of the lens.

Also, filters made from photographic film are unaffected by light after the developing process, whereas photorefractive materials remain sensitive to light in the absence of some fixing process [21]. Birefringent and optically active nonlinear media introduce more complications that can turn out to be useful for improving performance [22]. Finally, we know that volume gratings have amplitude transmittances that depend strongly on the wavelength and angle of illumination [23]. So, the synthesis of a dynamic volume filter must be done keeping the intensity, direction, wavelength, and polarization of the readout beam in mind.

For real-time operation of the processor,  $h$  and  $u$  must be present concurrently. Since they can no longer both be on axis, the filter cannot be read from the same angle at which it was written. For thin nonlinear filters, this is not a problem since the amplitude transmittance does not depend strongly on the angle of illumination. However, the diffraction efficiency will be limited due to the thinness of the filter, and, if a thin saturable absorber is used as the nonlinear medium, the requisite writing intensity may have to be provided by a Q-switched laser [19].

So, we need to write the filters (gratings) in thick media, subject to the above thickness constraint, but wish to avoid the concomitant angular dependence, particularly on the polar angle relative to the average grating vector.

One approach is to illuminate at the same polar angle, but a different azimuthal angle about the grating vector [24]. This introduces an astigmatic aberration into the filter output, but satisfactory results were obtained in a system which writes absorption gratings in cryptocyanine dye with  $\text{MW}/\text{cm}^2$  intensities.

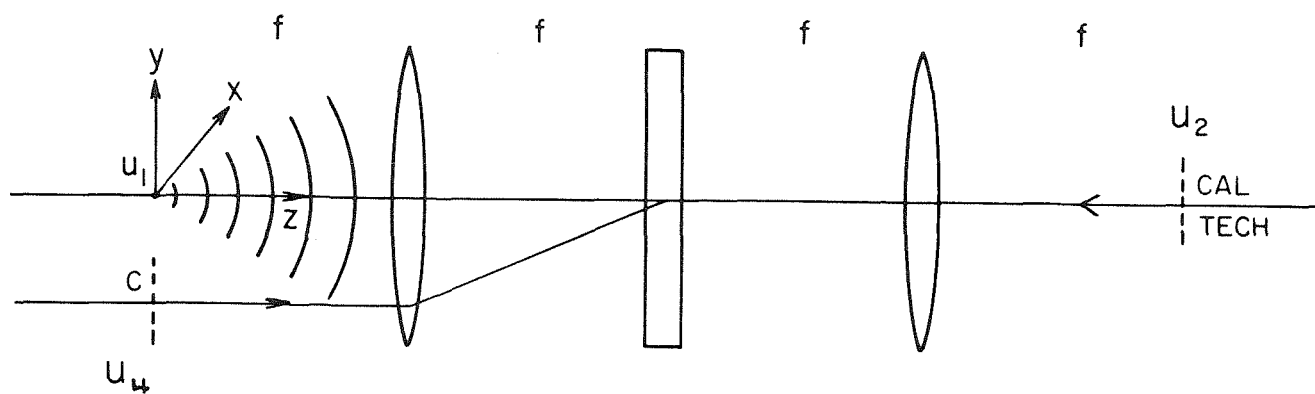
Another approach is to use different wavelengths so that the two input beams can be superimposed. Convolution and correlation can be generated in this way by sum and difference frequency mixing in KDP [25,26]. No reference is needed, but the use of multiple wavelengths (first, second, and third harmonics of Nd:YAG) introduces spatial scaling which may be objectionable. Dispersion in the medium may require precise alignment in order to achieve phase matching.

Another system illuminated both input objects with the 488nm wavelength from an argon laser, and used a 632.8nm HeNe beam for the reference [27]. In contrast to the Van der Lugt sequence, here two transformed input fields interfere to write a complicated index pattern in a photorefractive medium. Readout is performed by the reference beam, which is almost superimposed with one of the inputs, but misaligned slightly so as to be incident at the Bragg angle. The photorefractive material was BSO, which is less sensitive to red than blue, so the reference beam provides a nearly nondestructive readout.

A solution involving 4WM, which requires only one wavelength, has been proposed and demonstrated in our laboratory [28,29]. In the grating picture, it corresponds to illumination at the Bragg angle, but in the reverse direction. Again the nonlinear medium is placed in the common focal plane of a two lens system as shown in Fig. 5.8. Let us examine its operation in the nonlinear optics picture, and let all three input fields contain arbitrary amplitude and phase information. The input complex amplitudes  $u_1(x,y)$ ,  $u_2(x,y)$ , and  $u_4(x,y)$ , in the outer focal planes are Fourier transformed by propagating to the common focal plane. The transformed fields  $U_1$ ,  $U_2$ , and  $U_4$  induce nonlinear polarizations in the medium. The polarization

$$P = \chi^{(3)} U_1 U_2 U_4^*$$

radiates an output field that propagates essentially backward relative to beam four, returning through lens L. The convolution theorem says that the



**Figure 5.8.** Four-wave mixing configuration for performing spatial convolution and correlation of images.

transform of the product  $U_1 U_2$  is the convolution of the transforms  $u_1 * u_2$ . Accordingly, it can be shown that the output field, when evaluated at the plane located a distance  $f$  in front of lens  $L$ , is of the form

$$u_3 \propto u_1(\mathbf{x}) * u_2(\mathbf{x}) * u_4^*(\mathbf{x})$$

The performance of this processor can be understood in more detail by a) propagating each of the three input fields to the NLM, b) obtaining the third-order nonlinear polarization  $P_{NL}$  in the medium, and c) evaluating the field radiated by  $P_{NL}$  at the output plane of the processor.

The derivations of the Fourier transforming and imaging (see §5.3) properties of lenses are very similar. Using Fresnel diffraction (3), and the thin lens transmission function (5), one can show that the field,  $E_b$ , in the neighborhood of

the back focal plane of a lens, is related to the field,  $u$ , in the front focal plane by

$$E_b(\mathbf{x}, z) = \frac{\exp i k (n\Delta + z)}{i\lambda f} F \left\{ u(\mathbf{x}) \exp \frac{i k}{2f} \frac{2f - z}{f} |\mathbf{x}|^2 \right\} \quad (\mathbf{f} \rightarrow \frac{\mathbf{x}}{\lambda f})$$

where  $F\{\dots\}$  stands for the two dimensional Fourier transform, and  $\mathbf{f} = (f_x, f_y)$ .

When the transverse spatial extent,  $r_{\max}$ , of  $u(\mathbf{x})$ , and the  $z$  dimension of the NLM are small enough so that  $|2f - z| \ll 2f^2 / r_{\max}^2$  then

$$E_b(\mathbf{x}, z) = \frac{\exp i k (n\Delta + z)}{i\lambda f} U(\frac{\mathbf{x}}{\lambda f}) \quad (12)$$

where  $U(\mathbf{f}) = F\{u(\mathbf{x})\}$ . Therefore, within the NLM, the three input fields are given by

$$E_1(\mathbf{x}, z) = \frac{\exp i k (n\Delta + z)}{i\lambda f} U_1(\frac{\mathbf{x}}{\lambda f}) \quad (14a)$$

$$E_2(\mathbf{x}, z) = \frac{\exp i k (n\Delta + 4f - z)}{i\lambda f} U_2(\frac{\mathbf{x}}{\lambda f}) \quad (14b)$$

$$E_4(\mathbf{x}, z) = \frac{\exp i k (n\Delta + z)}{i\lambda f} U_4(\frac{\mathbf{x}}{\lambda f}) \quad (14c)$$

In a NLM possessing a third-order nonlinear optical susceptibility, a polarization is induced which is proportional to the cube of the total optical field. The particular term of interest is

$$P_{NL} = \chi^{(3)} E_1 E_2 E_4^* \quad (15)$$

which radiates a field, propagating backwards relative to  $E_4$ , of the same frequency. The field, at an observation point  $\mathbf{r}_0$ , induced by this polarization, is given by the Green's function solution (10). Applying the Fresnel approximation to this solution, we can show that the field radiated by this polarization is also transformed by propagating through a lens, in analogy to (13).

$$E_3(\mathbf{x}, 0) = \int_{2f - z_0/2}^{2f + z_0/2} \frac{\exp i k (n\Delta + z)}{i\lambda f} F \left\{ \frac{i 4 \pi^2}{\lambda} P_{NL}(\mathbf{x}, z) \right\} dz \quad (\mathbf{f} \rightarrow \frac{\mathbf{x}}{\lambda f})$$

$$= \int_{2f-z_0/2}^{2f+z_0/2} \frac{\exp i k(2n\Delta + 4f)}{-(i\lambda f)^4} \frac{i4\pi^2}{\lambda} \chi^{(3)} F \left\{ U_1\left(\frac{\mathbf{x}}{\lambda f}\right) U_2\left(\frac{\mathbf{x}}{\lambda f}\right) U_4^*\left(\frac{\mathbf{x}}{\lambda f}\right) \right\} dz \quad \left( f \rightarrow \frac{\mathbf{x}}{\lambda f} \right)$$

This result for the output of the processor can be simplified with the convolution theorem [20] which states that the transform of the product equals the convolution of the transforms, *i.e.*,

$$F\{GH\} = g * h$$

Therefore

$$E_S(\mathbf{x}, 0) = -i \frac{4\pi^2}{\lambda} \frac{\chi^{(3)} z_0}{\lambda^4 f^4} u_1(\mathbf{x}) * u_2(\mathbf{x}) \otimes u_4(-\mathbf{x}) \exp i k(2n\Delta + 4f)$$

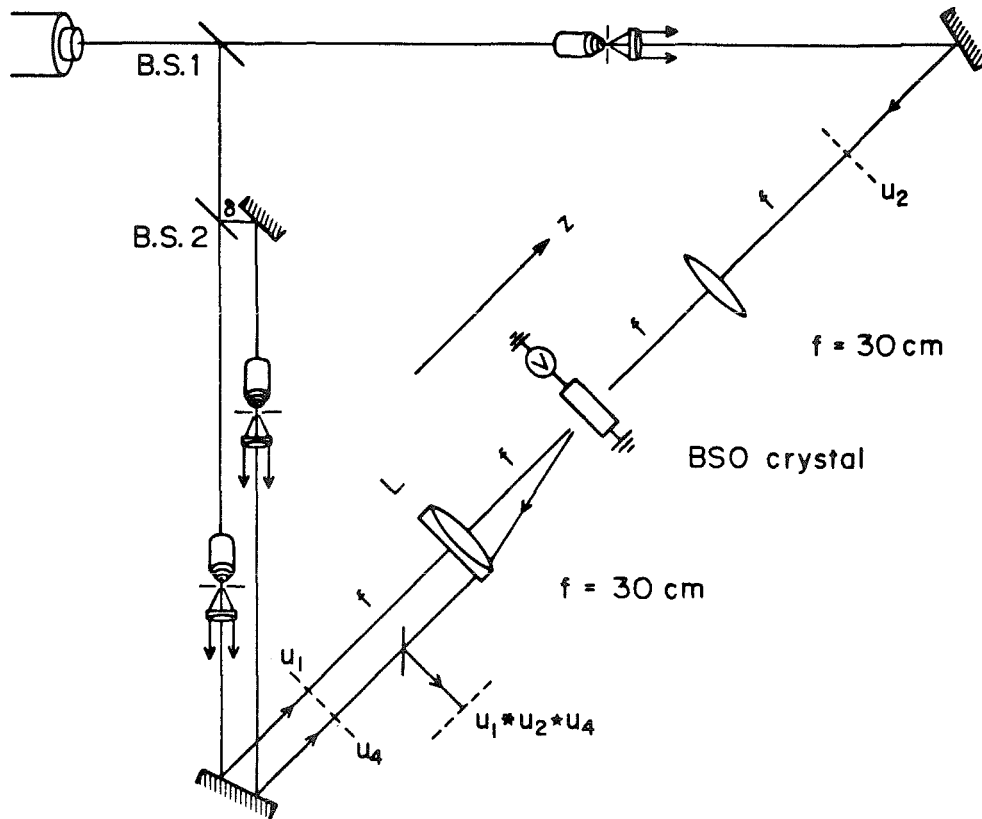
where we have used the definition of correlation  $g \otimes h \equiv g(\mathbf{x}) * h^*(-\mathbf{x})$ .

Two-image processing is performed by simulating a  $\delta$  function for the third input, *i.e.* focusing the third beam at its input plane to give a collimated beam at the transform plane. The interaction is exactly phase matched only when  $U_1$  and  $U_2$  are counterpropagating. If, say,  $U_2$  is a plane wave, then phase matching (Bragg condition along with conservation of photon energy) will put a constraint on the angular spread,  $\delta\vartheta$ , of  $U_1$ , which is known to be  $\delta\vartheta \sim \Lambda/t$  for a grating of period  $\Lambda$  and thickness  $t$  [23]. The angular spread of  $U_1$  at the transform plane is related to the spatial extent  $d$  of  $u_1$  at the front focal plane by  $\delta\vartheta = d/f$ . So, the size of  $u_1$  is limited to  $d < \Lambda f/t$ . The average fringe spacing depends on the distance between  $u_1$  and  $u_4$ , which we assume to be  $d$ , as follows:  $\Lambda = \lambda/2 \sin\theta = \lambda f/2d$ . So, for this system, the input object size is limited to

$$d < f \sqrt{2\lambda/t} \quad (16)$$

This constraint is seen to be the same as the above constraint (12) on filter thickness.

This operation was demonstrated with the experimental arrangement shown in Fig. 5.9.



**Figure 5.9.** Experimental apparatus for performing spatial convolution and correlation of images.

The nonlinear medium was a  $10 \times 10 \times 3 \text{ mm}^3$  crystal of BSO. The application of a transverse ( $\perp$  to  $z$ ) 5 to 7 kV/cm dc electric field enhances the hologram formed between beams 1 and 4. The lenses had focal lengths of 30 cm, restricting the size of the input objects to 3 mm by (16). The coherence length of the laser must be longer than the greatest optical path length difference,  $\delta$ , between the beams.



The continuous wave argon laser with a power output of 1.6W at 514.5nm was initially polarized perpendicular to the plane of the figure. Typical experimental results are shown in Fig. 5.10. The first three columns show the input fields  $u_1$ ,  $u_2$ , and  $u_4$ . The fourth column shows the photograph at the output plane. Rows (a) to (d) illustrate correlation, and row (e) illustrates convolution. The maximum resolution in row (c) was 28 lines/mm, compared to a theoretical maximum of 33 lines/mm determined by the transverse extent of the crystal in the transform plane. The output in row (d) clearly demonstrates pattern recognition.

The operation of the processor was also tested with purely phase objects. For inputs one and four, we used thin lenses having amplitude transmittances like (5). If two such lenses are correlated, the x and y dependence of the field in the output plane should be equivalent to that of a plane wave which has just passed through a lens having focal length equal to the difference in the input focal lengths.

$$u_1 \otimes u_4 \sim \frac{-i\pi}{k \left( \frac{1}{f_1} - \frac{1}{f_4} \right)} \exp \left( \frac{-ik}{2} \frac{|\mathbf{x}|^2}{f_1 - f_4} \right)$$

We determined the general curvature of the output wave by simply looking for a focus at a distance  $f_1 - f_4$  behind the output plane. Table 5.1 summarizes the measurement results, which agree well with the prediction.

The versatility of this processor allows all three inputs to be time varying, but we measured the hologram writing time to be 30 msec so that rapidly changing input fields will cause the output to decrease. Another practical problem is that the range of input light intensities is limited by the saturation effect in BSO (see §2.4). The combination of sensitivity to both the amplitude and phase of the input fields indicates that the correlation processor might be useful for applica-



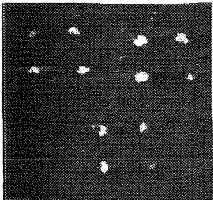

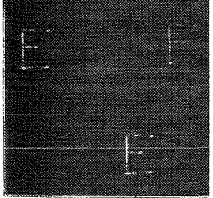
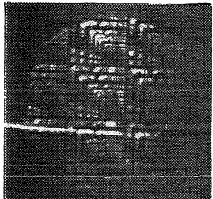
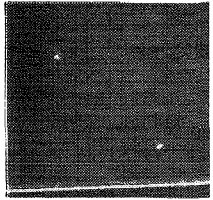

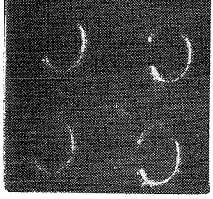
U <sub>1</sub>	U <sub>2</sub>	U <sub>4</sub>	U <sub>3</sub>
	DELTA FUNCTION		
	DELTA FUNCTION	E	
DELTA FUNCTION	DELTA FUNCTION	RESOLUTION CHART	
C	DELTA FUNCTION	CAL TECH	
C		DELTA FUNCTION	

Figure 5.10. Output of the processor shown in Fig. 5.9.

tions such as screening tissue samples for cancer cells.

**TABLE 5.1.** Correlation of phase objects

$f(\text{cm})$		Output wavefront	Radius of curvature (cm)
Lens at input plane 1	Lens at input plane 4		
33.3	50.0	diverging	...
33.3	-9.5	converging	41.4
33.3	-50.5	converging	81.0
33.3	20.0	converging	13.2

**References for Chapter 5**

1. M. Cronin-Golomb, B. Fischer, J. Nilsen, J.O. White & A. Yariv, Appl. Phys. Lett. **41**, 219 (1982).
2. Yu.A. Anan'ev, Sov. J. Quant. Elect. **4**, 7 (1975).
3. J. Feinberg, Opt. Lett. **7**, 486 (1982).
4. A. Litvinenko and S. Odoulov, Opt. Lett. **9**, 68 (1984).
5. S. Kawata and Y. Ichioka, J. Opt. Soc. of Am. **70**, 762 (1980).
6. H. Stark, D. Cahana & H. Webb, J. Opt. Soc. of Am. **71**, 635 (1981).
7. J.R. Fienup, Opt. Lett. **3**, 27 (1978).
8. R.J. Marks II, Appl. Opt. **19**, 1670 (1980).
9. J. Cederquist and S.H. Lee, J. Opt. Soc. of Am. **71**, 643 (1981).
10. J. Cederquist, J. Opt. Soc. of Am. **71**, 651 (1981).
11. H.H. Szu, "Foundations of Single Frame Image Processing." presented at ICO Conference, Optics in Four Dimensions, Ensenada, Mexico, August 4-8, 1980.
12. A. Yariv, Opt. Comm. **21**, 49 (1977).
13. D.M. Pepper and A. Yariv, Opt. Lett. **5**, 59 (1980).
14. J.W. Goodman, W.H. Huntley Jr., D.W. Jackson & M. Lehman, Appl. Phys. Lett. **8**, 311 (1966).
15. A. Yariv and T.L. Koch, Opt. Lett. **7**, 113 (1982).

16. B. Fischer, M. Cronin-Golomb, J.O. White & A. Yariv, Appl. Phys. Lett. **41**, 141 (1982).
17. J.P. Huignard and J.P. Herriau, Appl. Opt. **17**, 2671 (1978).
18. J. Feinberg, Opt. Lett. **5**, 330 (1980).
19. S.H. Lee, Opt. Engin. **13**, 196 (1974).
20. J.W. Goodman, *Introduction to Fourier Optics*, McGraw-Hill, New York, 1968
21. D.L. Staebler, W.J. Burke, W. Phillips & J.J. Amodei, Appl. Phys. Lett. **26**, 182 (1975).
22. J.P. Herriau, J.P. Huignard & P. Auborg Appl. Opt. **17**, 185 (1978).
23. H. Kogelnik, Bell Syst. Tech. J. **48**, 2909 (1969).
24. B. Carquille and C. Froehy, Appl. Opt. **19**, 207 (1980).
25. R.A. Ereemeeva, V.A. Kudryashov, I.N. Matveev, T.G. Usacheva & A.I. Chekmenev, Sov. J. Quant. Elect. **5**, 1429 (1975).
26. R.A. Ereemeeva, V.A. Kudryashov, I.N. Matveev, T.G. Usacheva & A.I. Chekmenev, Sov. J. Quant. Elect. **7**, 90 (1977).
27. L. Pichon and J.P. Huignard, Opt. Comm. **36**, 277 (1981).
28. D.M. Pepper, J. AuYeung, D. Fekete & A. Yariv, Opt. Lett. **3**, 7 (1978).
29. J.O. White and A. Yariv, Appl. Phys. Lett. **37**, 5 (1980).